NASA TECHNICAL NOTE

NASA TN D-6473

NASA TN D-6473

ANALYTICAL AND EXPERIMENTAL STUDIES OF NATURAL VIBRATION MODES OF RING-STIFFENED TRUNCATED-CONE SHELLS WITH VARIABLE THEORETICAL RING FIXITY

by Eugene C. Naumann, Donnell S. Catherines, and William C. Walton, Jr.

Langley Research Center
Hampton, Va. 23365

NATIONAL AERONAUTICS AND SPACE ADMINISTRATION • WASHINGTON, D. C. • OCTOBER 1971

1. Report No. NASA TN D-6473	2. Government Accession No.	3. Recipient's Catalog No.
4. Title and Subtitle ANALYTICAL AND EXPERIMENTAL STUDIES OF NATURAL VIBRATION MODES OF RING-STIFFENED TRUNCATED-CONE SHELLS WITH VARIABLE THEORETICAL RING FIXITY		5. Report Date October 1971 6. Performing Organization Code
7. Author(s) Eugene C. Naumann, Donnell S. Catherines, and William C. Walton, Jr.		8. Performing Organization Report No. L-7228
9. Performing Organization Name and Address NASA Langley Research Center Hampton, Va. 23365		10. Work Unit No. 114-08-13-04 11. Contract or Grant No.
12. Sponsoring Agency Name and Address National Aeronautics and Space Administration Washington, D.C. 20546		13. Type of Report and Period Covered Technical Note 14. Sponsoring Agency Code

15. Supplementary Notes

16. Abstract

Experimental and analytical investigations of the vibratory behavior of ring-stiffened truncated-cone shells are described. Vibration tests were conducted on (1) 60° conical shells having up to four ring stiffeners and for free-free and clamped-free edge constraints and (2) 9° conical shells, for two thicknesses, each with two angle rings and for free-free, free-clamped, and clamped-clamped edge constraints. The analytical method is based on linear thin-shell theory, employing the Rayleigh-Ritz method. Discrete rings are represented as composed of one or more segments, each of which is a short truncated-cone shell of uniform thickness. Equations of constraint are used to join a ring and shell along a circumferential line connection. Excellent agreement was obtained for comparisons of experimental and calculated frequencies.

17. Key Words (Suggested by Author(s))	18. Distribution Statement
Structural dynamics Ring-stiffened cones Natural vibration modes	Unclassified – Unlimited

19. Security Classif. (of this report)	20. Security Classif. (of this page)	21. No. of Pages	22. Price*
Unclassified	Unclassified	84	$3.00

*For sale by the National Technical Information Service, Springfield, Virginia 22151

ANALYTICAL AND EXPERIMENTAL STUDIES OF NATURAL VIBRATION MODES OF RING-STIFFENED TRUNCATED-CONE SHELLS WITH VARIABLE THEORETICAL RING FIXITY

By Eugene C. Naumann, Donnell S. Catherines, and William C. Walton, Jr.
Langley Research Center

SUMMARY

Results are reported from correlated experimental and analytical studies of models with semivertex angles of 60° and 9° and with various ring stiffeners and boundary conditions. In the experimental work for each model configuration, the natural modes of vibration were excited up to a point high in the frequency spectrum. In the analytical work an analysis previously developed to compute the vibration modes of truncated-cone shells without stiffeners is extended to include the effects of rings and boundary conditions other than free-free. A ring is represented as composed of one or more segments, each of which is a truncated-cone shell of uniform thickness. The connection of a ring to the shell is expressed by a rather general system of equations of constraint making it possible to represent different degrees of fixity in the connection.

An analytical determination has been made of the modes of the tested configurations covering the frequency ranges of the tests, and detailed correlations between experimental and analytical results are presented. Particular attention is given to the effect produced on the analytical results and their correlation with experiment when different degrees of fixity between ring and shell are used in the analysis.

Excellent agreement was obtained for comparisons of experimental and calculated frequencies for all model configurations and for tests of the unattached rings. The degree of fixity at ring-shell attachments was found to have an appreciable effect on calculated frequencies, particularly when the ring was not located at or near the edge of the shell.

Measured mode shapes generally exhibited considerable modal coupling; that is, the model resonant response was composed of two or more harmonics along a circumference and there could be different harmonic content on different circumferences.

INTRODUCTION

Shells with the shape of truncated cones are used extensively in space applications. The configurations employed vary from those with a wide apex angle such as the shield for

a planetary entry vehicle to those with a narrow apex angle such as a transition section in a launch vehicle fuselage. Usually, such shells are stiffened by rings or stringers or both to provide structural integrity and to provide attachment points for fixtures and payloads.

The agreement between experimental and calculated results for uniform, isotropic truncated-cone shells presented in references 1 to 5 indicates that the vibration characteristics of this class of unstiffened shells is adequately understood. Results presented in reference 6 for small-angle conical shells with closely spaced rings indicated good frequency agreement between experiment and an analysis using a theory involving an "equivalent orthotropic shell." The results in references 7 to 10, however, show considerable differences between experimental and calculated frequencies for conical shells with either large or small semivertex angles and widely spaced rings. This paper reports results from an analytical and experimental investigation undertaken in an attempt to resolve some of these differences. The investigation made use of a series of truncated-cone shell models with semivertex angles of 60° and 9° and with various ring stiffeners and boundary conditions.

In the experimental work for each configuration, the natural modes of vibration were excited up to a point very high in the frequency spectrum. For each mode both frequency and mode shapes were measured by use of the advanced equipment described in reference 11.

For the analytical work the method of reference 5, which was established to compute the vibration modes of conical shells without stiffeners, has been extended to include the effects of ring stiffeners and boundary conditions other than free-free. In this respect, an important objective of the analytical investigation is to provide the capability to attach a ring to a shell along one or more circumferences and to equate any combination of displacements and rotations along an attachment circumference. A ring is represented as composed of one or more segments, each of which is a short truncated-cone shell of uniform thickness. The connection of a ring to the shell is expressed by a rather general system of equations of constraint making it possible to represent different degrees of constraint in the connection. An analytical determination has been made of the modes of the tested configurations covering the frequency ranges of the tests, and detailed correlations between experimental and analytical results are presented. Particular attention is given to the effect produced on the analytical results and their correlation with experiment when different degrees of fixity between ring and shell are used in the analysis.

SYMBOLS

Any consistent system of units may be used in this analysis.

A	attachment circumference
A_r	assumed ring cross-sectional area
a_k,b_k,c_k	arbitrary coefficients in displacement polynomials
d,e,f,h_o,h_m,L_o	ring dimensions defined in figure 1
h	shell thickness
L	Lagrangian
L_r	idealized ring length
ℓ	radius to ring-segment center of gravity
m	meridional mode number
n	circumferential mode number
R_1,R_2	radius of curvature in s- and ϕ-directions, respectively
r	radius of shell middle surface
u,s	shell middle-surface meridional displacement and coordinate, respectively
v,ϕ	shell middle-surface circumferential displacement and coordinate, respectively
w,z	shell middle-surface normal displacement and coordinate, respectively

β shell middle-surface rotation

γ defined after equation (10)

δ shell middle-surface semivertex angle

ω frequency parameter

Matrix notation:

$\lfloor a \rfloor$ transpose of $\{a\}$

$\{a\}$ defined in equation (3)

$[C]$ defined in equation (14)

$[CA]$ defined in equation (8)

$[CC]$ defined in equation (12)

$[CP]$ defined in equation (6)

$[E]$ defined in equation (15)

$[GM]$ defined after equation (10)

$[K]$ defined in equation (2a)

$[M]$ defined in equation (2b)

$\lfloor P \rfloor$ defined after equation (6)

$\lfloor P' \rfloor$ defined after equation (6)

$\{q\}$ defined in equation (16)

$[ZP]$ defined in equation (7)

$[\beta]$ defined in equation (16)

$[\phi]$ defined in equation (6)

Subscripts:

1,2 refer to values at shell minimum and maximum radii, respectively

u,v,w refer to shell middle-surface displacement directions

Superscripts:

p,q refer to component and connection, respectively

T indicates transpose

bars refer to functions containing elements evaluated for two or more components

$\hat{}$ refer to uncoupled quantities

EXPERIMENTAL METHOD

Vibration surveys were conducted (1) on a 60° truncated-cone shell with up to 4 different ring stiffeners and with free-free and clamped-free boundaries; (2) on 9° truncated-cone shells, for two thicknesses, with end rings, and for free-free, free-clamped, and clamped-clamped boundaries; and (3) on individual rings while detached from the shells. The following sections present a description of the models and test procedures.

Models

Schematic views of the models are shown in figure 1. All model components were made of commercially available 6061-T6 aluminum alloy. The shells were formed from sheet stock and the rings were machined from plate stock. The 0.0635-cm-thick 60° and 9° shells were fabricated by first cutting two sections from sheet stock, then forming two halves, and finally joining the halves with machine butt welds along opposite shell generators. The shell was then placed on a metal die and the welds were mechanically worked to smooth out the seams to produce a model with essentially constant thickness. The 0.0419-cm-thick 9° shell was also fabricated from two formed halves; however, the halves were joined by using a commercial bonding agent and a 1.27-cm-wide strap, of the same

material as the shell, on the exterior side of the joint. (See detail in fig. 1(b).) As part of the fabrication process each shell section was checked at several locations for thickness value. The thickness values reported herein are average values with deviations on the order of ±0.0008 cm.

The rings for each shell were machined from a single piece of plate to insure against variation in material properties. As part of the machining process, the material was subjected to stress-relieving heat-treatment cycles at regular intervals and the final depths of cut were held to a minimum to reduce machining stresses in the rings. To facilitate the test program, the ring portion of the base plate for the 60° shell was duplicated and used interchangeably with the base plate to establish the required edge constraint. (See discussion under "Test Procedures.") In the cross-sectional shape of rings 1, 2, and 3 in figure 1(a), the top surface of the rings has a positive taper (taper angle, e) with respect to the bottom surface. This taper has been set so that the top surfaces of the rings when placed on the shell lie in a new conical surface which has a different semivertex angle than the bottom surface does. All rings were attached to the inner wall of the shell. For the 9° shells the rings were bonded to the shells with a commercial adhesive. For the 60° shell the rings were attached to the shell with both a bonding agent and 0.3175-cm-diameter, positive lock, blind rivets, having 0.635-cm grip length. The rings were drilled and countersunk to the required depth to accommodate the rivets. The rivet spacing was determined on the basis of bond integrity rather than strength requirements. The positive-lock blind rivets were used in lieu of other fasteners because of the excellent gripping characteristics without local material deformation. For the 9° shells the rings were bonded on as part of the fabrication process. For the 60° shell the rings were attached as part of a sequence in which model testing was interspersed with ring attachments so that a series of model configurations was obtained. Figure 2 summarizes all the model configurations and boundary conditions tested and establishes the nomenclature used subsequently in the paper to refer to particular model tests.

Test Procedures

Simulation of edge conditions.- Four combinations of edge conditions were investigated, namely, free-free, clamped-free, free-clamped, and clamped-clamped. The first word in the designation indicates the condition at the minimum diameter and the second word indicates the condition at the maximum diameter. The word "free" indicates no constraint and the word "clamped" indicates that the displacements and the rotation about the edge are constrained.

The basic method for simulating the free-free condition was to suspend the model at eight uniformly spaced points around a circumference on soft elastic bands. For the 60° shell models the suspension points were at the maximum circumference, whereas for the 9° shell models the suspension points were on the ring at the minimum circumference.

For free-free tests of the ring-stiffened 60° shell models (configurations 2 and 3), the base ring was used in lieu of the base plate. The eight-point elastic suspension was also used for the tests of the individual rings. For some tests of configuration 1, the unstiffened 60° shell with free edges, the free-free condition was also simulated by placing the model on a soft hair pad at the small diameter.

Clamped-edge conditions were simulated, for all models, by restraining the motions of the appropriate end ring. For the ring-stiffened 60° shell (configurations 4, 5, 6, and 7), the plate portion of the base plate was clamped between a massive support and a cover plate by means of a 2.54-cm-diameter bolt; thus, the plate was constrained and the ring was allowed to act as a cantilever. (See fig. 3.) For the 9° shells (configurations 9, 9A, 10, and 10A), clamped constraints were simulated at the maximum diameter by bolting the flange of ring B (see fig. 1(b)) to a massive steel structure. To simulate a clamp at the minimum diameter, the flange of ring A was bolted to a small steel structure (assumed rigid) that actually rested upon the conical shell. It may be argued that the attached structure has rigid-body degrees of freedom and therefore does not represent a clamp. This statement is quite true for modes with an axisymmetric shape ($n = 0$) and modes for which the circumferential wave number n is equal to 1, for when the shell is vibrating in such a mode there is a net force or moment on the end mass which would cause the mass to move. However, for modes with the circumferential mode number n greater than 1, there is no net force or moment on the end mass and consequently no need to restrain the rigid-body motions of the mass. No modes are presented for $n = 0$ or $n = 1$. The prestress due to the weight of the small steel structure was small enough to have negligible effect on the model natural frequencies.

Excitation of models.- Two types of shakers were used: An air shaker, as described in reference 12, was used for frequencies less than about 100 hertz. A 6.7-newton electrodynamic shaker was used for higher frequencies. The shaker was attached to the model with a small vacuum cup and was driven with the amplified output of a variable-frequency oscillator. As discussed in reference 5, the air shaker is desirable for low-energy modes of shell structures because the restraint offered by the electrodynamic shaker distorts the mode shape significantly and generally yields higher resonant frequencies. The electrodynamic shaker is desirable for the high-energy modes because, for these modes, the shaker effect is not significant and the electrodynamic shaker gives a more nearly harmonic force output. The frequency ranges of the two shaker systems were made to overlap to insure a smooth transition in frequency.

Mode shape and resonance detection.- For all the tests reported herein, the principal instrument for detecting vibration response of the models was a mobile, noncontacting, displacement-sensitive probe of the type described in reference 11. It is noted that the test apparatus is designed to excite, sense, and measure normal deflections only, as opposed to torsional or stretching deflections. For tests using the electrodynamic

shaker, the output of a miniature accelerometer attached to the shaker vacuum cup was also monitored to assist in resonance detection. The test procedure was as follows:

(1) Fix the location of the mobile displacement probe at a (somewhat arbitrary) point usually near the shaker.

(2) Increase the shaker frequency very slowly until a peak in the probe output is encountered.

(3) With a standard electronic counter, measure the frequency at the response peaks and identify such frequencies as natural frequencies and the associated steady-state responses as mode shapes.

(4) Hold the shaker frequency at the resonant frequency and traverse the model surface with the mobile probe to measure the scaled amplitude of the normal displacement.

In figure 3 may be seen the model, air shaker, edge clamp, and mobile sensor. Generally, the normal displacement of a mode was measured along three different circumferences and along one meridian.

Resonance classification.- Since the models are axisymmetric structures, the normal deflection in a mode should vary around any circumference as a harmonic wave with nodes and antinodes occurring at the same value of ϕ for all circumferences. A typical data sheet for this type of response, designated an uncoupled response, is shown in figure 4(a). Frequently, however, the response did not assume the classic harmonic form but was of the character illustrated by the results in figure 4(b). In these responses several different harmonics appear and there may be different harmonic content along different circumferences. Such a response is designated a coupled response. Experience has shown that such coupled responses are to be expected in a modal survey of an axisymmetric shell because shells normally exhibit several groups of two or more modes, each mode of the group having very nearly the same frequency.

The following procedure was used to classify measured resonant frequencies for comparison with analysis. First, the associated measured response shape was inspected and all readily apparent circumferential harmonics were identified by judgment. Each such circumferential harmonic was assigned an index n denoting the wave number. In this manner, one or more values of n were associated with each measured resonant frequency. Next, plots were made on which regular curves were faired through the groups of data as shown in figure 4(c). Resonances lying on or near these curves were identified by ascending values of an index m. For unconstrained models the lowest value of m was assigned to be zero. For constrained models the lowest value of m was assigned to be one.

ANALYTICAL METHOD

The analytical method reported herein is an extension of the linear analysis based on Novozhilov's thin-shell theory employing the Rayleigh-Ritz method, reported in reference 5. The extension permits representation of a broad range of constraint conditions, and representation of discrete rings attached to the shell. In the analysis it is assumed that a ring can be represented as composed of one or more segments each of which is a short truncated-cone shell of uniform thickness. The same energy expressions and assumed functions are used for the ring segments as are used in the shell analysis of reference 5. Constraint equations are used to establish the additional edge conditions and to relate displacements and rotations between the shell and a ring segment and between two ring segments. In this paper all connections among components are along discrete circumferences rather than at discrete points. There may be more than one attachment circumference between two components and such connections are referred to as circumferential line connections. The following sections present the relations developed to obtain the cited extensions to the analysis of reference 5.

Coordinate System

Figure 5 shows the coordinate system used for a truncated-cone-shell component which may be either the basic shell or a ring segment. It is emphasized that each component has its own coordinate system. The origin is at the imaginary apex of the component with the Y-axis of the coordinate system coincident with the axis of symmetry. The z-axis is normal to the component middle surface, positive outward. The radius r to the middle surface is taken normal to the Y-axis and is related to the middle surface slant length s by the relation $r = s \sin \delta$, where δ is the semivertex angle of the component. The circumferential coordinate ϕ is the angle formed by the radius r and the X-axis. The direction of the X-axis is arbitrary because the component is a body of revolution. It is assumed, however, that the location of the X-axis is coincident for all components. The orthogonal inplane and normal displacement components, hereinafter called displacements u, v, and w, are assigned directions as follows: inplane meridional displacement u, positive in positive s-direction; inplane circumferential displacement v, positive with increasing ϕ; and normal displacement w, positive outward. The middle-surface rotations β_u, β_v, and β_w are defined as shown in the sketches at the bottom of figure 5.

Component Stiffness and Mass Matrices

Under the assumptions of this analysis, the mass and stiffness matrices for the shell and each ring segment are readily available by using the shell equations of motion

formulated in reference 5. The derivation of the equations of motion in reference 5 is abstracted and presented in the appendix.

The Lagrangian L for a component is written as

$$L = \frac{1}{2}\{\hat{a}\}[\hat{K}]\{\hat{a}\} - \frac{1}{2}\omega^2\{\hat{a}\}[\hat{M}]\{\hat{a}\} \tag{1}$$

where

$[\hat{K}]$ stiffness matrix

$[\hat{M}]$ mass matrix

$\{\hat{a}\}$ matrix of generalized coordinates

Explicit formulations of the matrices $[\hat{K}]$ and $[\hat{M}]$ are given in the appendix. The generalized coordinates in $\{\hat{a}\}$ are coefficients in polynomial expansions of the displacements u, v, and w.

Uncoupled stiffness and mass matrices are obtained for each model component and are, respectively, formed as

$$[K] = \begin{bmatrix} [\hat{K}]^{(0)} & & & & \\ & [\hat{K}]^{(1)} & & & \\ & & \ddots & & \\ & & & [\hat{K}]^{(P-1)} & \\ & & & & [\hat{K}]^{(P)} \end{bmatrix} \tag{2a}$$

and

$$[M] = \begin{bmatrix} [\hat{M}]^{(0)} & & & & \\ & [\hat{M}]^{(1)} & & & \\ & & \ddots & & \\ & & & [\hat{M}]^{(P-1)} & \\ & & & & [\hat{M}]^{(P)} \end{bmatrix} \tag{2b}$$

where $p = 0,1,2,\ldots P$ identifies the model component. The superscript zero (0) is reserved for the basic shell and superscripts other than zero refer to ring segments.

A set of coordinates describing the deformation of the system and appropriate for use with the matrices $[K]$ and $[M]$ are the elements of the matrix $\{a\}$ where

$$\{a\} = \begin{Bmatrix} \{\hat{a}\}^{(0)} \\ \{\hat{a}\}^{(1)} \\ \vdots \\ \{\hat{a}\}^{(P-1)} \\ \{\hat{a}\}^{(P)} \end{Bmatrix} \tag{3}$$

in which the elements of $\{\hat{a}\}^{(p)}$ are the coordinates for the pth component. It is important to understand, however, that the coordinates comprising the matrix $\{a\}$ are not independent but are governed by equations of constraint which describe the connections between the components.

Constraint Equations

As previously noted, equations of constraint were used in this investigation to establish edge conditions other than free-free and to relate component displacements and rotations along circumferential line connections. To establish formulations for equations of constraint it will be necessary to evaluate displacements and rotations along any specific circumference A in a component. The double superscript (p,q) identifies the qth such circumference for the pth component. The position of the circumference within the component is determined by specification of the meridional coordinate $s = s^{(p,q)}$ and the normal coordinate $z = z^{(p,q)}$, and the coordinates are referred to the pth component coordinate system.

For the pth component the middle-surface displacements $u^{(p,q)}$, $v^{(p,q)}$, and $w^{(p,q)}$ evaluated along the circumference $s = s^{(p,q)}$, $z = 0$ become

$$\left.\begin{aligned} u^{(p,q)}\left(s^{(p,q)}, \phi, 0\right) &= \sum a_k^{(p)} \left(\frac{s}{s_2}\right)^k \cos n\phi \\ v^{(p,q)}\left(s^{(p,q)}, \phi, 0\right) &= \sum b_k^{(p)} \left(\frac{s}{s_2}\right)^k \sin n\phi \\ w^{(p,q)}\left(s^{(p,q)}, \phi, 0\right) &= \sum c_k^{(p)} \left(\frac{s}{s_2}\right)^k \cos n\phi \end{aligned}\right\} \tag{4}$$

The middle-surface rotations β_u, β_v, and β_w can be expressed in terms of the middle-surface displacements by the following relations:

$$\left.\begin{aligned}
\beta_u(s,\phi) &= \frac{v(s,\phi,0)}{R_2(s,\phi)} - \frac{1}{R(s,\phi)} \frac{\partial \left[w(s,\phi,0)\right]}{\partial \phi} \\
\beta_v(s,\phi) &= \frac{u(s,\phi,0)}{R_1(s,\phi)} + \frac{\partial \left[w(s,\phi,0)\right]}{\partial s} \\
\beta_w(s,\phi) &= -\frac{1}{2} \frac{1}{R(s,\phi)} \left\{ \frac{\partial}{\partial s} \left(R(s,\phi)\ v(s,\phi,0) \right) - \frac{\partial \left[u(s,\phi,0)\right]}{\partial \phi} \right\}
\end{aligned}\right\} \tag{5}$$

where

$$R(s,\phi) = s \sin \delta$$

$$\frac{1}{R_1}(s,\phi) = 0$$

$$\frac{1}{R_2}(s,\phi) = \frac{\cos \delta}{s \sin \delta}$$

Use of equations (4) and (5) yields the following matrix expressions for the middle-surface displacements and rotations:

$$\begin{Bmatrix}
u\left(s^{(p,q)}, \phi, 0\right) \\
v\left(s^{(p,q)}, \phi, 0\right) \\
w\left(s^{(p,q)}, \phi, 0\right) \\
\beta_u\left(s^{(p,q)}, \phi\right) \\
\beta_v\left(s^{(p,q)}, \phi\right) \\
\beta_w\left(s^{(p,q)}, \phi\right)
\end{Bmatrix}^{(p,q)} = \left[\phi\right] \left[\bar{C}\bar{P}\right]^{(p,q)} \left\{\hat{a}\right\}^{(p)} \tag{6}$$

where

$$\left[\phi\right] = \begin{bmatrix}
\cos n\phi & & & & & \\
& \sin n\phi & & & & \\
& & \cos n\phi & & & \\
& & & \sin n\phi & & \\
& & & & \cos n\phi & \\
& & & & & \sin n\phi
\end{bmatrix}$$

and

$$\left[CP\right]^{(p,q)} = \left[\begin{array}{ccc} \lfloor P \rfloor & 0 & 0 \\ 0 & \lfloor P \rfloor & 0 \\ 0 & 0 & \lfloor P \rfloor \\ 0 & \frac{1}{R_2}\lfloor P \rfloor & \frac{n}{R}\lfloor P \rfloor \\ 0 & 0 & \lfloor P' \rfloor \\ -\frac{1}{2}\frac{n}{R}\lfloor P \rfloor & -\frac{1}{2}\left(\frac{1}{s}\lfloor P \rfloor + \lfloor P' \rfloor\right) & 0 \end{array}\right]_{s = s^{(p,q)}}$$

in which

$$\lfloor P \rfloor = \left\lfloor 1, \left(\frac{s}{s_2}\right), \left(\frac{s}{s_2}\right)^2, \ldots \right\rfloor$$

$$\lfloor P' \rfloor = \left\lfloor 0, \frac{1}{s_2}, \frac{2}{s_2}\left(\frac{s}{s_2}\right), \frac{3}{s_2}\left(\frac{s}{s_2}\right)^2, \ldots \right\rfloor$$

It is assumed that lines originally normal to the middle surface remain straight, unextended, and normal after deformation. It then follows that the displacements and rotations on the general circumference A are

$$\left\{\begin{array}{l} u\left(s^{(p,q)}, \phi, z^{(p,q)}\right) \\ v\left(s^{(p,q)}, \phi, z^{(p,q)}\right) \\ w\left(s^{(p,q)}, \phi, z^{(p,q)}\right) \\ \beta_u\left(s^{(p,q)}, \phi\right) \\ \beta_v\left(s^{(p,q)}, \phi\right) \\ \beta_w\left(s^{(p,q)}, \phi\right) \end{array}\right\} = \left[ZP\right]^{(p,q)} \left\{\begin{array}{l} u\left(s^{(p,q)}, \phi, 0\right) \\ v\left(s^{(p,q)}, \phi, 0\right) \\ w\left(s^{(p,q)}, \phi, 0\right) \\ \beta_u\left(s^{(p,q)}, \phi\right) \\ \beta_v\left(s^{(p,q)}, \phi\right) \\ \beta_w\left(s^{(p,q)}, \phi\right) \end{array}\right\} \tag{7}$$

where

$$\left[ZP\right]^{(p,q)} = \left[\begin{array}{cccccc} 1 & 0 & 0 & 0 & -z^{(p,q)} & 0 \\ 0 & 1 & 0 & z^{(p,q)} & 0 & 0 \\ 0 & 0 & 1 & 0 & 0 & 0 \\ 0 & 0 & 0 & 1 & 0 & 0 \\ 0 & 0 & 0 & 0 & 1 & 0 \\ 0 & 0 & 0 & 0 & 0 & 1 \end{array}\right]$$

The reader is reminded that the eccentricity term $z^{(p,q)}$ takes on positive, zero, or negative values depending on whether the circumference A is, respectively, external, on, or internal to the component middle surface.

By substituting equations (6) into equations (7) and noting that, due to the special character of $[\phi]$ and $[\bar{ZP}]^{(p,q)}$, $[\bar{ZP}]^{(p,q)}[\phi] = [\phi][\bar{ZP}]^{(p,q)}$, there is obtained

$$\begin{Bmatrix} u\left(s^{(p,q)}, \phi, z^{(p,q)}\right) \\ v\left(s^{(p,q)}, \phi, z^{(p,q)}\right) \\ w\left(s^{(p,q)}, \phi, z^{(p,q)}\right) \\ \beta_u\left(s^{(p,q)}, \phi\right) \\ \beta_v\left(s^{(p,q)}, \phi\right) \\ \beta_w\left(s^{(p,q)}, \phi\right) \end{Bmatrix} = [\phi][\bar{CA}]^{(p,q)}\{\hat{a}\}^{(p)} \tag{8}$$

where

$$[\bar{CA}]^{(p,q)} = [\bar{ZP}]^{(p,q)}[\bar{CP}]^{(p,q)}$$

Consider now another component labeled $\bar{p}$ to be connected to component p along circumference A, and let the coordinates of the connection circumference A in the coordinate system of component $\bar{p}$ be denoted $s^{(\bar{p},\bar{q})}$ and $z^{(\bar{p},\bar{q})}$. Similar to the developments which led to equations (8), the displacements and rotations of component $\bar{p}$ along A referred to the $\bar{p}$ coordinate system are given by

$$\begin{Bmatrix} u\left(s^{(\bar{p},\bar{q})}, \phi, z^{(\bar{p},\bar{q})}\right) \\ v\left(s^{(\bar{p},\bar{q})}, \phi, z^{(\bar{p},\bar{q})}\right) \\ w\left(s^{(\bar{p},\bar{q})}, \phi, z^{(\bar{p},\bar{q})}\right) \\ \beta_u\left(s^{(\bar{p},\bar{q})}, \phi\right) \\ \beta_v\left(s^{(\bar{p},\bar{q})}, \phi\right) \\ \beta_w\left(s^{(\bar{p},\bar{q})}, \phi\right) \end{Bmatrix} = [\phi][\bar{CA}]^{(\bar{p},\bar{q})}\{\hat{a}\}^{(\bar{p})} \tag{9}$$

The displacements and rotations of component $\bar{p}$ may be expressed with reference to the coordinate system of the pth component by the following transformation:

$$\begin{Bmatrix} \bar{u}\left(s^{(\bar{p},\bar{q})}, \phi, z^{(\bar{p},\bar{q})}\right) \\ \bar{v}\left(s^{(\bar{p},\bar{q})}, \phi, z^{(\bar{p},\bar{q})}\right) \\ \bar{w}\left(s^{(\bar{p},\bar{q})}, \phi, z^{(\bar{p},\bar{q})}\right) \\ \bar{\beta}_u\left(s^{(\bar{p},\bar{q})}, \phi\right) \\ \bar{\beta}_v\left(s^{(\bar{p},\bar{q})}, \phi\right) \\ \bar{\beta}_w\left(s^{(\bar{p},\bar{q})}, \phi\right) \end{Bmatrix} = [GM]^{(p,\bar{p})} \begin{Bmatrix} u\left(s^{(\bar{p},\bar{q})}, \phi, z^{(\bar{p},\bar{q})}\right) \\ v\left(s^{(\bar{p},\bar{q})}, \phi, z^{(\bar{p},\bar{q})}\right) \\ w\left(s^{(\bar{p},\bar{q})}, \phi, z^{(\bar{p},\bar{q})}\right) \\ \beta_u\left(s^{(\bar{p},\bar{q})}, \phi\right) \\ \beta_v\left(s^{(\bar{p},\bar{q})}, \phi\right) \\ \beta_w\left(s^{(\bar{p},\bar{q})}, \phi\right) \end{Bmatrix} \tag{10}$$

where

$$[GM]^{(p,\bar{p})} = \begin{bmatrix} \cos\gamma & 0 & -\sin\gamma & 0 & 0 & 0 \\ 0 & 1 & 0 & 0 & 0 & 0 \\ \sin\gamma & 0 & \cos\gamma & 0 & 0 & 0 \\ 0 & 0 & 0 & \cos\gamma & 0 & -\sin\gamma \\ 0 & 0 & 0 & 0 & 1 & 0 \\ 0 & 0 & 0 & \sin\gamma & 0 & \cos\gamma \end{bmatrix}^{(p,\bar{p})}$$

and $\gamma^{(p,\bar{p})} = \delta^{(\bar{p})} - \delta^{(p)}$

Substitution of equations (9) into equations (10), with $[GM]^{(p,\bar{p})}[\phi] = [\phi][GM]^{(p,\bar{p})}$, yields

$$\begin{Bmatrix} \bar{u}\left(s^{(\bar{p},\bar{q})}, \phi, z^{(\bar{p},\bar{q})}\right) \\ \bar{v}\left(s^{(\bar{p},\bar{q})}, \phi, z^{(\bar{p},\bar{q})}\right) \\ \bar{w}\left(s^{(\bar{p},\bar{q})}, \phi, z^{(\bar{p},\bar{q})}\right) \\ \bar{\beta}_u\left(s^{(\bar{p},\bar{q})}, \phi\right) \\ \bar{\beta}_v\left(s^{(\bar{p},\bar{q})}, \phi\right) \\ \bar{\beta}_w\left(s^{(\bar{p},\bar{q})}, \phi\right) \end{Bmatrix} = [\phi][\overline{CA}]^{(p,\bar{p},\bar{q})} \{\hat{a}\}^{(\bar{p})} \tag{11}$$

where $[\overline{CA}]^{(p,\bar{p},\bar{q})} = [GM]^{(p,\bar{p})}[CA]^{(\bar{p},\bar{q})}$

Consider the case where it is desired to equate all displacements and rotations of the pth component on circumference A to the corresponding displacements and rotations of the $\bar{p}$th component on circumference A. Use of the preceding equations then leads to the equation

$$\left[CC\right]^{(p,\bar{p},q,\bar{q})}\left\{\bar{a}\right\}^{(p,\bar{p})} = \left\{0\right\} \tag{12}$$

where

$$\left[CC\right]^{(p,\bar{p},q,\bar{q})} = \left[\left[CA\right]^{(p,q)} - \left[\overline{CA}\right]^{(p,\bar{p},\bar{q})}\right]$$

and

$$\left\{\bar{a}\right\}^{(p,\bar{p})} = \begin{Bmatrix}\left\{\hat{a}\right\}^{(p)} \\ \left\{\hat{a}\right\}^{(\bar{p})}\end{Bmatrix}$$

Note that the coordinates $s^{(p,q)}$ and $s^{(\bar{p},\bar{q})}$ are related by the expression

$$s^{(p,q)} = \frac{\tan\delta^{(\bar{p})}\, s^{(\bar{p},\bar{q})} + \left(z^{(\bar{p},\bar{q})} - z^{(p,q)}\right)}{\tan\delta^{(p)}} \tag{13}$$

Equation (13) must be satisfied exactly in order to obtain zero-frequency rigid-body modes for free-free, ring-stiffened, conical shells.

With regard to equation (12), two points are now made. Firstly, the equation as written specifies a connection between any two components, labeled p and $\bar{p}$, where all displacements and rotations are equated along a common circumference. In the event that it is desired to match only certain ones of the displacements and rotations along the connection circumference, equation (12) is modified by replacing the rows in matrix $\left[CC\right]$ which correspond to the unconstrained displacements and rotations by null rows. Secondly, if it is desired to constrain to zero any specific displacement or rotation along circumference $s^{(p,q)}$, $z^{(p,q)}$, then the matrix $\left[\overline{CA}\right]^{(p,\bar{p},\bar{q})}$ is nulled and the rows in matrix $\left[CA\right]^{(p,q)}$ corresponding to the unconstrained displacements and rotations are replaced with null rows. This last device allows specification of the usual homogeneous boundary conditions at the edge of a shell.

Equation (12) can be generalized to give equations for the case where there are several rings, each of which may be connected to the shell at more than one circumference. Equation (12) then takes the form:

$$\left[C\right]\left\{a\right\} = \left\{0\right\} \tag{14}$$

To illustrate, figure 6 shows the form taken by the matrix $[C]$ for an example case of a free-free shell with two rings. In figure 6 the superscripts (p,q) for each connection x are shown in the exploded view. In the matrix $[C]$ there is a column of submatrices for each model element (p) and a row of submatrices for each connection circumference. For a model having one or more boundary constraints, an additional row of submatrices would be included for each component that is constrained.

Equations of Motion

The procedures described in reference 13 were used to establish the system equations of motion. From equation (14) form the symmetric matrix

$$[E] = [C]^T[C] \tag{15}$$

where the superscript T indicates the transpose. The most general solution of equation (15) can then be written as

$$\{a\} = [\beta]\{q\} \tag{16}$$

where $[\beta]$ is a matrix whose columns are the columns of any modal matrix of $[E]$ corresponding to zero eigenvalues of $[E]$ and where $\{q\}$ is an arbitrary column matrix comformable with $[\beta]$. The system equations of motion can now be written as

$$\left[[\beta]^T[K][\beta] - \omega^2[\beta]^T[M][\beta]\right]\{q\} = \{0\} \tag{17}$$

The familiar eigenvalue-eigenvector formulation of equation (17) is in the same form as the frequency equations of reference 5 and thus is amenable to solution by the same techniques.

Ring Idealization

The following sections describe the procedure used to obtain the idealized ring dimensions used in this investigation. Each of the rings used with the 60^o cone was represented by a single shell segment, whereas for the 9^o cone each ring was represented by two shell segments joined by using equations of constraint.

60^o rings.- The ring idealization consists of determining an equivalent ring which has a uniform cross section. For the rings used with the 60^o cone, this idealization involved two approximations. The tapered cross section was replaced by a constant-thickness section and the holes drilled to accommodate the rivets were accounted for by an effective reduced section. Sketch (a) shows actual sections of the 60^o rings (from fig. 1(a)) away from a hole, labeled "normal," and at a hole (including the rivet), labeled

"rivet hole." The method of analysis assumes a uniform section. Therefore, as one step in the idealization of the ring, the section labeled "assumed" was taken for every section of the ring. The volume of material removed by the assumed constant-section circumferential groove is approximately equal to the net volume of material removed by the drilled holes, excluding the volume replaced by rivets.

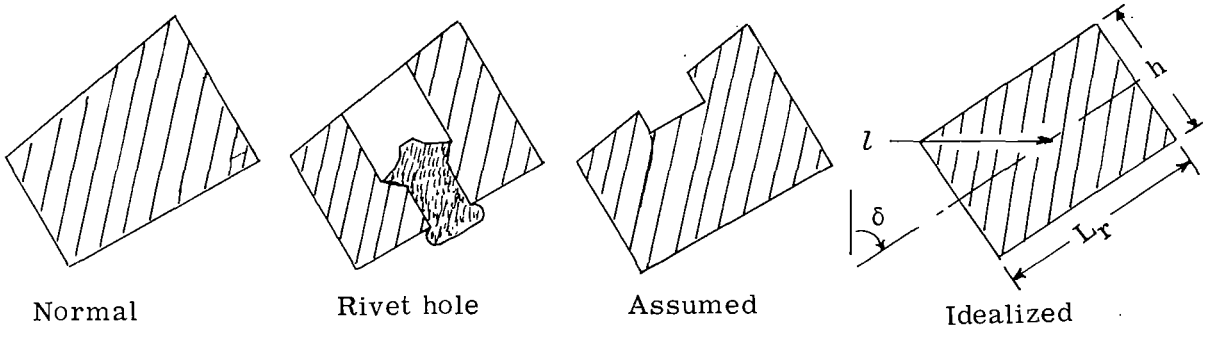

Sketch (a)

For the cross section labeled "assumed," section properties were determined and used in the following expressions to obtain the constant-thickness ring labeled "idealized" in sketch (a) (the idealized ring has the same area and ratio of inertias as the assumed ring):

$$h = \sqrt[4]{\frac{I_{min}}{I_{max}} A_r^2} \tag{18}$$

$$L_r = \frac{A_r}{h} \tag{19}$$

$$\left.\begin{aligned} r_1 &= l - \frac{1}{2} L_r \sin \delta \\ r_2 &= l + \frac{1}{2} L_r \sin \delta \end{aligned}\right\} \tag{20}$$

where

I_{max}, I_{min}, A_r principal moments and area for cross section labeled "assumed"

l radius of center of gravity

h thickness of idealized ring

L_r length of idealized ring

r_1 minimum radius of idealized ring

r_2 maximum radius of idealized ring

δ semivertex angle and principal axes orientation

In order to give some idea of the difference between the normal and assumed ring sections, this procedure was applied to both the normal and assumed cross sections. The section details obtained for each are presented in the following table:

Variable	Idealized dimensions of cross sections for –							
	Base ring		Ring 1		Ring 2		Ring 3	
	Normal	Assumed	Normal	Assumed	Normal	Assumed	Normal	Assumed
h, cm	0.254	0.2413	0.6737	0.6314	0.9670	0.9068	1.2591	1.2205
r_1, cm	7.62	7.544	25.831	25.852	42.692	42.705	59.710	59.586
r_2, cm	10.16	10.084	26.924	26.916	43.779	43.792	60.482	60.622
δ, deg	60	60	59.40	59.39	58.98	59.07	37.32	54.54

An examination of the table shows that the primary effect of accounting for the taper and holes in the manner described was to obtain an idealized ring section which was slightly thinner and longer than would have been obtained by use of the normal ring cross section.

9^o rings.- The idealizations used for rings A and B on the 9^o cone (fig. 1(b)) consisted of representing the two legs of the rings with shells and then tying the two shells together by use of equations of constraint. For each of these rings the outstanding leg had holes.

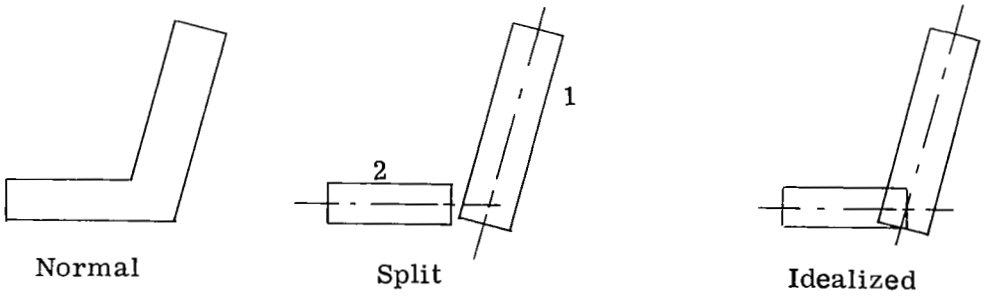

Sketch (b)

The cross section in sketch (b) labeled "normal" is the actual ring cross section away from a hole. The cross section labeled "split" is the result of splitting the ring into

two pieces, piece 1 being the structure attached to the shell and piece 2 being the flange. Piece 2 has a reduced section to account for holes. This reduced section was determined by a procedure similar to that described previously for 60° rings. A comparison of the idealized dimensions of the normal and assumed sections is shown in the following table:

Variable	Idealized dimensions of cross sections for –			
	Ring A		Ring B	
	Normal	Assumed	Normal	Assumed
Piece 1				
h, cm	0.4318	0.4318	0.4318	0.4318
r_1, cm	19.084	19.084	32.847	32.847
r_2, cm	19.345	19.345	33.067	33.067
δ, deg	8.967	8.967	8.967	8.967
Piece 2				
h, cm	0.4318	0.4318	0.4318	0.4318
r_1, cm	17.958	18.009	33.032	33.032
r_2, cm	19.119	19.119	34.176	34.063
δ, deg	90	90	90	90

The third cross section in sketch (b), labeled "idealized," shows the idealized ring, where the two rings are attached at the intersection of the middle surfaces by using four equations of constraint. The displacements u, v, and w, and the rotation β_v about the normal to the paper are equated.

DISCUSSION OF RESULTS

The organization of this section is as follows:

(1) The results of a study to investigate convergence of the computed frequencies are presented.

(2) Measured and calculated natural frequencies for the free rings and for each of the model configurations are presented and compared.

(3) Mode shape data are presented and discussed.

(4) Results are presented from a study to evaluate the effect on the calculated frequencies of the assumed connection between the shell and rings.

In the subsequent discussion it is necessary to distinguish between different assumptions made in the analysis regarding the connection between ring and shell. A two-digit designation (I_1-I_2) is used. The first digit (I_1 = 1,2,3) indicates one of the three attachment circumference configurations shown in the upper part of figure 7. For example, if $I_1 = 2$, there are two attachment circumferences at the intersection of the shell inner surface and normals to the middle surface of the ring at the minimum ring radius r_1 and the maximum ring radius r_2. The second index $(I_2 = 3,4,5,6)$ indicates that compatibility is established at each connection between the corresponding set of displacements and rotations shown at the bottom of figure 7. For example, if $I_2 = 5$, the three displacements and the rotations β_v and β_u are matched at each connection.

Frequency Convergence

Frequency convergence studies were reported in reference 5 for an unstiffened truncated-cone shell model nominally identical to model configuration 1. These studies (ref. 5) indicated that use of 12 terms in each of the polynomial series for the displacements u, v, and w (eq. (A3)) was adequate for convergence of the computed natural frequencies. Additional convergence evaluation was deemed to be necessary for the configurations of this paper because of the consideration of stiffeners and new boundary conditions.

Table I gives the results of the convergence study. Natural frequencies were computed for a number of modes of configuration 5 (three rings, clamped-free) by varying the number of polynomial terms representing the displacements of both the basic shell and the ring stiffeners and considering different connections between one of the rings and the basic shell. Table I shows the calculated frequencies for (1-4), (1-3), and (1-4) connections at the base ring, ring 2, and ring 3, respectively. The calculated frequencies in table I appear to be essentially converged, that is, less than 0.5-percent variation occurred for one added term, when 15 and 5 terms are used for the shell and rings, respectively. In table I ((1-4), (2-3), and (1-4) connections) the frequencies corresponding to $n = 4$, $m = 1$, $m = 3$ and $n = 8$, $m = 2$, $m = 3$ appear to be converged. For the frequencies corresponding to $n = 4$, $m = 2$ and $n = 8$, $m = 1$, changes of up to 3 percent occurred in going from 14 to 15 terms in the shell displacement polynomials. Increasing the number of terms in the polynomial representations of the ring displacements from 5 to 6 resulted in negligible changes in the calculated frequencies.

Increasing the terms in the shell displacements beyond 15 and in the ring displacements beyond 6 sometimes resulted in catastrophic loss of significance in the computed results. It may be noted that 28 significant figures were carried. This tendency to loss of significance is considered a drawback of the analytical method.

Except for special connection studies, all calculated results presented in this paper are based on the assumption of only one attachment circumference in each connection, as in table I ((1.4), (1.3), and (1.4) connections), and were obtained for 12 terms and 5 terms, respectively, in the shell and ring segment displacement polynomial. Although it is recognized that the use of 12 terms, in lieu of 15 terms, in the shell displacement polynomials may lead to calculated results which are not completely converged, it is thought that the errors produced do not have an appreciable effect on the comparisons presented subsequently.

Frequency Results and Comparisons

The resonant frequencies which were detected experimentally are presented in tables II to V together with associated calculated frequencies. Table II gives the frequencies of the individual rings. Table III gives frequencies for model configurations 1, 2, and 3, the 60° cones with free-free edge conditions. Table IV gives frequencies for model configurations 4, 5, 6, and 7, the 60° cones with clamped-free edge conditions. Table V gives the frequencies for model configurations 8, 8A, 9, 9A, 10, and 10A, the 9° cones with free-free, free-clamped, and clamped-clamped boundary conditions. Under the resonance classification which has been described, it was possible for more than one number pair (m,n) to be assigned to the same frequency, and also more than one frequency can be assigned to the same number pair. (See fig. 4(c).) When this condition occurred, only dominant harmonics of these modes are entered in tables II to V. The calculated frequencies presented in tables II to V were obtained by using the input parameters presented in table VI under the following conditions:

(1) Each displacement polynomial series contained 12 and 5 terms for the shell and ring segment, respectively.

(2) Type (1-4) connections were used to join ring segment to ring segment and to join ring segment to shell when the ring segment was located at or near the shell edge.

(3) Type (1-3) connections were used to join ring segments to the shell when the ring segment was located in the shell interior. (See subsequent discussion under connection studies.)

(4) Edge conditions are imposed on ring segments which are connected to the shell, rather than on the end of the shell itself.

The frequency results of tables II to V are presented graphically along with mode shape data (to be discussed subsequently) in figures 8 to 18. The comparisons (table II and fig. 8) between measured and calculated frequencies for several different ring configurations indicate that the method of this paper adequately predicts the $m = 0$ and $m = 1$ bending mode frequencies for the free rings. Similar comparisons for the shell model configurations (tables III, IV, and V and figs. 9 to 18) show very good agreement

between experimental and calculated frequencies over the entire range of modes investigated, even though, as discussed previously, considerable coupling of modes was evident in the experimental tests. A possible exception to the conclusion of generally very good frequency correlation lies in the fact that in some instances a measured resonance corresponding to a calculated natural frequency was not identified. See, for example, figure 12(a), $n = 16$, $m = 1$. In all cases this result may reasonably be attributed to failure to separate modes with nearly equal frequencies.

Some observations are now made regarding trends in the behavior of the natural frequencies. All statements are based on calculated values of frequency which show the same trends as the experimental values except for occasional unimportant details.

60° cones.- Figures 9 and 10(a), respectively, show results for the free-free 60° shell with no ring stiffeners and with a base ring. For both $m = 0$ and $m = 1$, the frequencies for $n = 2$ to $n \approx 5$ are significantly affected by the addition of the base ring with substantial percentage increases in the frequencies for $n = 2$, 3, and 4. (See also table III.) These increases are particularly large in the $m = 1$ modes. For $n > 5$, the frequencies are little affected.

Figure 11(a) shows the results when an end ring (ring 3) is added to the configuration of figure 10(a). Adding this ring produces a substantial increase in the frequencies of all the $m = 0$ modes, compared with the base ring case of figure 10(a). The general effect on the $m = 1$ modes is also to increase the frequency. However, there are exceptions in the cases of $n = 2$, 3, and 4 for which the calculated frequencies are somewhat reduced.

Figure 12(a) shows the frequency curves when the base ring is replaced by the clamped base plate. From comparison of figures 11(a) and 12(a), it may be seen that for n greater than about 4, the two lower frequency curves are the same whether the base ring is free or clamped.

Parts (a) of figures 12, 13, 14, and 15 show frequency curves for the clamped-free 60° shell with various combinations of rings. Consider first the minimum frequency which occurs in all cases for $n = 2$, $m = 1$. Figure 12(a) gives the results when the only stiffener (in addition to the base ring) is ring 3. As interior rings are added (figs. 13(a) and 14(a)), the minimum frequency is little affected. Removal of ring 3 while retaining rings 1 and 2 (fig. 15(a)) results in approximately a 30-percent increase in the minimum frequency. As in previous discussion, addition of the rings generally increases frequencies with an occasional reduction of the frequencies for lower values of n.

9° cones.- Effects of shell thickness on frequency for the 9° cones can be seen by comparing parts (a) and (b) of figures 16, 17, and 18. The frequencies tend to increase with shell thickness for higher values of n, the percentage increase in frequency being somewhat less than the percentage increase in thickness (50 percent). For the smaller

values of n, the behavior of the frequencies is erratic. Cases may be found where the frequency increases, others where it is unaffected, and even some where there is a slight decrease. It is noted that there is no particular reason to expect uniformity in the trends of the frequencies because changing the shell thickness only changes part of the system, the mass and stiffness of the rings being unaffected.

It may also be observed from figures 16, 17, and 18 (model configurations 8, 9, 10, 8A, 9A, and 10A) that as boundary conditions change from free-free to clamped-clamped, the frequency curves become more regular and simpler in character.

Mode Shapes

As previously noted, mode shapes were measured for each resonant frequency. The typical test data sheets in figures 4(a) and 4(b) give a clear indication of the complexity that the measured mode shapes can obtain. Not all the measured mode shapes are presented. The mode shapes which are presented were selected mainly for minimum coupling and in some cases to illustrate trends or typical behavior.

Selected measured mode shapes for model configurations 2 to 7 are presented in parts (b) of figures 10 to 15, respectively, and for model configurations 8 to 10 in parts (c) of figures 16 to 18, respectively. In these figures the first mode number entry identifies the mode judged to be strongest; the second mode number, the next strongest; and so forth. It may be noted that in many cases in these figures, there are more mode number entries than for the corresponding frequency in the frequency tables. The additional entries in the figures correspond to harmonics which were not considered strong enough to be used in the frequency classification procedure but which nevertheless could be observed to be present in the measured mode shape. The assignment of the index m in such cases was based largely on the proximity of the frequencies.

Mode shapes for model configuration 1 have already been presented in reference 5 and will not be repeated. Model configurations 8 and 8A, 9 and 9A, and 10 and 10A differ only in shell thickness and the mode shapes for the thinner shell were only slightly different from those of the thicker shell. For this reason, the mode shapes for model configurations 8A, 9A, and 10A are omitted.

Two characteristics are noted in the experimental mode shapes. First, there are modes for which the rings exhibit considerable motion and indeed seem to be pulling the shell locally. This effect can be seen for model configuration 3 in figure 11(b) ($n = 2$, 3, and 4; $m = 0$ and $n = 5$ and 6; $m = 1$) and for model configuration 5 in figure 13(b) ($n = 3$, 4, and 5; $m = 1$ and $n = 4$ and 5; $m = 2$). Figure 13(b) shows that this "pulling" occurs for interior as well as end rings. The second trend noted is related to mode shapes for modes in which the rings are essentially motionless and, in fact, act as local

constraints. See, for example, configuration 8, figure 16(c) ($n = 5$ to 11; $m = 0$). For these modes the point of shell maximum motion is seen to move toward the shell maximum diameter (1.0 on normalized shell length) as the circumferential mode number increases.

Several calculated meridional mode shapes for model configuration 5 are presented in figures 13(c) and 13(d) for $m = 1$ and $m = 2$ modes, respectively. Comparisons between the measured mode shapes in figure 13(b) and corresponding calculated mode shapes in figures 13(c) and 13(d) show generally good agreement in overall appearance. Superposition of calculated and measured mode shapes in most cases yields generally poor agreement in the vicinity of rings. Comparisons between calculated and measured mode shapes for other model configurations result in similar observations.

In the discussion of frequency results, several references were made to changes in the character (or shape) of the frequency curves. In reference 5 changes in the frequency curves were shown to be associated with changes in the meridional mode shapes. This is also true in the present investigation. To illustrate this point, calculated mode shapes will be used in lieu of measured mode shapes because of the absence of modal coupling in the calculated shapes. Referring first to the frequency curves for model configuration 5 in figure 13(a) and the calculated $m = 1$ mode shapes in figure 13(c), the following observations are made. The mode shape varies from an essentially straight line ($n = 1$, fig. 13(c)) with large motions at both ring 2 and ring 3 (respectively 0.67 and 1.0 on normalized shell length) to large relative motion in the shell panel between the base ring and ring 2 at $n = 6$. This transition in mode shapes corresponds to the dipping part of the $m = 1$ frequency curve of figure 13(a) between $n = 0$ and $n = 6$. The second dip in the frequency curve of figure 13(a) ($n = 6$ to $n = 12$) is characterized by progressive changes in the mode shapes in which the point of maximum motion in the shell panel approaches ring 2. As the shell maximum deflection approaches ring 2, the shell panel between rings 2 and 3 begins to increase in amplitude until at $n = 13$ the point of maximum shell motion passes from the inner panel to the outer panel. This point ($n = 13$) also marks the end of the second dip and beginning of the third dip in the $m = 1$ frequency curve. For $n > 13$ the mode shape is characterized by movement of the point of maximum deflection toward ring 3 and a corresponding decrease in deflection in the inner shell panel. Note also that for $n > 6$, nodes occur at both ring 2 and ring 3.

The $m = 2$ frequency curve (fig. 13(a)) and the calculated mode shapes (fig. 13(d)), also show the correspondence between transitions in the frequency curves and in the mode shapes. The transitions of the frequency curve are at $n \approx 4$, 7, and 12. As figure 13(d) shows, the mode shape assumes a distinct new character in the vicinity of these n-values.

Ring Connection Studies

One objective in developing the analytical method previously described was to provide the capability to attach a ring to a shell along one or more circumferences and to equate any combination of displacements and rotations along an attachment circumference. A study was carried out to ascertain effects of using different types of connections between the shell and ring segments. The study utilized model configurations 2, 4, and 5 for which each ring could be represented by a single shell segment as discussed previously. The results of this study are presented in table VII and in figures 19 and 20, discussion of which follows.

Effect of number of attachment circumferences.- Figure 19 shows results obtained from varying the number of attachment circumferences while holding constant the number of rotations equated. Two model configurations (configurations 2 and 4) were utilized. The trends are as one might expect. The frequencies increase as the number of attachment circumferences is increased and appear to be converging. It can be deduced mathematically that the frequencies using three attachment circumferences should be equal to or greater than the frequencies for one or two attachment circumferences. However, it is noted that it is not a mathematical necessity that the frequencies for two attachment circumferences be higher than those for one attachment circumference because the single attachment circumference does not coincide with either of those for two attachment circumferences.

Effect of number of rotations equated.- Figure 20 shows frequency results for configurations 2, 4, and 5 obtained by utilizing various numbers of attachment circumferences and equating several combinations of rotations at each attachment circumference. (Recall that three displacements are always equated.)

In figure 20(a) one attachment circumference is used in representing the connection between the base ring and the shell for configuration 2, a one-ring configuration. The number of rotations equated is varied. It can be seen that the calculated frequency either increases or remains the same as additional rotations are equated, which is consistent with the mathematical concept employed. Equating the rotation β_u does not increase the calculated frequency because in the present formulation β_u is not linearly independent of the other variables. Figure 20(b) shows results for model configuration 4 which has two end rings (base ring and ring 3). Results are shown for (1-3), (2-3), and (1-4) type connections at each ring. It is observed that the variations in calculated frequency which were produced by making the different connection assumptions are generally in the range of 5 to 10 percent. The frequencies correponding to the (1-4) connection are higher than those for the (1-3) connection, as would be expected. As in figure 19,

the frequencies computed for the (2-3) connection are higher than those for the (1-3) connection and indeed are the highest. This condition is not a mathematical necessity.

Figure 20(c) shows results for configuration 5, a three-ring configuration (base ring, ring 2, and ring 3). Shown in figure 20(c) are the calculated results obtained for (1-3) connections at all rings (dash-dot curve), (1-4) connections at all rings (short-dash curve), and for the combination of connections (1-4), (1-3), and (1-4) (solid curve). It is observed that varying the ring connections results in frequency variations on the order of 10 to 15 percent for $m = 1$, $n > \approx 5$ and $m = 2$, $n > \approx 7$. As the discussion of mode shapes has shown in the modes $m = 1$; $n = 0$ to ≈ 5, rings 2 and 3 are undergoing substantial normal (w) deflection whereas for $m = 1$, $n > 5$ and for $m = 2$, $n > 7$, the rings exhibit essentially no normal motion. Thus, the larger effect of ring connections occurs in regions where the rings are deflecting least, a fact which might not have been anticipated. In these regions the (1-4) connection frequencies are again higher than the (1-3) connection frequencies. The combination of connections (1-4), (1-3), and (1-4) resulted in frequencies which were significantly higher than those obtained for (1-3) connections for $m = 1$, $n > \approx 12$, whereas for $m = 2$ the significant increase was in the range $n = 7$ to $n \approx 12$. For the modes $m = 1$; $n = 0$ to ≈ 5, varying the connections produced no appreciable effect on frequency. Calculated frequencies for connections of (1-4), (2-3), and (1-4) (not shown in fig. 20(c), see table VII(c)) were found to be slightly higher than those obtained for (1-4) connections, a result similar to that noted for model configuration 4.

In order to determine the connection or connections which resulted in the best agreement between experimentally measured frequencies and calculated frequencies, the calculated frequencies of table VII were compared with appropriate experimental frequencies (symbols in figs. 20(b) and 20(c)). As a result of these comparisons, the following connection rules were established and were used for all calculated frequencies reported herein:

1. For end rings – (1-4) connections; that is, one attachment circumference, three displacements, and one rotation (β_V) equated.
2. For interior rings – (1-3) connections; that is, one attachment circumference, three displacements equated.

Finally, the previous discussion related to frequency convergence is recalled. It is possible that some of the computed frequencies are not completely converged. Thus the true values may be slightly lower than shown. See, for example, calculated frequencies for $n = 4$ and $n = 8$ in table VII(c). However, considering that the largest final change in frequency in table I ((1-4), (2-3), and (1-4) connections) is about 3 percent, it is doubtful that any important conclusions would be changed by further convergence.

CONCLUDING REMARKS

An experimental investigation of the vibration characteristics of ring-stiffened truncated-cone shells has been described and the results presented for tests on 13 model configurations. Additionally, an analytical procedure, developed for the purpose of predicting the vibratory behavior of ring-stiffened truncated-cone shells, has been described and the results obtained from applying the procedure to the tested configurations have been presented. Observations of and comparisons between the experimental and calculated results lead to the following remarks:

1. Variation in calculated frequency on the order of 10 to 15 percent can be obtained by varying the degree of fixity in ring to shell connections, the frequency increasing as the fixity increases. The larger effect of assumed ring connections occurs in modes for which the rings are deflecting least.

2. Very good agreement was obtained for comparisons of measured and calculated frequencies for all of the model configurations tested, by using the following assumed connections:

   (a) For end rings – one attachment circumference, three displacements, and one rotation equated.

   (b) For interior rings – one attachment circumference, three displacements equated.

3. Measured mode shapes generally exhibited considerable modal coupling; that is, the model resonant response was composed of two or more different harmonics along a circumference and there could be different harmonic content on different circumferences. Comparisons between measured uncoupled (or very lightly coupled) meridional mode shapes and calculated meridional mode shapes show generally good agreement in overall appearance. Agreement is sometimes poor in the vicinity of the rings. Abrupt changes in the curvature of the frequency-modal number curves are shown to be associated with changes in the characteristics shape of the meridional mode shapes.

4. The analytical procedure developed for this investigation utilized simple polynomials in the shell displacement approximations. This assumption leads to the requirement for high-precision calculations (28 significant figures) to insure against catastrophic loss of numerical significance. This characteristic is considered a drawback to the analytical procedure.

Langley Research Center,
National Aeronautics and Space Administration,
Hampton, Va., August 27, 1971.

APPENDIX

DERIVATION OF MASS AND STIFFNESS MATRICES FOR TRUNCATED CONICAL SHELLS, FROM REFERENCE 5

The following derivation and list of symbols are abstracted from reference 5.

Symbols

Any consistent system of units may be used in this analysis.

a,b,c	arbitrary coefficients in mode shapes
C	shell extensional stiffness, $\frac{Eh}{1 - \mu^2}$
D	shell bending stiffness, $\frac{Eh^3}{12(1 - \mu 2)}$
E	shell modulus of elasticity
h	shell thickness
n	circumferential mode number
r	radius of middle surface of shell
s	meridional coordinate of shell middle surface
t	time
T	kinetic energy
u	meridional displacement
U	strain energy
v	circumferential displacement
w	normal displacement

$\left.\begin{matrix}\alpha,\beta,\gamma,\theta,\psi,\\ \lambda,\epsilon,\eta,\kappa\end{matrix}\right\}$ matrix elements in frequency equation

δ semivertex angle

μ Poisson's ratio

ρ shell mass density

ω frequency parameter

Subscripts:

j,k identify modal components

1,2 refer to values at shell minimum and maximum radii, respectively

,s;,ϕ;,t denote partial differentiation with respect to that variable

Primes denote transpose.

Derivation of Energy Expressions and Matrices

The strain energy expression obtained by use of the shell theory of Novozhilov is:

$$U = \frac{C}{2}\int_0^{2\pi}\int_{s_1}^{s_2}\left[u_{,s}^2 + \left(\frac{1}{s}u + \frac{1}{s\sin\delta}v_{,\phi} + \frac{\cos\delta}{s\sin\delta}w\right)^2 + 2\mu\left(u_{,s}\right)\left(\frac{1}{s}u + \frac{1}{s\sin\delta}v_{,\phi} + \frac{\cos\delta}{s\sin\delta}w\right)\right.$$

$$\left. + \frac{1-\mu}{2}\left(\frac{1}{s\sin\delta}u_{,\phi} - \frac{v}{s} + v_{,s}\right)^2\right] s\sin\delta\, ds\, d\phi + \frac{D}{2}\int_0^{2\pi}\int_{s_1}^{s_2}\left[\left(-w_{,ss}\right)^2\right.$$

$$+ \left(\frac{\cos\delta}{s^2\sin^2\delta}v_{,\phi} - \frac{1}{s}w_{,s} - \frac{1}{s^2\sin^2\delta}w_{,\phi\phi}\right)^2 + 2\mu\left(-w_{,ss}\right)\left(\frac{\cos\delta}{s^2\sin^2\delta}v_{,\phi} - \frac{1}{s}w_{,s} - \frac{1}{s^2\sin^2\delta}w_{,\phi\phi}\right)$$

$$\left. + 2(1-\mu)\left(\frac{\cos\delta}{s\sin\delta}v_{,s} - \frac{\cos\delta}{s^2\sin\delta}v - \frac{1}{s\sin\delta}w_{,s\phi} + \frac{1}{s^2\sin\delta}w_{,\phi}\right)^2\right] s\sin\delta\, ds\, d\phi \qquad \text{(A1)}$$

where $C = \frac{Eh}{1-\mu^2}$ and $D = \frac{Eh^3}{12(1-\mu^2)}$. The first integral in equation (A1) gives the shell extensional energy and the second integral gives the shell bending energy.

The kinetic energy of a conical shell may be written in the following general form:

$$T = \frac{\rho h}{2} \int_0^{2\pi} \int_{s_1}^{s_2} \left(u_{,t}^2 + v_{,t}^2 + w_{,t}^2\right) s \sin \delta \, ds \, d\phi \tag{A2}$$

Let

$$\left.\begin{aligned} u(s,\phi,t) &= \sum_k a_k(t)\left(\frac{s}{s_2}\right)^k \cos n\phi \\ v(s,\phi,t) &= \sum_k b_k(t)\left(\frac{s}{s_2}\right)^k \sin n\phi \\ w(s,\phi,t) &= \sum_k c_k(t)\left(\frac{s}{s_2}\right)^k \cos n\phi \end{aligned}\right\} \qquad (k = 0,1,2, \ldots,N) \tag{A3}$$

where $a_k(t) = \bar{a}_k \cos \omega t$, $b_k(t) = \bar{b}_k \cos \omega t$, and $c_k(t) = \bar{c}_k \cos \omega t$.

The equations of motion are obtained by substituting equations (A3) into equations (A1) and (A2) and using the relations

$$\begin{aligned} \frac{\partial}{\partial a_j}\left[U\left(a_k,b_k,c_k\right) - \omega^2 T\left(a_k,b_k,c_k\right)\right] &= \frac{\partial}{\partial b_j}\left[U\left(a_k,b_k,c_k\right) - \omega^2 T\left(a_k,b_k,c_k\right)\right] \\ &= \frac{\partial}{\partial c_j}\left[U\left(a_k,b_k,c_k\right) - \omega^2 T\left(a_k,b_k,c_k\right)\right] \\ &= 0 \end{aligned} \tag{A4}$$

The operations represented by equation (A4) produce the familiar eigenvalue-eigenvector formulation which can be written in matrix form as follows:

$$\left[\begin{array}{c|c|c} \alpha & \beta & \gamma \\ \hline \beta' & \theta & \lambda \\ \hline \gamma' & \lambda' & \kappa \end{array}\right] \left\{\begin{array}{c} a_k \\ \hline b_k \\ \hline c_k \end{array}\right\} - \omega^2 \left[\begin{array}{c|c|c} \eta & 0 & 0 \\ \hline 0 & \epsilon & 0 \\ \hline 0 & 0 & \psi \end{array}\right] \left\{\begin{array}{c} a_k \\ \hline b_k \\ \hline c_k \end{array}\right\} = \left\{\begin{array}{c} 0 \\ \hline 0 \\ \hline 0 \end{array}\right\} \tag{A5}$$

or equation (A5) is of the form used in equation (17)

$$\left[\hat{K}\right]\{\hat{a}\} - \omega^2 \left[\hat{M}\right]\{\hat{a}\} = \{0\} \tag{A5a}$$

In equation (A5) the prime denotes a transpose and $\alpha,\beta, \ldots \psi$ each represent a submatrix whose elements are specified (for $j + k \neq 0$; $j + k + 2 \neq 0$) as follows:

$$\alpha_{jk} = \left[jkC_{11} + C_{22} + (j + k)C_{12} + \frac{n^2}{\sin^2\delta}C_{66}\right]\frac{1}{j + k}\left[1 - \left(\frac{r_1}{r_2}\right)^{j+k}\right]$$

$$\beta_{jk} = \frac{n}{\sin\delta}\left[C_{22} + jC_{12} - (k - 1)C_{66}\right]\frac{1}{j + k}\left[1 - \left(\frac{r_1}{r_2}\right)^{j+k}\right]$$

$$\gamma_{jk} = \frac{\cos\delta}{\sin\delta}\left(C_{22} + jC_{12}\right)\frac{1}{j + k}\left[1 - \left(\frac{r_1}{r_2}\right)^{j+k}\right]$$

$$\theta_{jk} = \left[\frac{n^2}{\sin^2\delta}C_{22} + (j - 1)(k - 1)C_{66}\right]\frac{1}{j + k}\left[1 - \left(\frac{r_1}{r_2}\right)^{j+k}\right]$$

$$+ \frac{\cos^2\delta}{\sin^2\delta}\left[\frac{n^2}{\sin^2\delta}D_{22} + (j - 1)(k - 1)D_{66}\right]\frac{\sin^2\delta}{r_2{}^2(j + k - 2)}\left[1 - \left(\frac{r_1}{r_2}\right)^{j+k-2}\right]$$

$$\lambda_{jk} = \frac{n\cos\delta}{\sin^2\delta}\left\{C_{22}\frac{1}{j + k}\left[1 - \left(\frac{r_1}{r_2}\right)^{j+k}\right] + \left[\left(\frac{n^2}{\sin^2\delta} - k\right)D_{22} - k(k - 1)D_{12}\right.\right.$$

$$\left.\left. + (k - 1)(j - 1)D_{66}\right]\frac{\sin^2\delta}{(j + k - 2)r_2{}^2}\left[1 - \left(\frac{r_1}{r_2}\right)^{j+k-2}\right]\right\}$$

$$\kappa_{jk} = \frac{\cos^2\delta}{\sin^2\delta}C_{22}\frac{1}{j + k}\left[1 - \left(\frac{r_1}{r_2}\right)^{j+k}\right] + \left\{jk(j - 1)(k - 1)D_{11} + \left(\frac{n^2}{\sin^2\delta} - j\right)\left(\frac{n^2}{\sin^2\delta} - k\right)D_{22}\right.$$

$$- \left[j(j - 1)\left(\frac{n^2}{\sin^2\delta} - k\right) + k(k - 1)\left(\frac{n^2}{\sin^2\delta} - j\right)\right]D_{12}$$

$$\left. + \frac{n^2}{\sin^2\delta}(j - 1)(k - 1)D_{66}\right\}\frac{\sin^2\delta}{(j + k - 2)r_2{}^2}\left[1 - \left(\frac{r_1}{r_2}\right)^{j+k-2}\right]$$

$$\eta = \epsilon = \psi = \frac{\rho h r_2{}^2}{\sin^2\delta(j + k + 2)}\left[1 - \left(\frac{r_1}{r_2}\right)^{j+k+2}\right]$$

where

$$C_{11} = C_{22} = \frac{Eh}{1 - \mu^2} \qquad D_{11} = D_{22} = \frac{Eh^3}{12(1 - \mu^2)}$$

$$C_{12} = \mu C_{11} \qquad D_{12} = \mu D_{11}$$

$$C_{66} = \frac{1 - \mu}{2} C_{11} \qquad D_{66} = 2(1 - \mu) D_{11}$$

In the preceding expressions the following evaluations are made for exceptional cases $j + k = 0,2$:

$$\frac{1}{j + k}\left[1 - \left(\frac{r_1}{r_2}\right)^{j+k}\right] = \log_e \frac{r_2}{r_1} \qquad (j + k = 0)$$

$$\frac{\sin^2\delta}{(j + k - 2)r_2^2}\left[1 - \left(\frac{r_1}{r_2}\right)^{j+k-2}\right] = \frac{\sin^2\delta}{r_2^2} \log_e \frac{r_2}{r_1} \qquad (j + k = 2)$$

REFERENCES

1. Seide, Paul: On the Free Vibrations of Simply Supported Truncated Conical Shells. Israel J. Technol., vol. 3, no. 1, Feb. 1965, pp. 50-61.

2. Weingarten, V. I.: Free Vibrations of Conical Shells. J. Eng. Mech. Div., Amer. Soc. Civil Eng., vol. 91, no. EM 4, Aug. 1965, pp. 69-87.

3. Lindholm, Ulric S.; and Hu, William C. L.: Non-Symmetric Transverse Vibrations of Truncated Conical Shells. Int. J. Mech. Sci., vol. 8, no. 9, Sept. 1966, pp. 561-579.

4. Swaney, Thomas George: Free Vibration of Conical Shells. Ph. D. Diss., Kansas State Univ., 1967.

5. Naumann, Eugene C.: On the Prediction of the Vibratory Behavior of Free-Free Truncated Conical Shells. NASA TN D-4772, 1968.

6. Weingarten, V. I.: Free Vibrations of Ring-Stiffened Conical Shells. AIAA J., vol. 3, no. 8, Aug. 1965, pp. 1475-1481.

7. Godzevich, V. G.; and Ivanova, O. V.: Free Oscillations of Circular Conical and Cylindrical Shells Reinforced by Rigid Circular Ribs. NASA TT F-291, 1965.

8. Crenwelge, O. E., Jr.; and Muster, D.: Free Vibrations of Ring-and-Stringer-Stiffened Conical Shells. J. Acoust. Soc. Amer., vol. 46, no. 1, July 1969, pp. 176-185.

9. Sewall, John L.; and Catherines, Donnell S.: Analytical Vibration Study of a Ring-Stiffened Conical Shell and Comparison With Experiment. NASA TN D-5663, 1970.

10. Dixon, Sidney C.; Miserentino, Robert; and Hudson, M. Latrelle: Theoretical and Experimental Vibration and Buckling Results For Blunt Truncated Conical Shells With Ring-Supported Edges. NASA TN D-7003, 1970.

11. Naumann, Eugene C.; and Flagge, Bruce: A Noncontacting Displacement Measuring Technique and Its Application to Current Vibration Testing. Preprint No. 16.18-5-66, Instrum. Soc. Amer., Oct. 1966.

12. Herr, Robert W.: A Wide-Frequency-Range Air-Jet Shaker. NACA TN 4060, 1957.

13. Walton, William C., Jr.; and Steeves, Earl C.: A New Matrix Theorem and Its Application for Establishing Independent Coordinates for Complex Dynamical Systems With Constraints. NASA TR R-326, 1969.

TABLE I.- RESULTS OF FREQUENCY CONVERGENCE STUDY USING MODEL CONFIGURATION 5

Number of terms/Displacement series for –				Frequency, Hz, for –					
				n = 4			n = 8		
Shell	Base ring	Ring 2	Ring 3	m = 1	m = 2	m = 3	m = 1	m = 2	m = 3
Connections (1-4), (1-3), (1-4)									
12	5	5	5	128.7	211.7	449.0	233.9	422.1	461.0
13	5	5	5	128.5	210.8	448.5	233.6	420.9	456.5
14	5	5	5	128.3	209.4	443.3	233.0	419.8	456.0
15	5	5	5	128.2	208.3	442.6	232.8	418.4	455.9
15	6	6	6	128.2	208.2	442.4	232.8	418.4	455.8
Connections (1-4), (2-3), (1-4)									
12	5	5	5	130.0	228.0	454.6	250.5	454.3	495.1
13	5	5	5	129.9	227.4	452.8	247.6	450.7	480.6
14	5	5	5	129.6	225.0	447.9	247.4	447.2	474.6
15	5	5	5	129.2	217.8	446.1	244.2	446.8	473.6
15	6	6	6	129.2	216.7	445.9	244.2	446.8	473.5

TABLE II.- RESULTS FOR FREE RINGS

(a) Rings used with 60^{o} cones

n	Frequency Hz, for –							
	Base ring		Ring 1		Ring 2		Ring 3	
	Experiment	Analysis	Experiment	Analysis	Experiment	Analysis	Experiment	Analysis
	m = 0							
0	-----	0	----	0	----	0	----	0
1	-----	0	----	0	----	0	----	0
2	196.1	194.9	57.0	57.9	30.2	30.9	20.5	21.3
3	539.0	542.2	162.2	161.5	85.4	86.3	59.5	60.0
4	1025.0	1032.6	307.9	307.9	163.9	164.6	114.0	114.6
5	-----	-----	497.2	496.7	265.6	265.4	184.7	184.9
6	-----	-----	727.0	727.7	389.0	388.9	271.2	270.9
7	-----	-----	996.2	1000.8	534.7	534.8	372.7	372.6
8	-----	-----	----	-----	699.8	703.2	490.1	489.9
	m = 1							
0	-----	0	----	0	----	0	----	0
1	-----	0	----	0	----	0	----	0
2	-----	879.3	104.3	106.0	44.6	41.8	27.6	22.3
3	-----	2390.6	305.4	305.5	119.0	118.6	63.7	62.3
4	-----	3805.1	587.6	589.2	227.7	227.5	121.8	119.0
5	-----	-----	957.5	953.6	367.9	367.8	196.6	192.1
6	-----	-----	----	1396.6	523.9	539.0	288.8	281.4
7	-----	-----	----	1916.0	740.0	740.7	397.0	386.8
8	-----	-----	----	-----	----	972.5	520.8	508.2

(b) Rings used with 9^{o} cones

n	Frequency, Hz, for –							
	Ring A				Ring B			
	m = 0		m = 1		m = 0		m = 1	
	Experiment	Analysis[a]	Experiment	Analysis	Experiment	Analysis[a]	Experiment	Analysis
0	----	0	----	0	----	0	----	0
1	----	0	----	0	----	0	----	0
2	143.3	143.8	244.7	236.9	53.5	47.8	72.4	71.1
3	424.0	427.4	786.8	774.5	144.6	144.0	221.2	222.4
4	817.1	829.7	----	1606.1	280.3	281.7	448.4	452.8
5	----	----	----	-----	455.6	459.1	750.1	754.2
6	----	----	----	-----	667.1	675.0	----	1118.2

[a]Two-segment representing connection (1-4).

TABLE III.- FREQUENCIES FOR FREE-FREE 60° CONES

n	Frequency, Hz, for –											
	Configuration 1 (no rings)				Configuration 2 (one ring)				Configuration 3 (two rings)			
	m = 0		m = 1		m = 0		m = 1		m = 0		m = 1	
	Experiment	Analysis	Experiment	Analysis	Experiment	Analysis[a]	Experiment	Analysis	Experiment	Analysis[b]	Experiment	Analysis
0	----	0	----	0	----	0	----	0	---------	0	----	0
1	----	0	----	0	----	0	----	0	---------	0	----	0
2	3.6	2.7	31.1	31.4	5.9	5.7	171.8 179.3	179.9	17.7	19.3	182.6 183.2	161.3
3	7.1	7.0	70.4	71.9	10.4	10.8	299.0	300.3	52.5	56.0	262.7	256.6
4	12.2	12.7	115.5	116.4	14.9	15.6	213.8 223.8	228.1	102.9	108.2	191.0	194.2
5	19.3	19.5	----	139.8	20.3	20.8	164.4	173.2	128.4, 130.7 135.6	131.1	198.1	203.2
6	26.2	26.5	140.3	139.3	26.6	26.9	143.1	147.7	117.3	118.8	284.4 292.7	288.3
7	33.1	33.5	134.6	138.8	33.4	33.6	127.8	140.4	115.2 117.3	116.5	292.7 298.2	296.0
8	40.8	41.0	140.3	141.9	40.7	41.0	132.9	142.0	120.0	120.4	276.3 280.0	278.6
9	48.4	49.2	146.1 150.1	147.4	49.2	49.2	143.1 146.9	147.4	126.5 130.7	127.1	270.0	272.0
10	57.9	58.1	153.2	155.0	58.6	58.1	153.9	155.0	135.6	135.7	270.0	271.5
11	69.9	67.9	164.3	164.3	68.4	67.9	163.0	164.3	145.5	146.0	270.4	275.0
12	79.3	78.4	174.7	175.3	78.5	78.5	171.8 176.4	175.3	156.6	157.7	280.0	282.0
13	90.0	89.9	186.8 190.5	187.8	90.4	89.9	184.4	187.8	169.5	170.7	284.4	291.8
14	101.0 105.2	102.2	197.8	201.7	104.2	102.2	193.2	201.7	182.6 184.0	185.1	302.5	304.0
15	114.0	115.3	----	216.9	117.5	115.3	208.2	216.9	198.1	200.7	----	318.3
16	128.5 130.4	129.4	----	233.4	128.0 132.9	129.4	----	233.4	----	217.5	----	334.6
17	140.3	144.3	----	251.2	143.1	144.3	----	251.2	----	235.5	----	352.7
18	166.4	160.1	----	270.3	163.0	160.1	265.8	270.3	270.0	254.6	----	372.6
19	180.2	176.8	----	290.5	179.3	176.8	----	290.6	280.0	274.8	----	394.2
20	----	194.4	----	312.0	193.2	194.4	----	312.0	298.2	296.1	----	417.4

[a]Connection (1-4).

[b]Connection (1-4), (1-4).

TABLE IV.- FREQUENCIES FOR CLAMPED-FREE 60° CONE

(a) Model configuration 4 (two rings)

n	Frequency, Hz, for –					
	m = 1		m = 2		m = 3	
	Experiment	Analysis[a]	Experiment	Analysis	Experiment	Analysis
0	----	[b]189.2 353.0	----	667.6	----	814.9
1	62.0	69.6	----	616.2	----	770.1
2	34.0	34.4	----	489.6	----	724.2
3	54.2	57.8	298.5	300.6	----	640.8
4	103.2	109.1	195.6 201.5	202.8	----	521.5
5	130.1 136.0	134.0	199.6 201.5	203.8	412.8	416.3
6	116.5	119.7	284.0	288.6	346.0	348.4
7	112.3	116.7	298.5	296.6	408.0	411.0
8	119.0 116.5	120.4	273.5	278.7	431.0	432.7
9	124.5	127.1	263.0	272.0	412.8 425.9	413.4
10	136.0 130.1	135.7	265.9	271.5	----	404.5
11	146.0	146.0	272.0	275.1	402.5	402.1
12	158.0	157.6	279.1	282.0	399.7	404.5
13	171.2	170.7	287.7	291.8	412.8	410.9
14	186.5	185.1	304.1	304.0	416.8	420.9
15	201.5 199.6	200.7	319.6	318.3	432.0 439.2	433.9
16	----	217.5	346.0	334.6	461.4	450.0
17	233.4	235.5	----	352.7	----	468.5
18	246.6	254.6	----	372.6	----	490.7
19	279.1 265.0	274.8	----	394.2	----	516.8
20	298.5 304.1	296.1	416.8 425.9	417.4	----	546.4
21	319.6	318.6	439.2	442.5	----	579.2
22	----	342.1	----	469.4	----	614.6
23	----	366.8	----	498.1	----	651.9
24	----	392.5	----	528.6	----	690.5
25	425.9 431.0	419.4	----	560.7	----	730.0
26	461.4	447.3	----	594.2	----	769.9

[a]Connection (1-4), (1-4).

[b]Lower frequency corresponds to torsion mode.

TABLE IV.- FREQUENCIES FOR CLAMPED-FREE 60° CONE – Continued

(b) Model configuration 5 (three rings)

n	Frequency, Hz, for –							
	m = 1		m = 2		m = 3		m = 4	
	Experiment	Analysis[a]	Experiment	Analysis	Experiment	Analysis	Experiment	Analysis
0	----	[b]176.0 338.2	----	562.3	----	720.3	----	902.0
1	56.1	64.8	529.2	565.3	----	714.3	----	752.5
2	34.4	35.4	----	421.1	----	721.5	----	772.7
3	63.6	68.5	252.1 258.4	263.0	550.7	586.2	----	692.0
4	121.9	128.7	203.9 211.7	211.7	436.5	449.0	----	641.6
5	196.4	202.3	225.7	238.7	376.7 372.5	390.2	545.7	585.7
6	237.5	240.7	297.9	296.8	413.7	448.9	508.9	526.9
7	----	232.3	435.7	407.6	468.3 476.5	467.1	479.4	485.5
8	230.3	233.9	----	422.1	----	461.0	----	542.1
9	238.9	242.6	----	387.9	452.0	451.9	----	648.4
10	252.1 257.4	255.1	----	359.2	452.0	456.0	----	637.5
11	269.4 274.8	269.6	----	337.4	466.0 468.3	468.4	----	634.1
12	284.9 297.9	282.5	----	326.2	466.0 475.0	486.7	----	638.2
13	----	285.8	323.0	333.0	529.2	507.6	----	652.6
14	----	283.0	----	353.9	536.6 545.7	529.4	----	677.0
15	----	281.6	372.5	380.6	529.2 550.7	552.1	----	707.6
16	284.9	283.4	----	410.3	----	576.9	----	740.6
17	----	288.8	413.0 452.0	441.9	----	604.1	----	775.1
18	297.9	297.6	----	474.9	----	632.7	----	812.7
19	----	309.4	----	509.1	----	662.0	----	855.7
20	----	323.8	----	544.0	----	691.6	----	905.6
21	----	340.8	----	579.2	----	722.1	----	962.8
22	----	359.9	----	613.8	----	754.7	----	1027.0
23	----	381.0	----	647.1	----	791.0	----	1097.6
24	413.7	403.9	----	678.6	----	832.0	----	1173.9
25	435.7 436.5	428.5	----	708.5	----	877.9	----	1255.4
26	----	454.6	----	737.2	----	928.6	----	1341.8

[a]Connections (1-4), (1-3), (1-4).

[b]Lower frequency corresponds to torsion mode.

TABLE IV.- FREQUENCIES FOR CLAMPED-FREE 60° CONE – Continued

(c) Model configuration 6 (four rings)

n	Frequency, Hz, for –					
	m = 1		m = 2		m = 3	
	Experiment	Analysis[a]	Experiment	Analysis	Experiment	Analysis
0	329.3	[b]174.5 336.4	----	559.6	----	719.1
1	55.6	64.3	----	558.2	----	710.7
2	37.2	36.3	344.4	393.2	----	669.2
3	67.7	71.3	249.0	262.0	----	509.8
4	122.8	129.0	251.5	273.6	407.9	448.7
5	195.7	203.2	309.1 328.5	337.6	----	536.6
6	285.9	296.3	407.9	440.4	----	526.0
7	388.8 390.2	407.5	431.1	466.1	----	485.2
8	----	415.4	----	454.0	527.7	542.1
9	363.0	375.9	----	423.7	----	564.3
10	333.0	344.2	----	399.4	----	600.9
11	----	320.3	----	383.5	----	628.8
12	----	302.9	----	376.7	----	637.6
13	----	291.2	363.0	378.4	----	641.1
14	----	284.3	----	387.5	----	646.0
15	285.9	281.9	407.9	403.0	----	653.4
16	----	283.5	431.1	423.8	----	662.9
17	----	288.9	----	449.1	----	674.2
18	----	297.6	----	478.0	----	687.2
19	309.1	309.4	527.0	510.0	----	702.0
20	328.5	323.9	----	544.1	----	719.3
21	----	340.8	----	579.4	----	740.0
22	----	360.0	----	614.7	----	765.3
23	393.0	381.1	----	648.8	----	796.4
24	407.9	404.0	----	680.8	----	834.1
25	431.1	428.6	----	710.7	----	878.4

[a]Connections (1-4), (1-3), (1-3), (1-4).

[b]Lower frequency corresponds to torsion mode.

TABLE IV.- FREQUENCIES FOR CLAMPED-FREE 60° CONE – Concluded

(d) Model configuration 7 (three rings)

n	Frequency, Hz, for –					
	m = 1		m = 2		m = 3	
	Experiment	Analysis[a]	Experiment	Analysis	Experiment	Analysis
0	----	[b]244.5 436.3	----	658.7	----	711.5
1	----	90.6	----	661.3	----	717.7
2	45.0	46.4	----	482.3	----	678.7
3	68.4	75.6	----	319.8	----	550.9
4	114.5	124.4	292.9	316.3	439.1	472.7
5	145.5 149.2	155.9	331.1 344.4	360.6	493.2	541.7
6	142.0	146.5	410.0	452.6	----	553.3
7	124.8	124.9	----	482.7	----	546.4
8	----	107.2	----	440.3	493.2	511.8
9	97.3	95.6	----	406.2	----	477.5
10	91.0	89.9	----	378.7	----	445.8
11	91.0	89.2	367.9	359.8	----	419.8
12	95.7	92.5	----	347.8	----	401.8
13	102.0	99.1	----	339.3	----	394.3
14	110.5 114.5	108.2	----	332.4	----	397.8
15	124.8	119.3	----	327.6	410.0	410.6
16	142.0	131.9	----	325.8	----	430.1
17	149.2	146.0	331.1	327.6	----	454.8
18	162.7	161.2	----	332.9	493.2	483.7
19	178.9	177.6	344.4	341.7	----	515.7
20	195.8	194.9	----	353.6	----	550.0
21	----	213.2	----	368.4	----	585.3
22	233.2	232.5	----	385.8	----	620.0
23	----	252.7	----	405.6	----	652.4
24	----	273.8	----	427.5	----	682.0
25	292.9	295.9	----	451.4	----	709.3
26	----	318.8	----	477.0	----	735.7
27	----	342.6	----	504.2	----	762.1
28	367.9	367.2	----	533.0	----	789.2
29	410.0	392.8	----	563.2	----	817.4
30	----	419.2	----	594.7	----	846.8

[a]Connections (1-4), (1-3), (1-3).

[b]Lower frequency corresponds to torsion mode.

TABLE V.- FREQUENCIES FOR 9° CONE

(a) Model configurations 8 and 8A (free-free)

n	Frequency, Hz, for –							
	m = 0		m = 1		m = 2		m = 3	
	Experiment	Analysis[a]	Experiment	Analysis	Experiment	Analysis	Experiment	Analysis
Configuration 8								
0	----	0	----	0	----	1370.7	----	1895.0
1	----	0	----	0	----	1389.0	----	1685.4
2	40.7	41.9	141.0	138.0	----	693.5	----	1417.6
3	110.8	114.3	269.6	275.2	----	557.4	----	922.5
4	138.5 140.6	143.8	281.0 283.5	286.3	----	558.6	----	940.1
5	116.4	119.5	332.2 336.6	342.7	495.7	496.5	----	749.5
6	110.8 114.3	115.7	269.6 281.0	285.4	520.2	527.5	----	709.2
7	128.6	129.0	245.8	248.1	----	445.0	----	676.9
8	152.5	151.6	232.4	239.9	379.4 384.5	388.3	520.2	580.4
9	179.6	178.7	254.5	253.8	351.4	363.3	----	515.8
10	211.1	209.0	281.0 283.5	280.9	349.5	365.6	----	483.4
11	245.3	242.2	318.6	314.0	379.4	388.7	477.5 486.4	479.8
12	284.6	278.2	349.5	350.6	427.3	423.2	----	500.3
13	332.2	317.3	396.0	390.6	----	463.4	----	537.0
14	----	359.2	----	433.8	----	507.3	----	580.5
Configuration 8A								
0	----	0	----	0	----	1234.0		
1	----	0	----	0	----	1278.0		
2	43.9	46.1	148.7	149.0	----	642.8		
3	119.0 126.0	125.9	248.7 267.0 268.2	273.5	----	558.6		
4	138.6 139.2	147.1	----	297.3	----	549.2		
5	108.2	114.4	330.9 343.5	351.5	----	504.8		
6	95.0	100.6	268.2	280.5	----	533.0		
7	95.6	101.5	221.2	232.0	----	437.2		
8	108.2	112.1	----	207.4	----	368.3		
9	126.0	128.7	----	201.6	315.5	325.4		
10	138.6 148.7	148.6	221.2	210.4	----	304.2		
11	----	170.7	----	228.9	----	301.8		
12	----	194.6	248.4	252.4	315.5	314.8		
13	----	220.4	267.0	278.4	330.9	337.8		
14	----	248.0	----	306.5	----	365.5		

[a]Connections (1-4), (1-4). Rings represented by two segments.

TABLE V.- FREQUENCIES FOR 9° CONE – Continued

(b) Model configurations 9 and 9A (free-clamped)

n	Frequency, Hz, for –							
	m = 1		m = 2		m = 3		m = 4	
	Experiment	Analysis	Experiment	Analysis	Experiment	Analysis	Experiment	Analysis
				Configuration 9				
0	----	[b]1034.7 1304.6	----	2492.5	----	2758.5	----	2935.3
1	----	484.1	----	1257.7	----	2038.7	----	2327.4
2	194.0	236.4	----	706.6	----	1376.3	----	1919.3
3	289.5	321.7	----	565.9	----	917.7	----	1393.4
4	219.3 223.9	230.3	----	570.8	----	936.7	----	1159.6
5	164.4	171.4	412.8	424.5	----	744.4	----	1073.2
6	145.8	148.8	321.5 327.1	332.1	558.3	586.4	----	864.7
7	149.6	151.2	277.9	281.2	475.2	480.9	----	712.7
8	168.3	168.6	260.5	262.4	409.9 417.2	415.5	----	606.4
9	194.0	193.5	270.5	269.0	----	383.2	----	537.2
10	223.9	222.1	289.5	292.4	----	379.5	----	500.0
11	254.8 258.2	253.8	319.1 329.1	323.8	391.2 397.3 401.9	398.5	459.3	491.5
12	289.5	288.6	361.7	359.3	426.3 444.0	431.3	558.3	508.9
13	332.7	326.4	391.2 397.3	398.2	475.2	470.2	----	543.5
14	370.4	367.2	426.3 444.0	440.5	----	513.3	----	586.1
15	417.2	411.1	459.3 471.6 485.0	486.1	----	559.7	----	632.7
16	459.3	458.0	----	535.0	----	609.5	----	685.2
				Configuration 9A				
0	----	[b]972.3 1211.0	----	2480.2	----	2588.5		
1	----	444.4	----	1215.1	----	1950.9		
2	201.6 210.0 217.9	230.9	----	685.5	----	1356.2		
3	277.4 295.0	330.1	----	570.8	----	903.1		
4	210.0 217.9	230.3	----	573.5	----	945.4		
5	154.6	167.1	----	423.6	----	744.4		
6	128.6	135.4	308.5	326.7	----	583.4		
7	121.0	124.3	255.0	266.6	----	472.2		
8	122.7	127.6	----	232.4	----	396.3		
9	136.9 137.9	140.4	----	218.7	334.0	347.1		
10	154.6	158.5	210.0 217.9	221.9	----	320.1		
11	175.5 180.8	179.3	233.9	237.3	----	313.0		
12	196.4 201.6	202.1	255.0	259.3	----	322.6		
13	217.9	227.0	277.4 286.1	284.4	----	343.8		
14	----	253.8	----	311.8	----	370.6		
15	277.4	282.7	----	341.4	----	400.5		

[b]Lower frequency corresponds to torsion mode.

TABLE V.- FREQUENCIES FOR 9° CONE – Concluded

(c) Model configurations 10 and 10A (clamped-clamped)

n	Frequency, Hz, for –							
	m = 1		m = 2		m = 3		m = 4	
	Experiment	Analysis	Experiment	Analysis	Experiment	Analysis	Experiment	Analysis
	Configuration 10							
3	----	417.9	----	888.4	----	1379.5		
4	255.9	278.2	----	626.4	----	1022.4		
5	197.1	201.6	----	462.9	----	780.0		
6	160.0	164.8	348.2	359.8	----	614.2		
7	153.5	157.2	293.7	298.9	497.4	501.7		
8	167.9	170.0	265.8	271.7	423.8 428.4	429.6		
9	184.0 186.3	193.6	272.4	272.4	412.2	391.4		
10	220.8 223.8	222.1	291.2 298.6	293.0	375.6 380.2	383.1		
11	250.9	253.8	317.1	323.9	397.7	399.5		
12	291.5 293.7	288.6	361.9	359.3	428.4	431.4		
13	330.6	326.4	397.7	398.2	464.9	470.2		
14	370.9	367.2	428.4	440.5	497.4	513.3		
15	423.8 428.4	411.1	474.3	486.1	----	559.7		
16	464.9	458.0	----	535.0	----	609.4		
	Configuration 10A							
3	----	420.5	----	891.0	----	1381.7	----	1780.7
4	241.8	279.3	----	628.5	----	1024.5	----	1396.6
5	180.0	198.6	394.3	463.0	----	780.9	----	1104.0
6	135.5	153.4	----	355.3	----	612.1	----	887.1
7	124.7 124.9	132.7	272.0	285.4	----	493.4	----	726.5
8	124.7 124.9	130.5	229.5	243.4	394.3	410.8	----	607.7
9	135.5	141.1	----	224.2	----	356.2	----	521.3
10	152.7 154.6	158.5	218.9	224.0	317.0	325.3	----	461.4
11	169.0	179.3	229.5 237.1	237.8	----	315.3	----	424.6
12	198.2	202.1	255.3 259.2	259.4	317.0 323.3	323.3	----	409.2
13	218.9 229.5	227.0	280.1	284.4	----	343.9	394.3 404.0	412.8
14	241.8 248.0	253.8	301.6 304.2	311.8	----	370.6	435.1	432.0
15	268.9 272.0	282.7	----	341.4	394.3	400.5	----	460.4
16	301.6 304.2	313.5	----	373.2	----	432.8	----	492.3
17	----	346.3	----	407.1	----	467.1	----	----
18	----	381.0	435.1	443.1	----	503.6	----	----

TABLE VI.- MODEL COMPONENT DIMENSIONS AND MATERIAL PROPERTIES

Listed material properties (all components): Aluminum alloy (6061-T6); Young's modulus, $E = 68.95\ GN/m^2$; Poisson's ratio, $\mu = 0.315$; Mass density, $\rho = 2.715\ kg/m^3$

Component	Semivertex angle, δ, deg	Maximum radius, r_2, cm	Minimum radius, r_1, cm	Thickness h, cm
60^o Shell	60	60.960	7.620	0.0635
Base ring	60	10.084	7.544	.2413
Ring 1	59.39	26.916	25.852	.6314
Ring 2	59.07	43.792	42.705	.9068
Ring 3	54.54	60.622	59.586	1.2205
9^o Shell 1	8.967	33.249	19.390	.0635
9^o Shell 2	8.967	33.239	19.380	.0419
Ring A	8.967	19.345	19.084	.4318
Ring A1	90	19.119	18.009	.4318
Ring B	8.967	33.067	32.847	.4318
Ring B1	90	34.063	33.032	.4318

TABLE VII.- FREQUENCY RESULTS OF RING TO SHELL CONNECTION STUDY

(a) Model configuration 2 (one ring)

n	Frequency, Hz, for connection –					
	(1-3)	(1-4)	(1-5)	(1-6)	(2-3)	(3-3)
m = 0						
0	0	0	0	0	0	0
1	0	0	0	0	0	0
2	5.7	6.0	6.0	7.1	7.2	7.5
3	10.3	11.2	11.2	12.6	12.6	13.1
4	14.9	15.8	15.8	16.5	16.5	16.9
5	20.5	20.9	20.9	21.0	21.0	21.2
m = 1						
0	0	0	0	0	0	0
1	0	0	0	0	0	0
2	187.0	190.0	190.0	194.3	222.0	223.3
3	306.7	306.8	306.8	308.6	320.9	322.1
4	224.8	229.5	229.5	234.3	237.8	240.6
5	167.6	173.9	173.9	176.6	179.0	181.9
m = 2						
0	----	----	----	----	----	----
1	----	----	----	----	----	----
2	680.8	681.1	681.1	681.8	683.0	683.2
3	646.1	646.5	646.5	646.5	654.4	654.8
4	568.5	571.7	571.7	575.2	578.6	580.5
5	460.1	468.3	468.3	472.2	476.3	480.1

TABLE VII.- FREQUENCY RESULTS OF RING TO SHELL CONNECTION STUDY – Continued

(b) Model configuration 4 (two rings)

n	Frequency, Hz, for connection[a] –																	
	(1-3) (1-3)	(2-3) (2-3)	(3-3) (3-3)	(1-4) (1-4)	(2-4) (2-4)	(3-4) (3-4)	(1-3) (1-3)	(2-3) (2-3)	(3-3) (3-3)	(1-4) (1-4)	(2-4) (2-4)	(3-4) (3-4)	(1-3) (1-3)	(2-3) (2-3)	(3-3) (3-3)	(1-4) (1-4)	(2-4) (2-4)	(3-4) (3-4)
	m = 1						m = 2						m = 3					
0	[b]189.2 312.2	210.0 370.2	[b]213.2 380.6	[b]189.2 353.0	[b]210.0 404.5	[b]213.2 415.3	597.4	691.4	706.6	667.6	780.9	850.0	774.2	824.9	833.4	814.9	886.1	912.8
1	69.3	76.7	78.3	69.6	77.2	79.3	574.5	645.6	660.0	616.2	719.7	768.7	743.0	782.2	788.0	770.1	816.8	837.8
2	33.7	37.3	38.1	34.3	37.5	38.6	486.8	507.4	512.5	489.6	521.4	535.9	700.0	735.8	744.0	724.2	795.4	832.3
3	55.6	59.3	60.0	57.8	60.4	60.8	297.0	316.5	321.1	300.6	323.9	333.8	631.3	653.6	660.0	640.8	687.9	714.8
4	105.5	111.0	111.9	109.1	112.6	113.4	196.2	214.5	218.9	202.8	224.8	234.7	513.2	536.7	541.8	521.5	560.3	580.5
5	130.5	138.5	140.1	134.0	142.3	149.2	194.3	209.0	212.8	203.8	220.1	225.7	405.6	429.7	434.3	416.3	452.6	475.1
6	116.4	122.5		119.7			280.5	292.1		288.6			335.9	357.8		348.4		
7	114.3	118.2		116.7			291.6	300.9		296.6			398.0	415.2		411.0		
8	117.9	121.9		120.4			275.1	281.6		278.7			424.3	439.3		432.7		
9	123.9	128.8		127.1			268.2	274.7		272.0			406.3	418.4		413.4		
10	131.8	137.7		135.7			266.9	274.3		271.4			396.9	409.1		404.5		
11	141.2	148.1		146.0			269.7	278.1		275.1			393.6	406.9		402.1		
12	152.0	160.1		157.7			275.7	285.4		282.0			395.2	409.4		404.5		
13	164.1	173.4		170.7			284.5	295.5		291.8			400.9	415.8		410.9		
14	177.5	188.0		185.1			295.7	308.0		304.0			410.2	425.8		420.9		
15	192.0	203.9		200.7			309.1	322.6		318.3			422.5	438.9		433.9		

[a]Upper connection is for base ring; lower connection is for ring 3.

[b]Lower frequency corresponds to torsion modes.

TABLE VII.- FREQUENCY RESULTS OF RING TO SHELL CONNECTION STUDY – Concluded

(c) Model configuration 5 (three rings)

n	Frequency, Hz, for connection[a] –											
	(1-3)(1-3)(1-3)	(1-4)(1-3)(1-4)	(1-4)(1-4)(1-4)	(1-4)(2-3)(1-4)	(1-3)(1-3)(1-3)	(1-4)(1-3)(1-4)	(1-4)(1-4)(1-4)	(1-4)(2-3)(1-4)	(1-3)(1-3)(1-3)	(1-4)(1-3)(1-4)	(1-4)(1-4)(1-4)	(1-4)(2-3)(1-4)
	m = 1				m = 2				m = 3			
0	[b]176.0 306.2	[b]176.0 338.2	[b]176.0 344.1	[b]176.4 345.7	506.3	562.3	623.8	623.9	691.6	720.3	770.1	770.4
1	64.4	64.8	64.8	64.9	532.5	565.3	570.4	576.6	703.3	714.4	748.5	752.3
2	34.9	35.4	35.6	35.9	418.5	421.1	421.2	437.4	698.0	721.5	722.2	733.2
3	67.2	68.5	68.7	69.5	259.7	263.0	270.0	278.4	581.5	586.2	594.2	596.3
4	124.9 [c]123.9	128.7 [c]128.2	128.7 [c]128.2	130.1 [c]129.2	207.1 [c]205.0	211.7 [c]208.2	226.1 [c]216.9	228.0 [c]217.8	442.2 [c]438.8	449.0 [c]442.4	451.3 [c]443.8	454.6 [c]446.1
5	194.4	202.3	203.9	204.8	234.3	238.7	252.6	253.3	383.0	390.2	390.3	394.1
6	235.2	240.7	253.1	255.0	287.6	296.8	297.4	298.0	441.8	448.9	449.0	454.0
7	229.9	232.3	244.7	246.7	398.9	407.6	409.6	410.0	451.9	467.1	480.0	484.9
8	233.4 [c]232.6	233.9 [c]232.8	248.8 [c]242.7	250.5 [c]244.2	410.7 [c]406.8	422.1 [c]418.4	449.4 [c]440.7	454.3 [c]446.8	455.7 [c]451.0	461.0 [c]455.9	489.9 [c]470.5	495.1 [c]473.6
9	242.4	242.6	260.9	262.4	375.1	387.9	420.1	424.9	450.4	451.9	481.4	483.9
10	254.3	255.1	277.5	278.7	345.7	359.2	393.7	397.6	455.4	456.0	490.0	491.6
11	267.5	269.6	297.3	298.4	324.3	337.4	372.0	374.9	467.9	468.4	511.4	512.6
12	275.5	282.5	318.8	320.0	317.0	326.2	357.4	359.4	485.6	486.7	544.2	545.3
13	272.3	285.8	329.2	331.0	329.5	333.0	362.8	363.6	504.7	507.6	587.1	588.2
14	266.8	283.0	325.1	326.7	352.3	353.9	391.8	392.4	520.7	529.4	636.8	638.1
15	264.2	281.0	321.7	323.1	379.5	380.6	428.7	429.3	532.5	552.1	688.7	690.2

[a]First connection is for base ring; second, for ring 2; third, for ring 3.

[b]Lowest frequency corresponds to torsion mode.

[c]Lower frequencies obtained for 15 terms in each shell displacement polynomial.

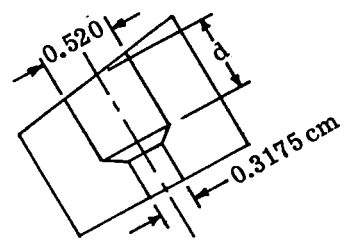

Ring rivet hole detail

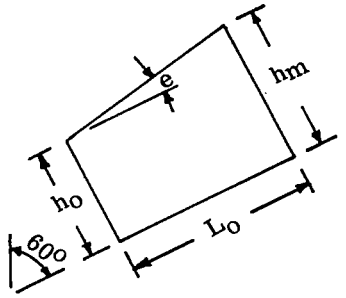

Ring taper detail

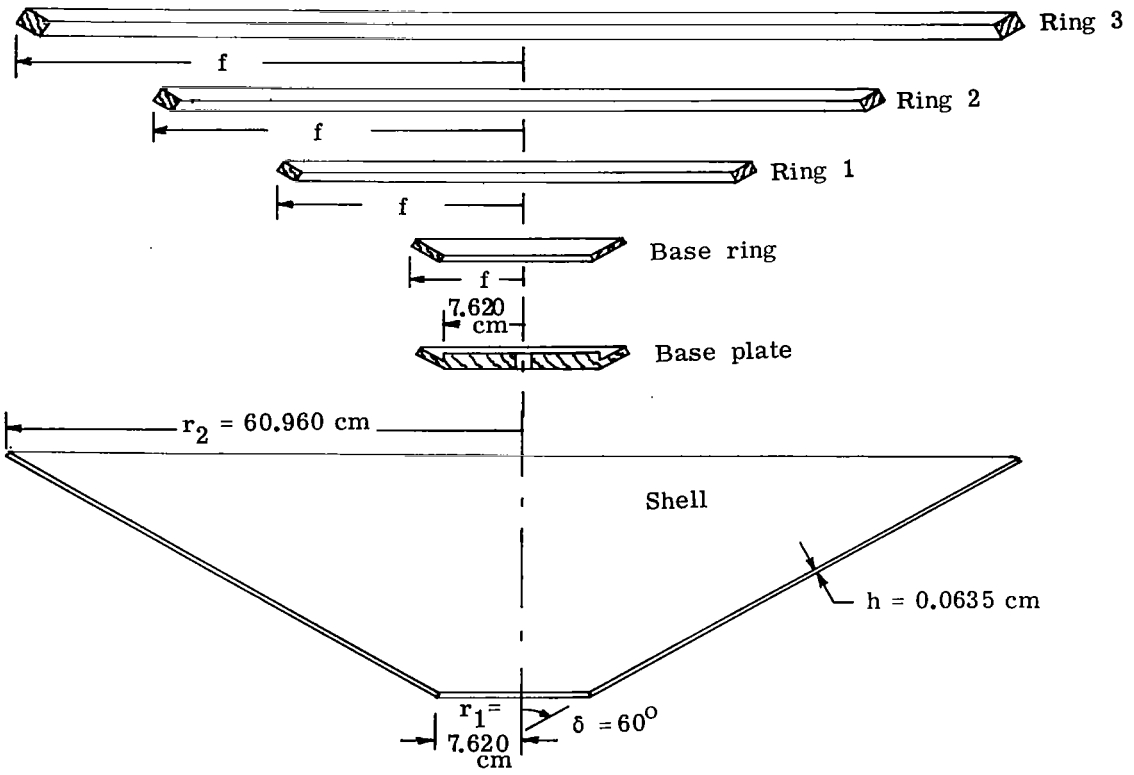

Ring	h_o, cm	e	h_m, cm	L_o, cm	radius f, cm	d, cm	Number of rivets
Base	0.2540	0.	0.2540	2.933	10.146	0	22
1	.6642	0.15	.6833	1.270	27.087	0.165	64
2	.9576	0.15	.9766	1.270	44.003	.460	112
3	1.2510	0.15	1.2700	1.270	60.945	.752	144

(a) 60^o cone model.

Figure 1.- Schematic representations of models.

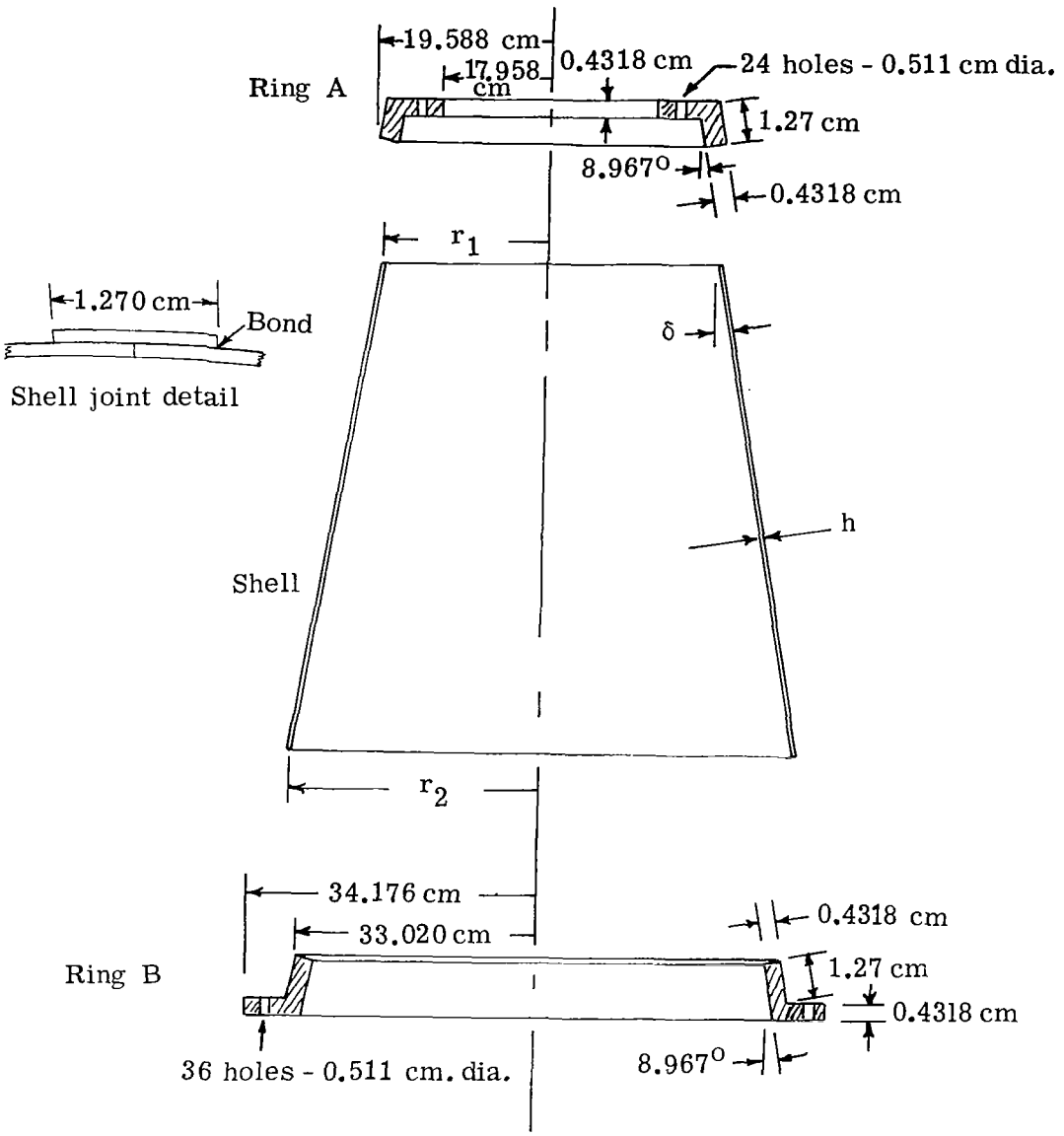

Shell	r_1, cm	r_2, cm	δ, deg	h, cm
1	19.390	33.249	8.967	0.0635
2	19.380	33.239	8.967	0.0419

(b) 9° cone models.

Figure 1.- Concluded.

Configuration	60° Shell +				Edge constraints*	Representation
	Base ring	Ring 1	Ring 2	Ring 3		
1					f-f	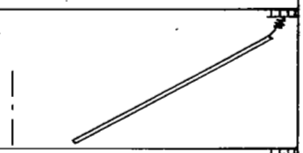
2	x				f-f	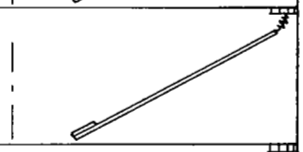
3	x			x	f-f	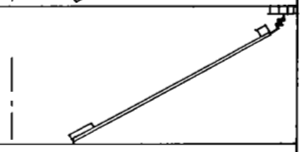
4	x			x	c-f	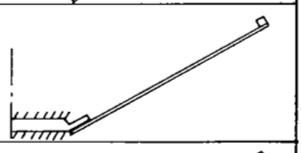
5	x		x	x	c-f	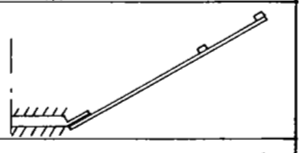
6	x	x	x	x	c-f	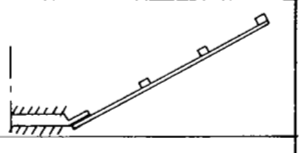
7	x	x	x		c-f	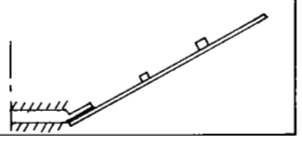

* f denotes free;
c, clamped

Configuration	9° Shell + rings A & B h=0.0635 cm	9° Shell + rings A & B h=0.0419 cm	Edge constraints*	Representation
8	x		f-f	
8A		x		
9	x		f-c	
9A		x		
10	x		c-c	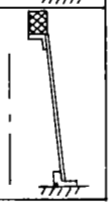
10A		x		

Figure 2.- Model configuration descriptions.

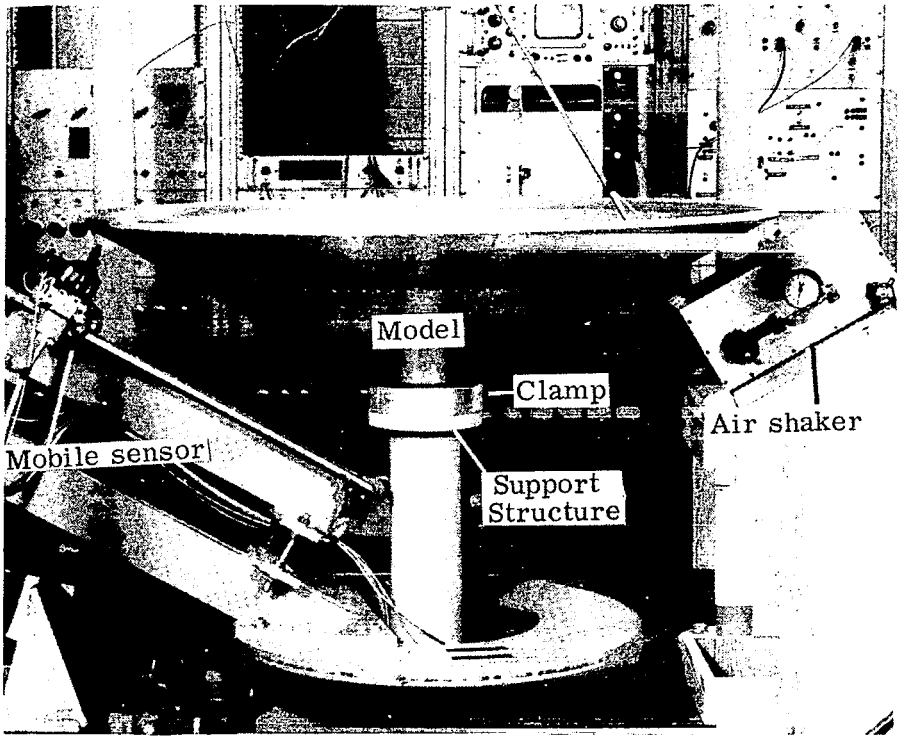

L-67-7546.1

Figure 3.- Test setup.

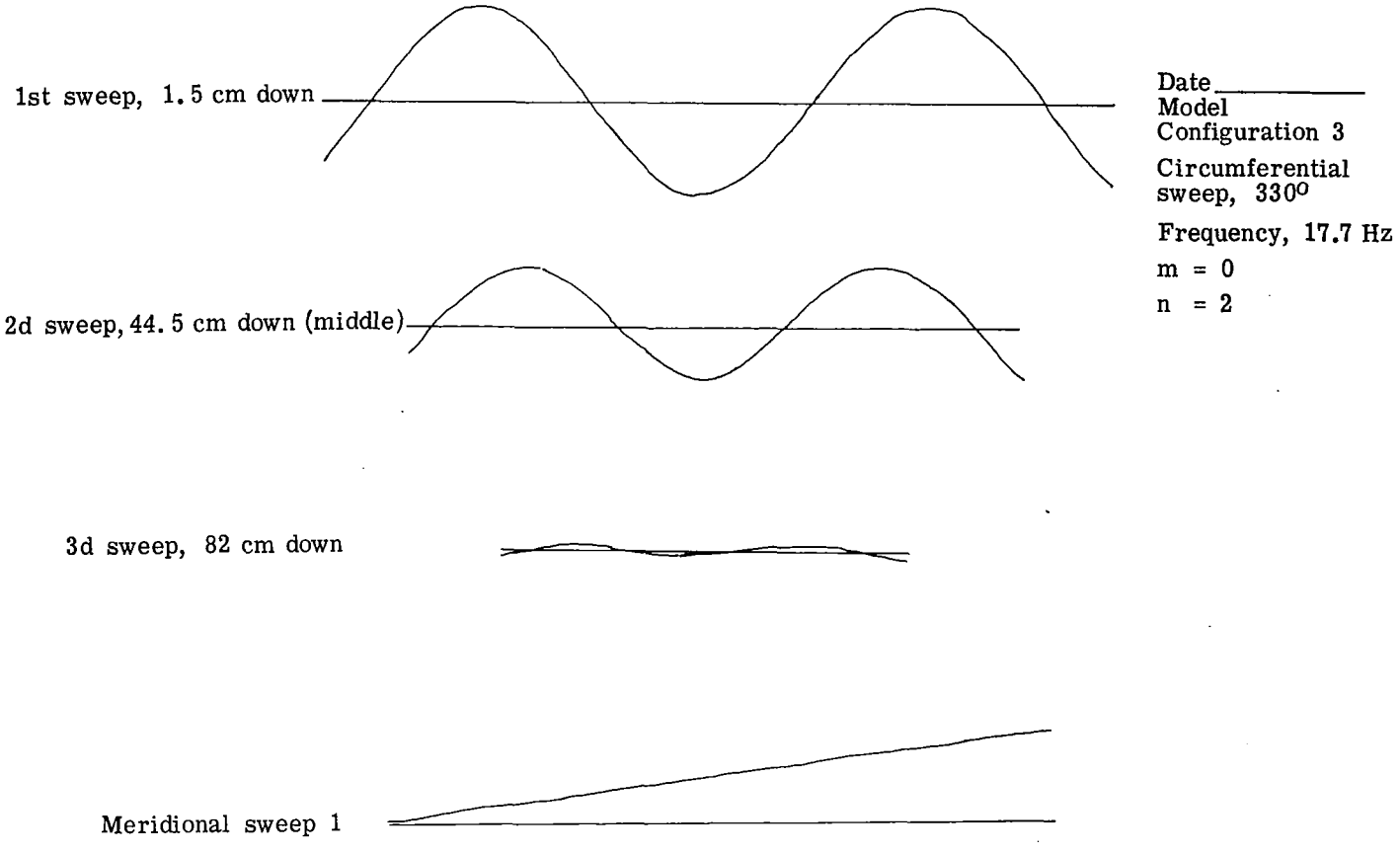

(a) Uncoupled mode.

Figure 4.- Reproduction of typical test data sheets illustrating resonance classification.

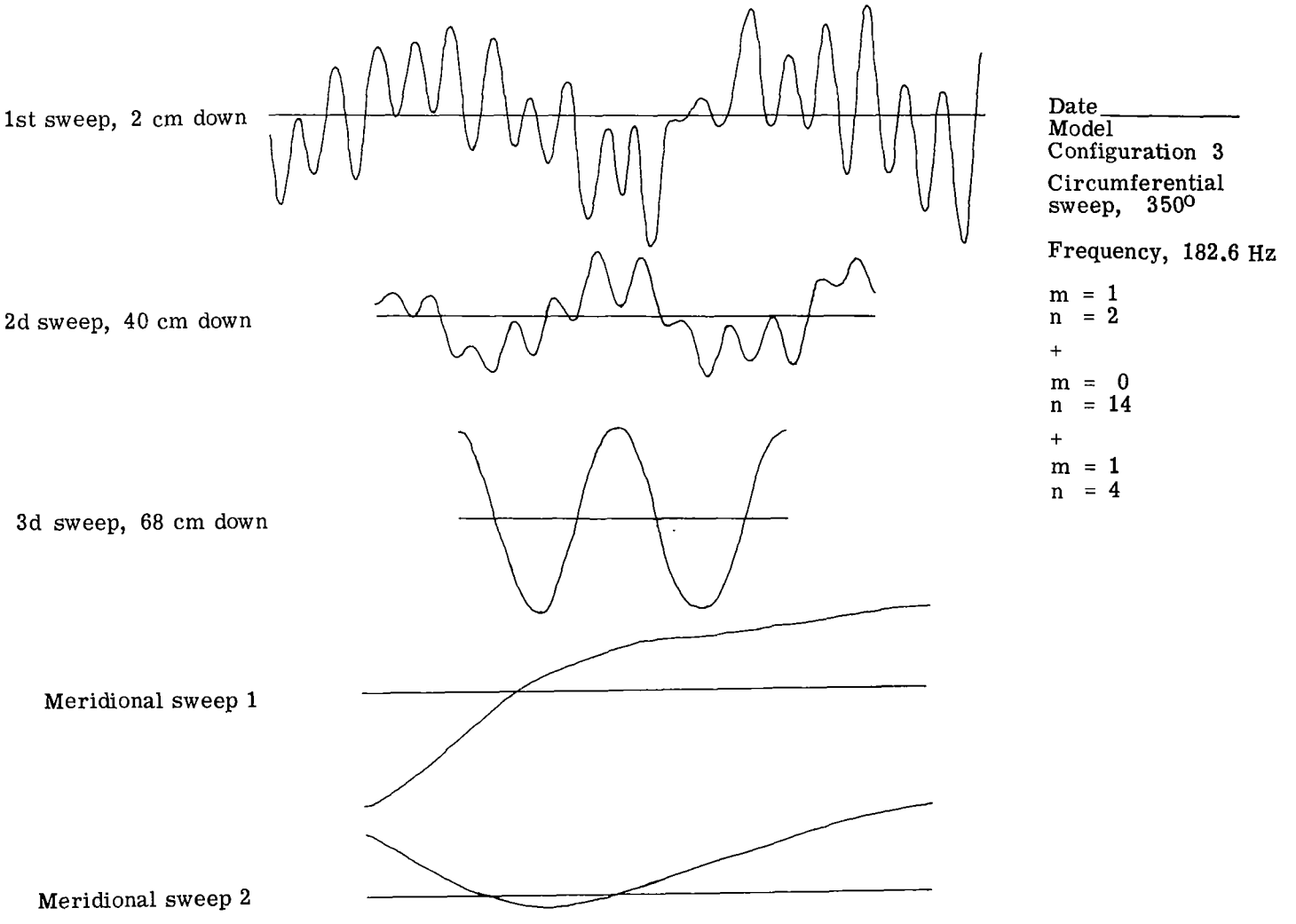

(b) Coupled modes.

Figure 4.- Continued.

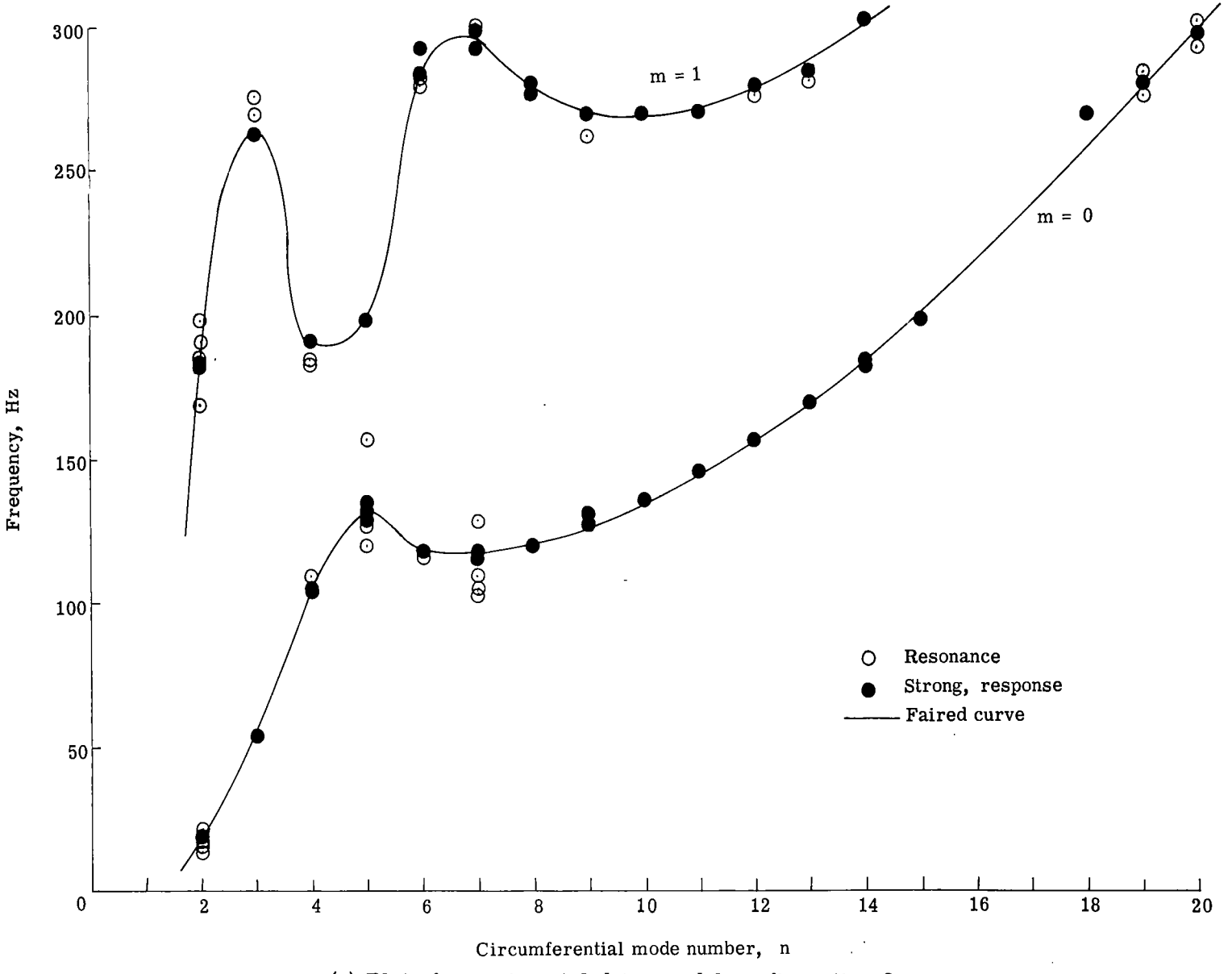

(c) Plot of experimental data; model configuration 3.

Figure 4.- Concluded.

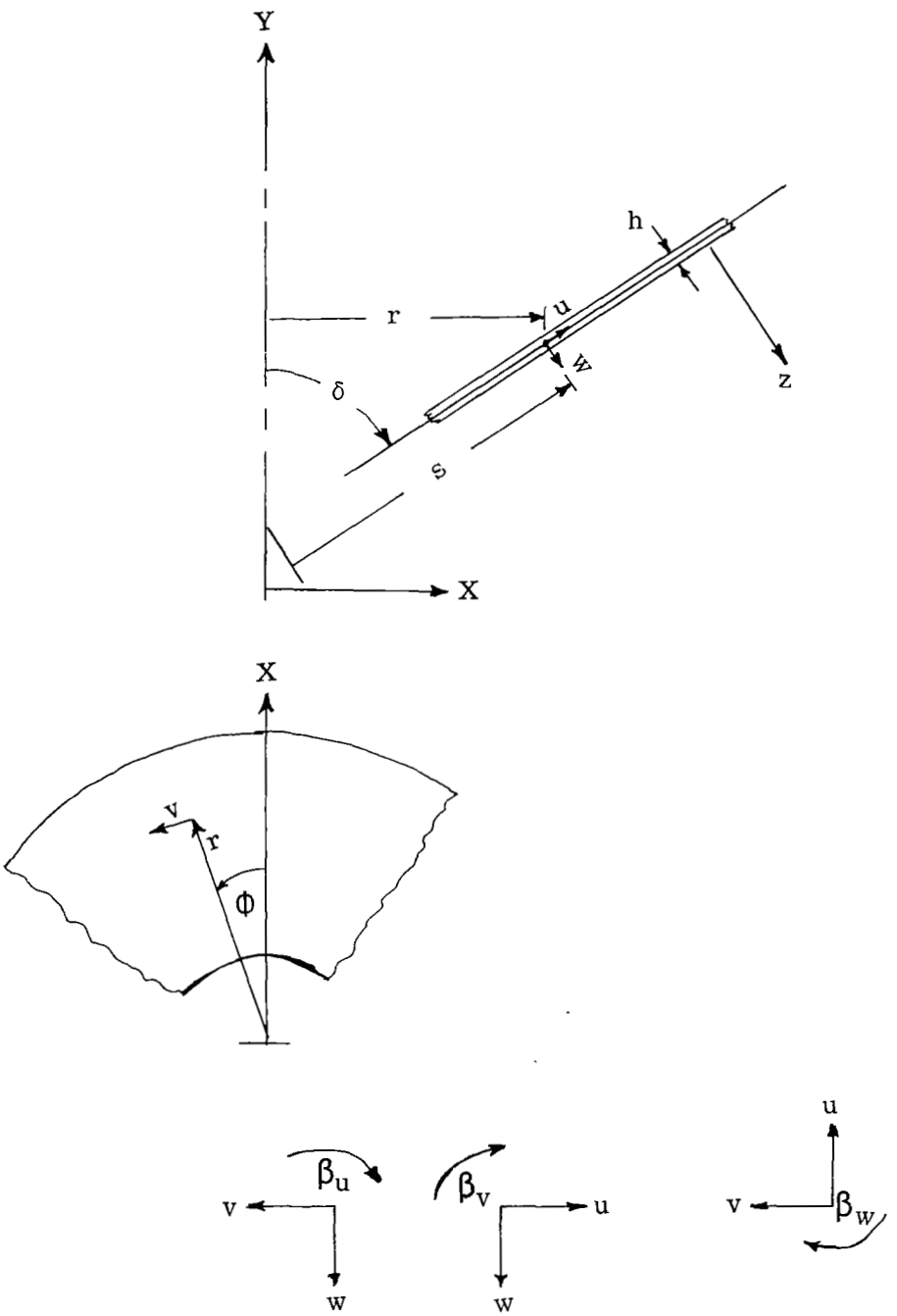

Figure 5.- Coordinate system.

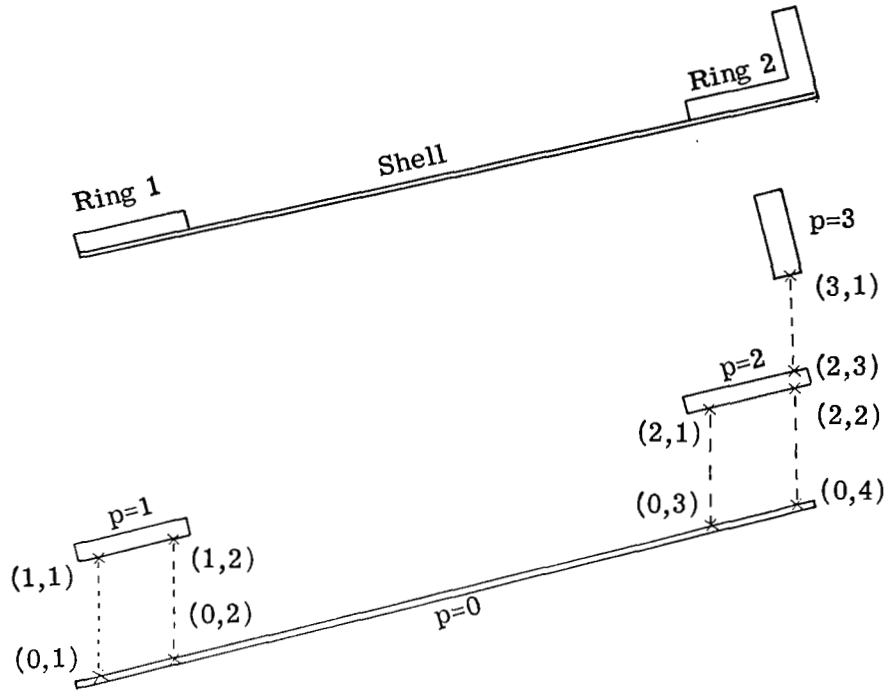

$$[C] = \begin{bmatrix} [CA]^{(0,1)} & -[\overline{CA}]^{(0,1,2)} & & \\ [CA]^{(0,2)} & -[\overline{CA}]^{(0,1,2)} & & \\ [CA]^{(0,3)} & & & \\ [CA]^{(0,4)} & & -[CA]^{(2,3,2)} & \\ & & [CA]^{(2,3)} & -[\overline{CA}]^{(2,3,1)} \end{bmatrix}$$

x denotes attachment circumference (p, q) location

Figure 6.- Illustration of constraint matrix $[C]$.

Index I_1	Number of connections	Location of normal	Schematic representation*
1	1	$\frac{r_1 + r_2}{2}$	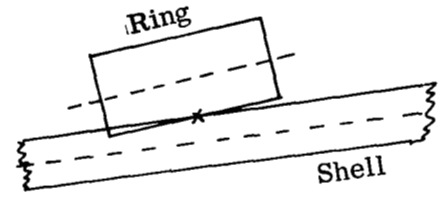
2	2	r_1 ; r_2	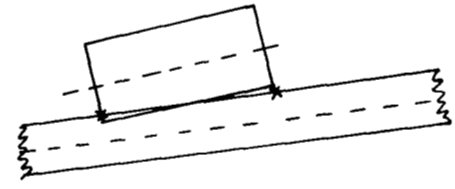
3	3	$r_1, \frac{r_1+r_2}{2}, r_2$	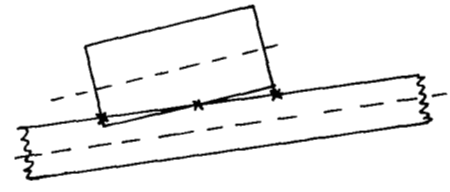

* x denotes connection

Index I_2	Compatibility required for -	
	Displacements	Rotations
3	3	0
4	3	1 (β_v)
5	3	2 (β_v, β_u)
6	3	3 (β_v, β_u, β_w)

Figure 7.- Ring segment to shell connection nomenclature.

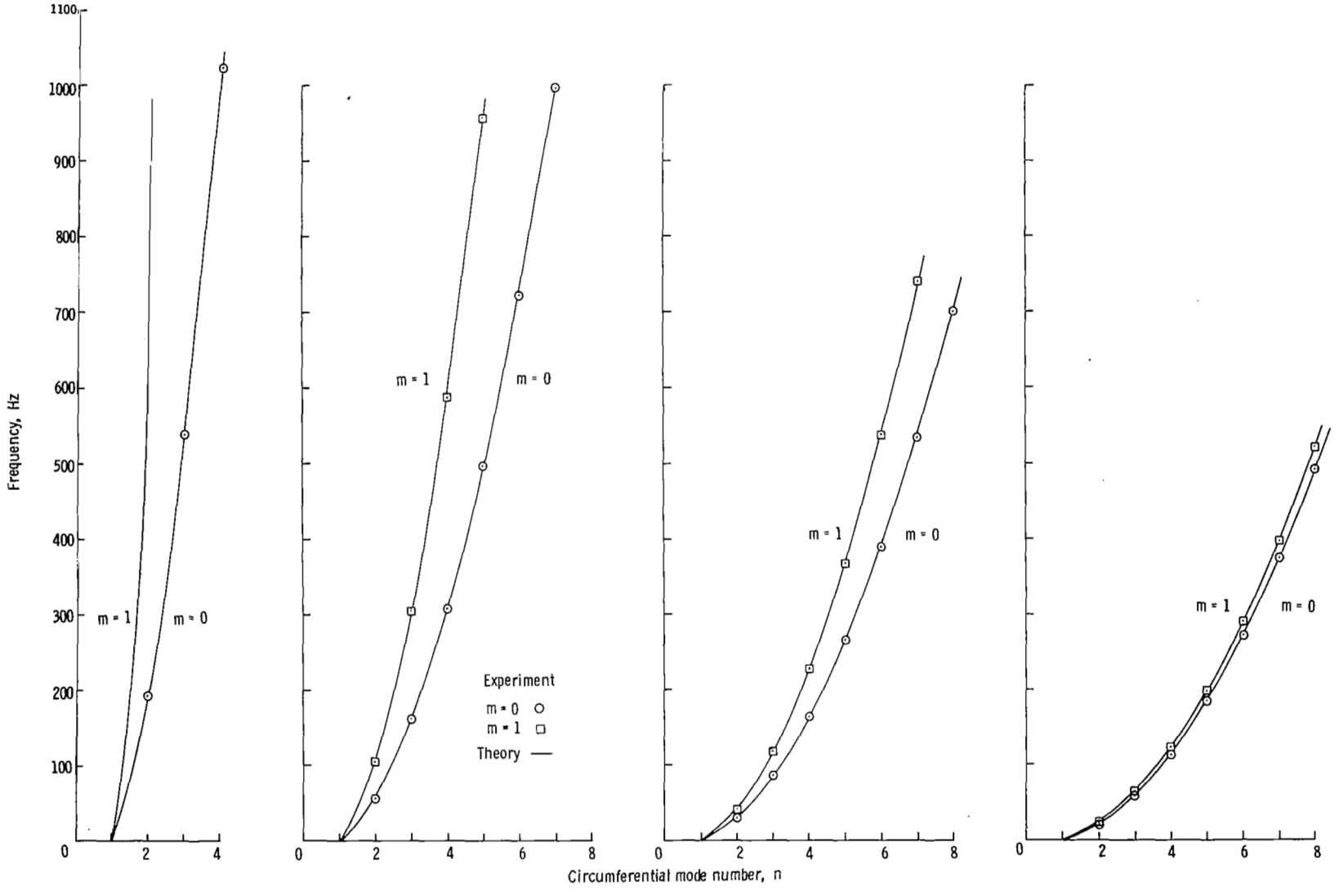

(a) Base ring. (b) Ring 1. (c) Ring 2. (d) Ring 3.

Figure 8.- Comparison of analysis and experiment data for free-free rings.

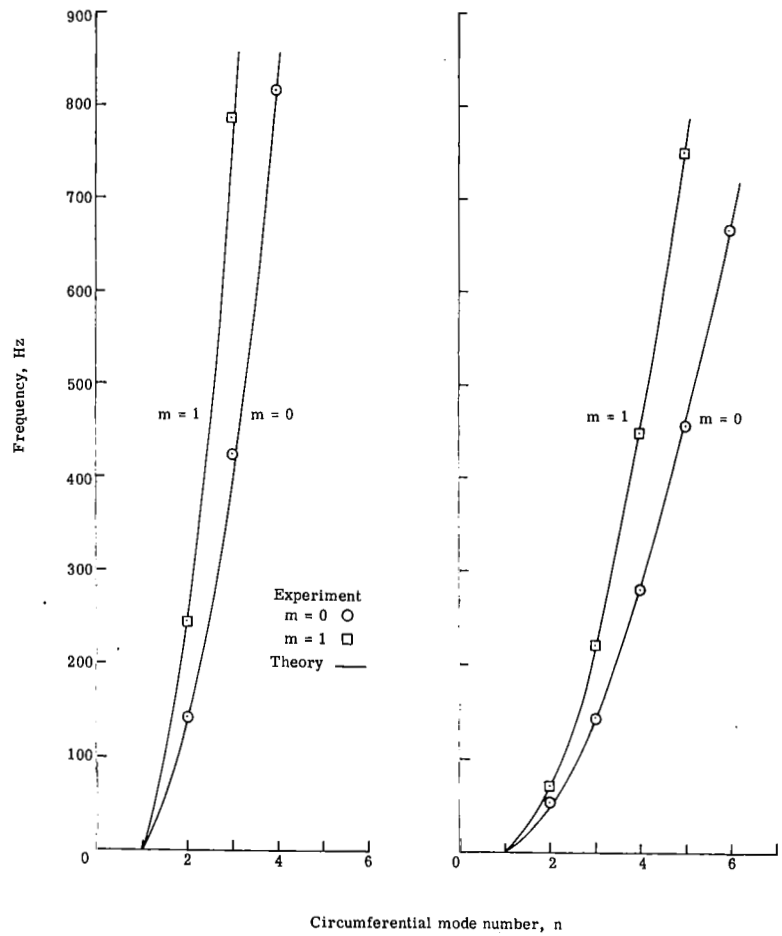

(e) Ring A.

(f) Ring B.

Figure 8.- Concluded.

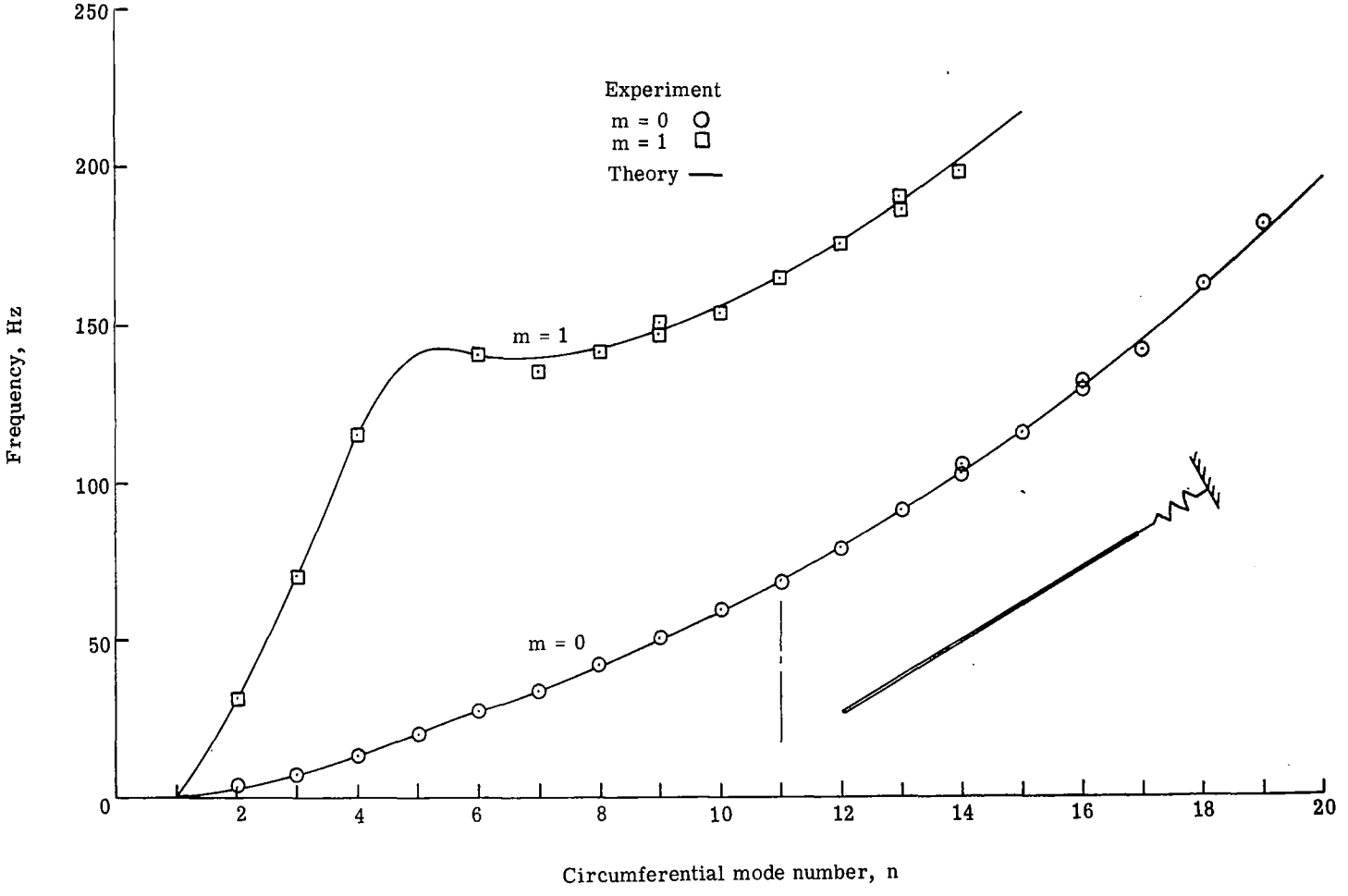

Figure 9.- Comparison of analysis and experiment for model configuration 1.

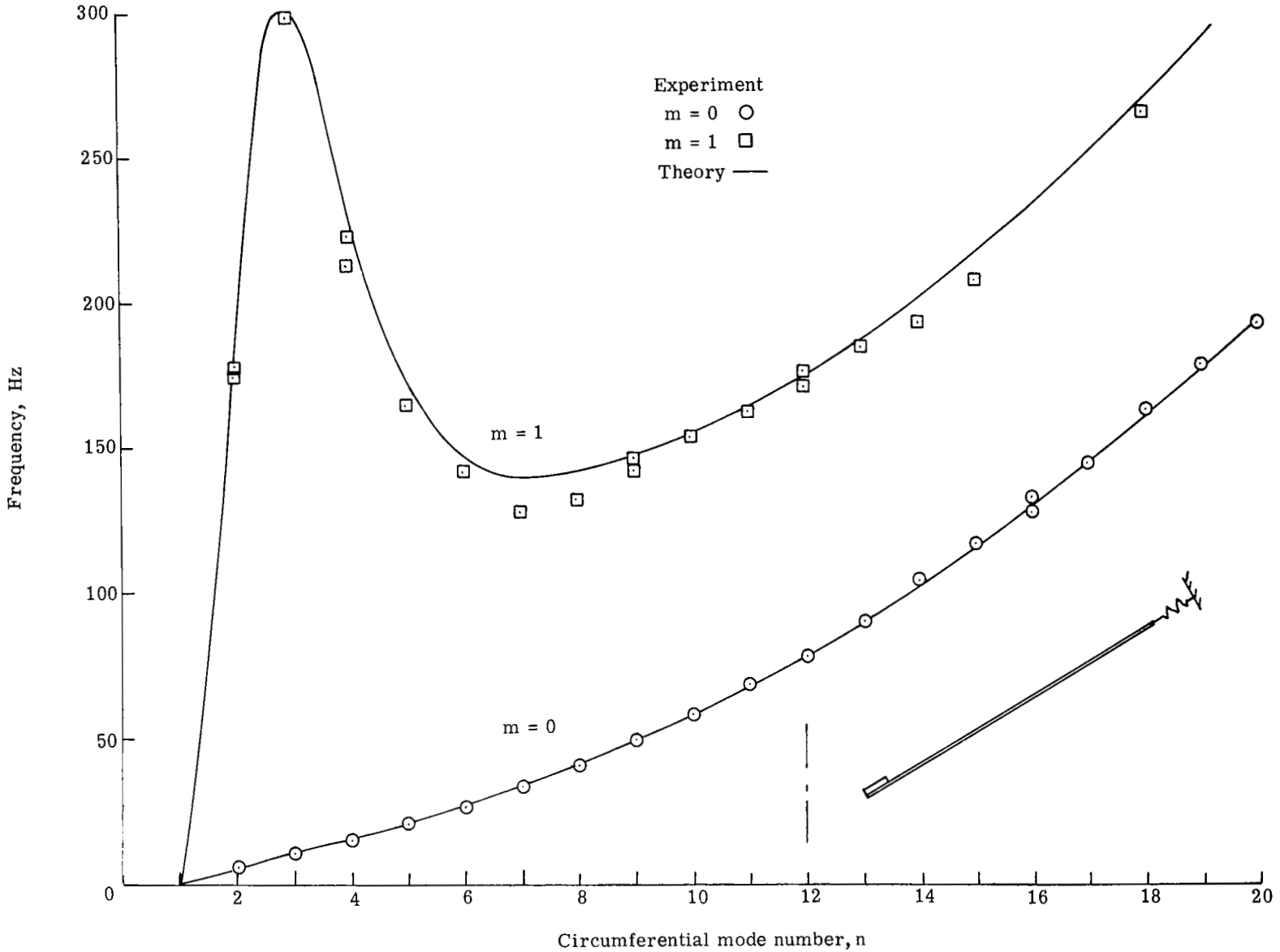

(a) Frequency.

Figure 10.- Comparison of analysis and experiment for model configuration 2.

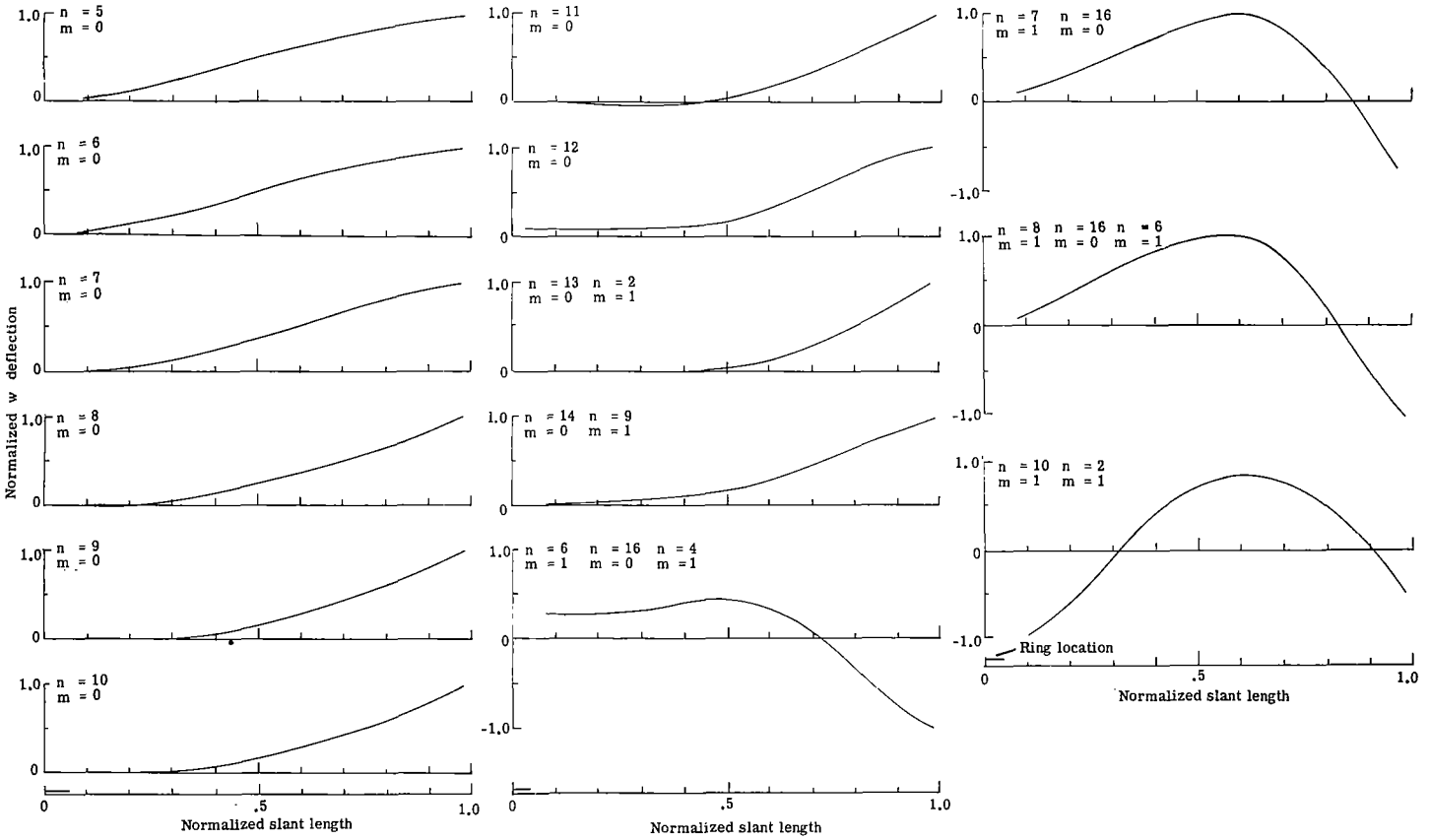

(b) Normalized experimental mode shapes.

Figure 10.- Concluded.

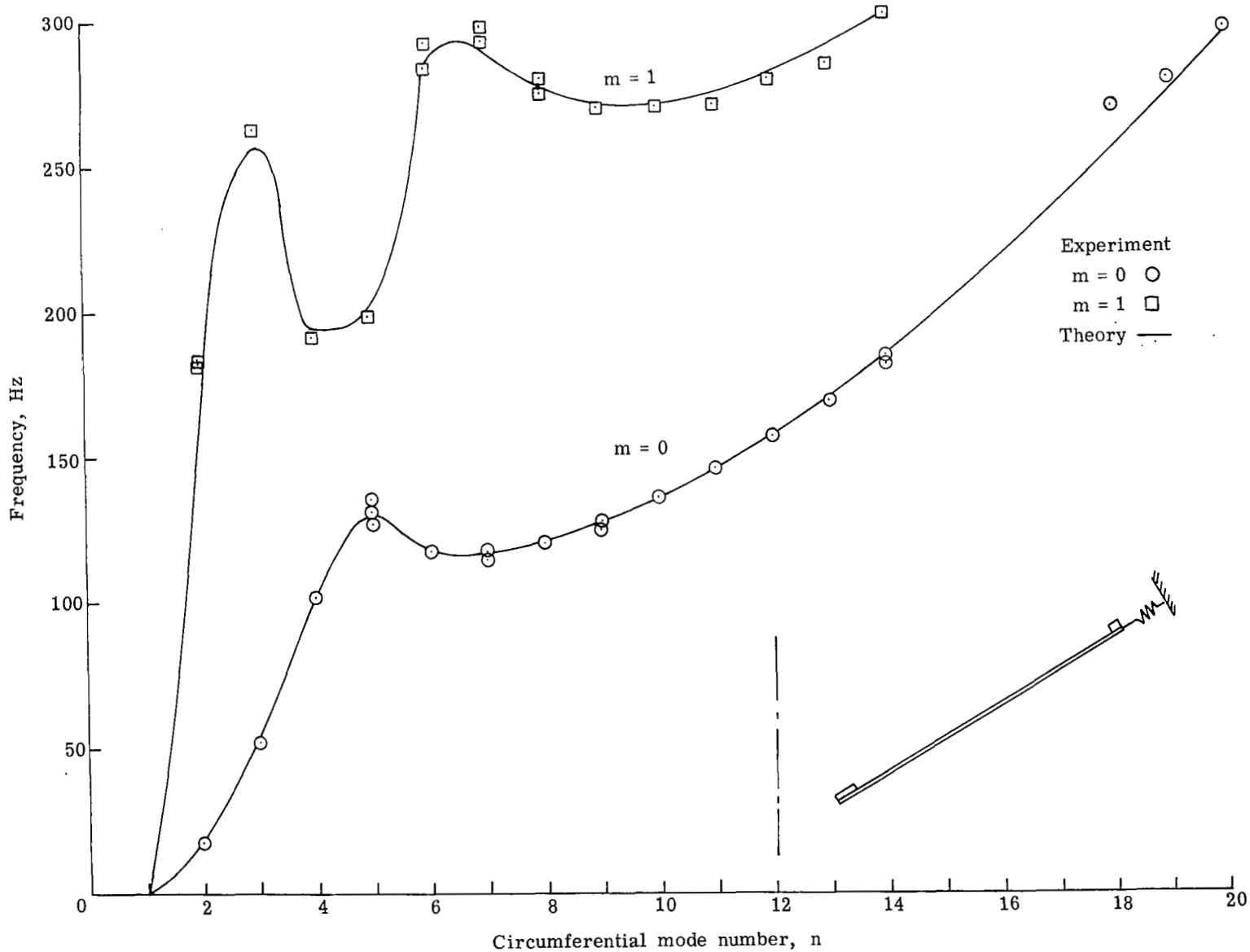

(a) Frequency.

Figure 11.- Comparison of analysis and experiment for model configuration 3.

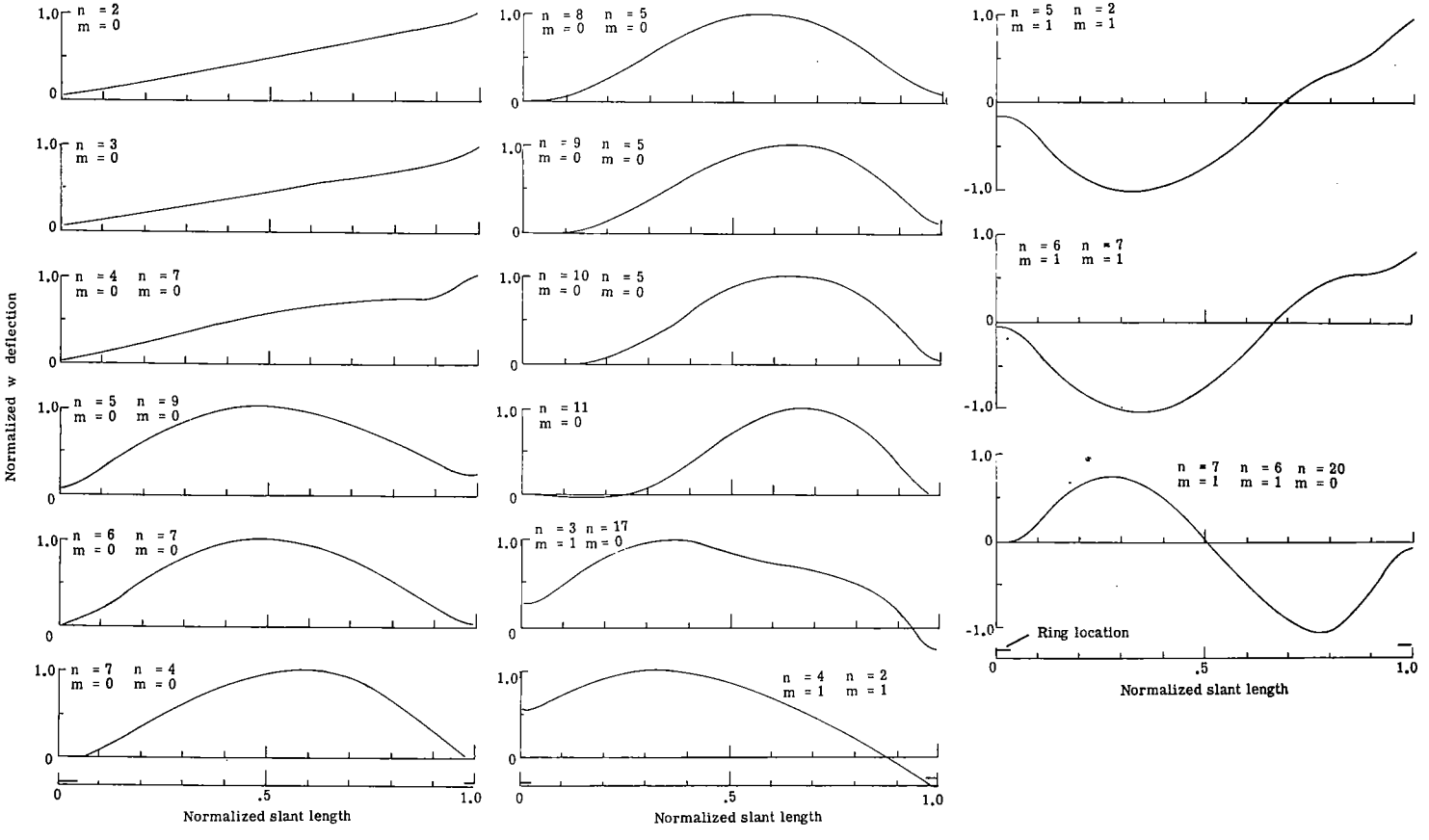

(b) Normalized experimental mode shapes.

Figure 11.- Concluded.

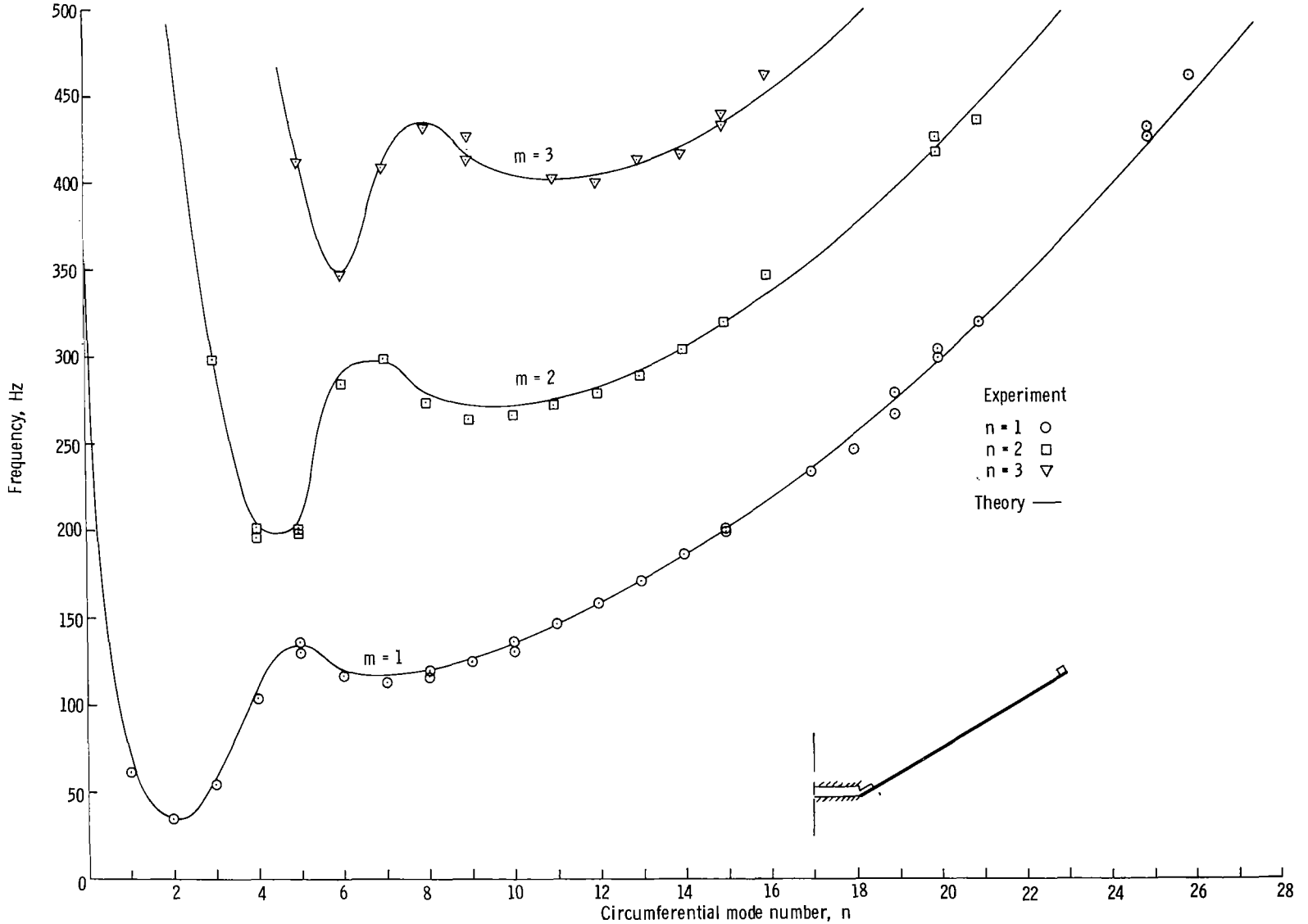

(a) Frequency.

Figure 12.- Comparison of analysis and experiment for model configuration 4.

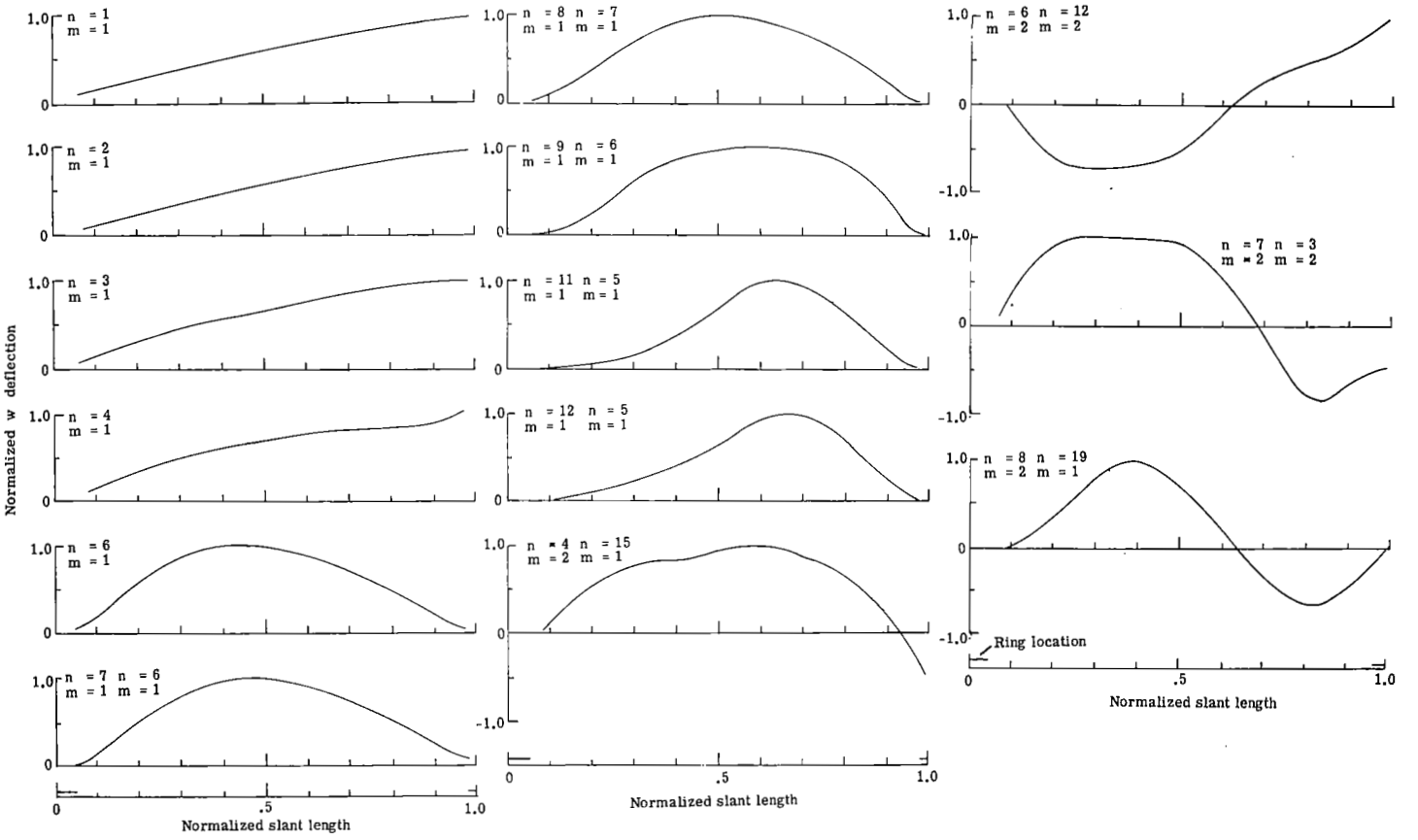

(b) Normalized experimental mode shapes.

Figure 12.- Concluded.

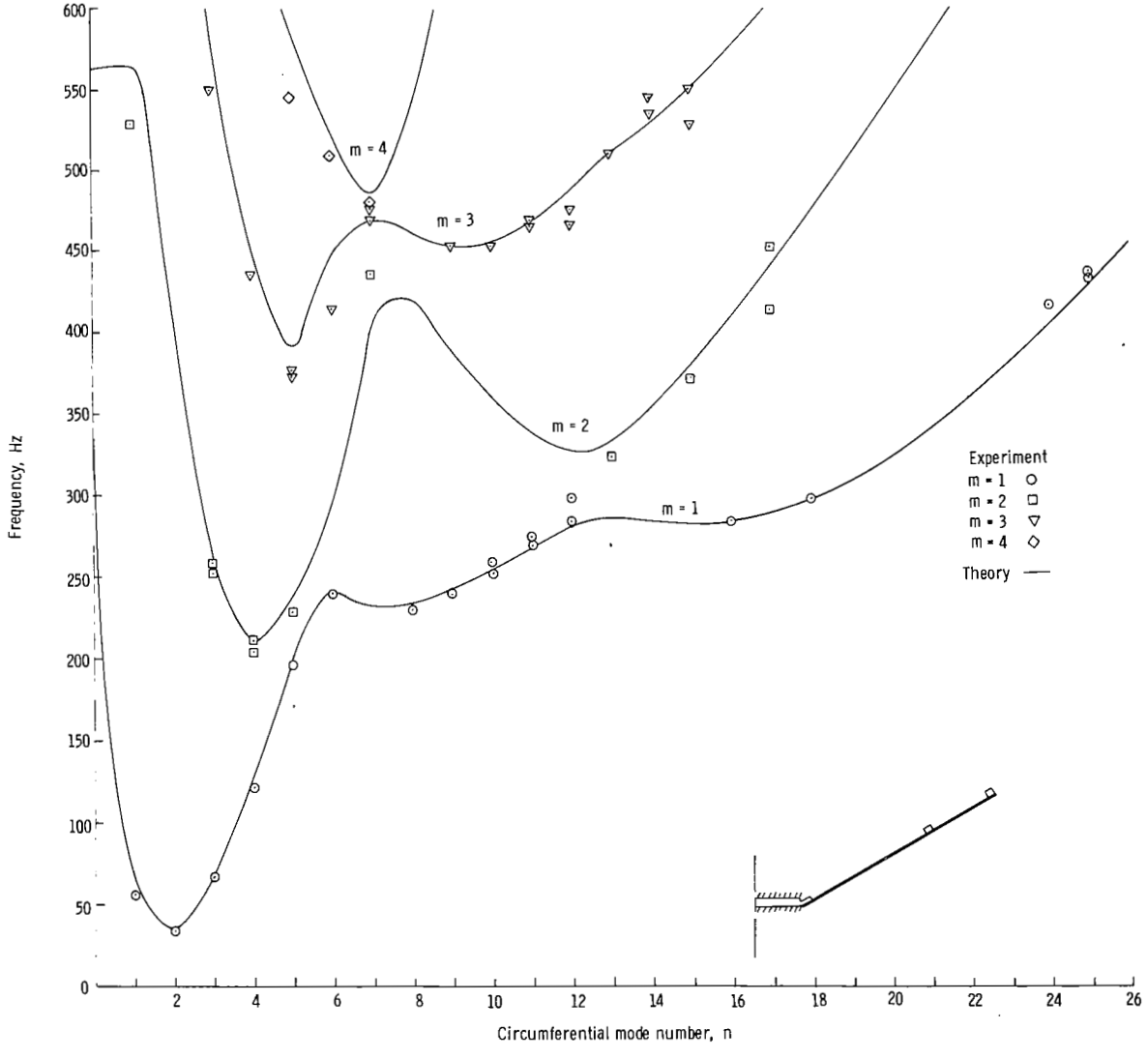

(a) Frequency.

Figure 13.- Comparison of analysis and experiment for model configuration 5.

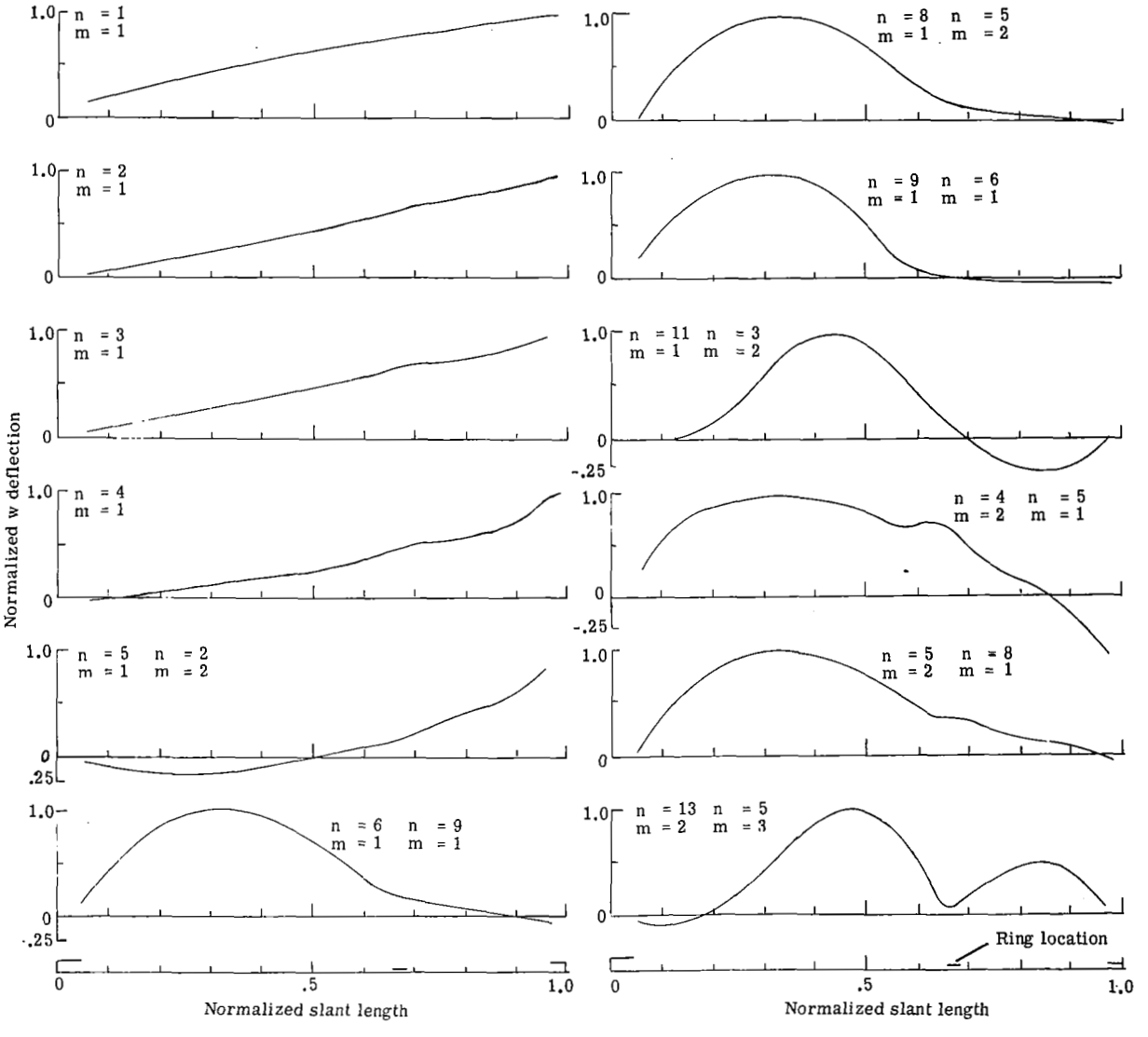

(b) Normalized experimental mode shapes.

Figure 13.- Continued.

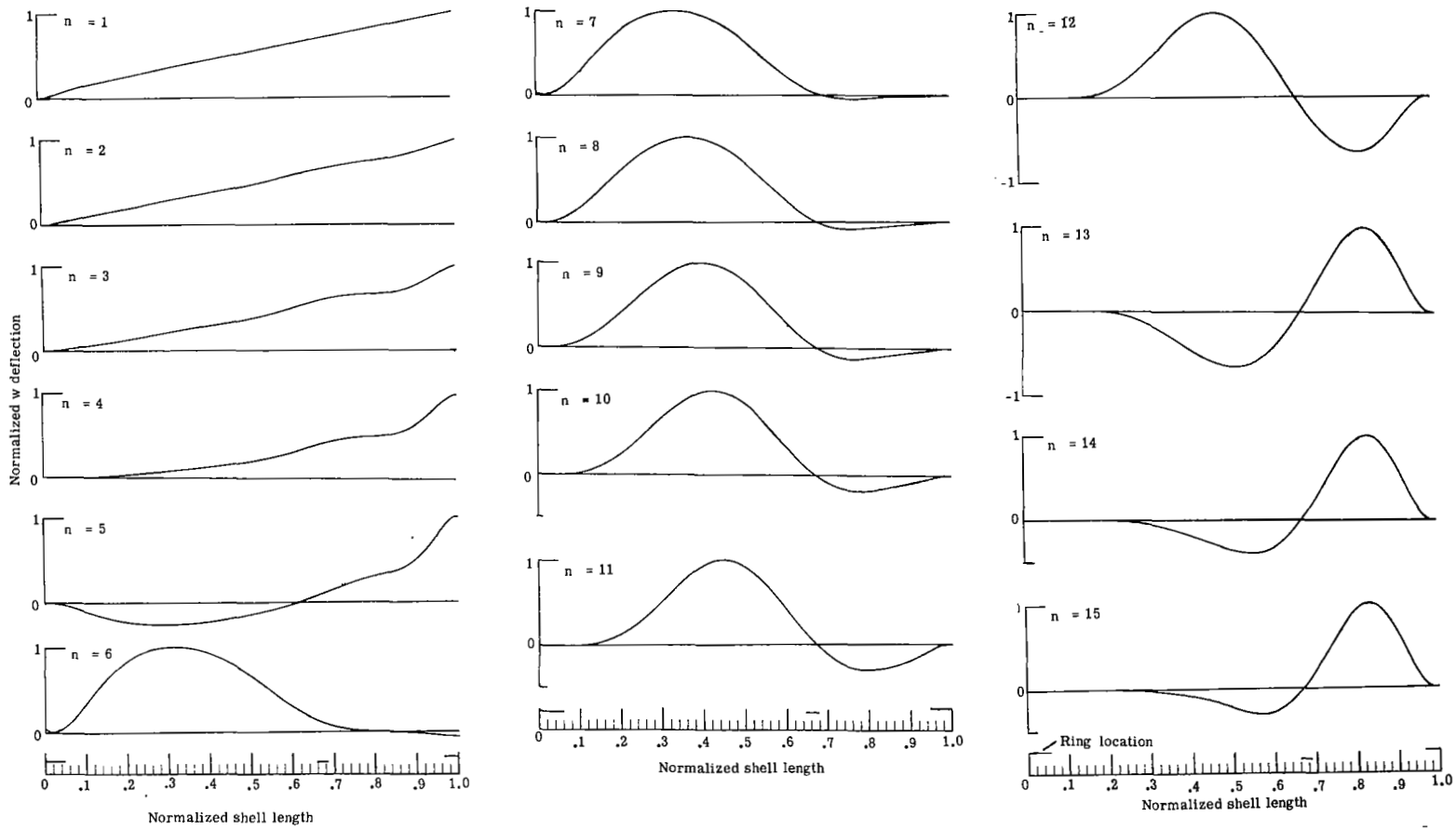

(c) Normalized calculated mode shapes. m = 1.

Figure 13.- Continued.

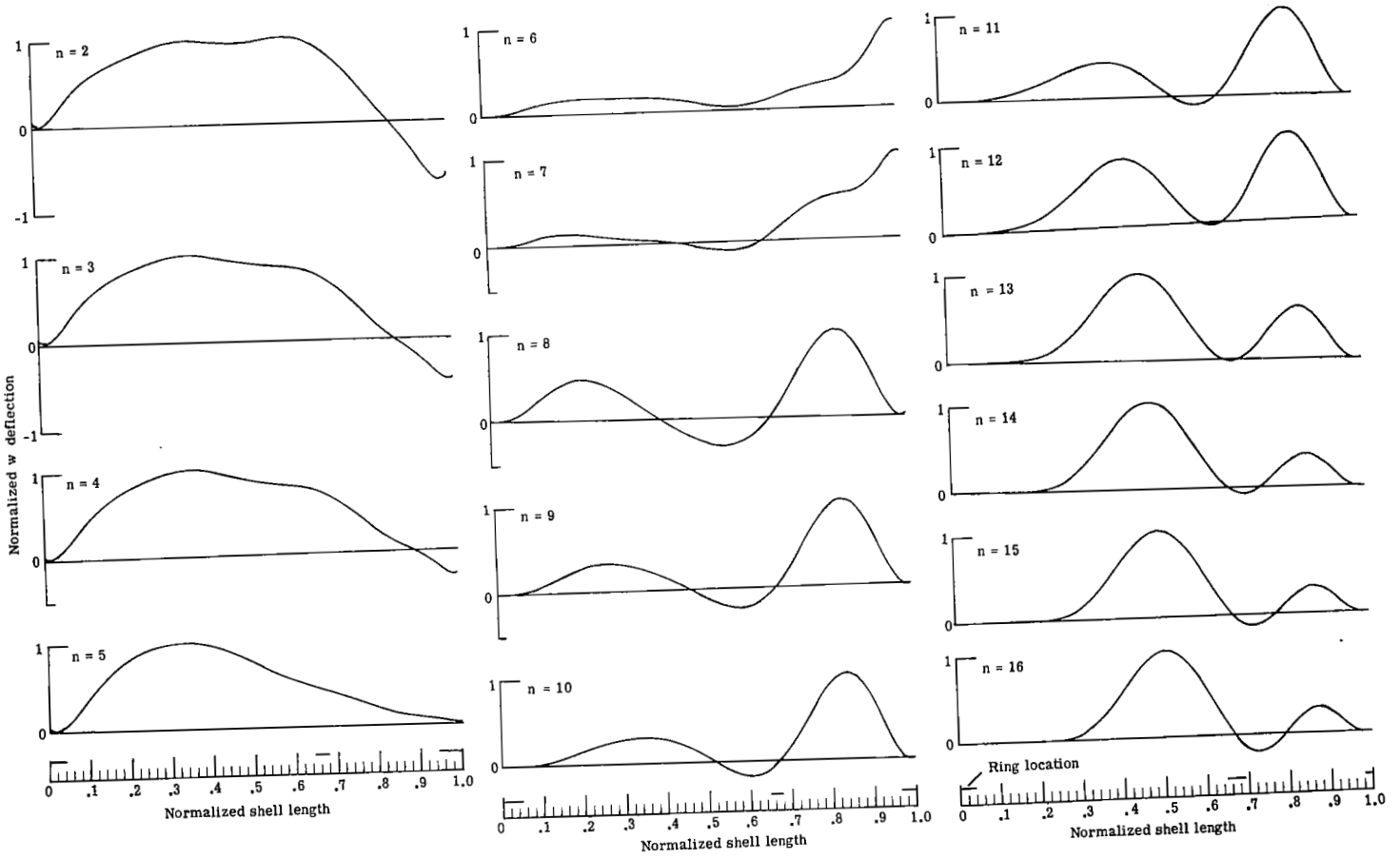

(d) m = 2.

Figure 13.- Concluded.

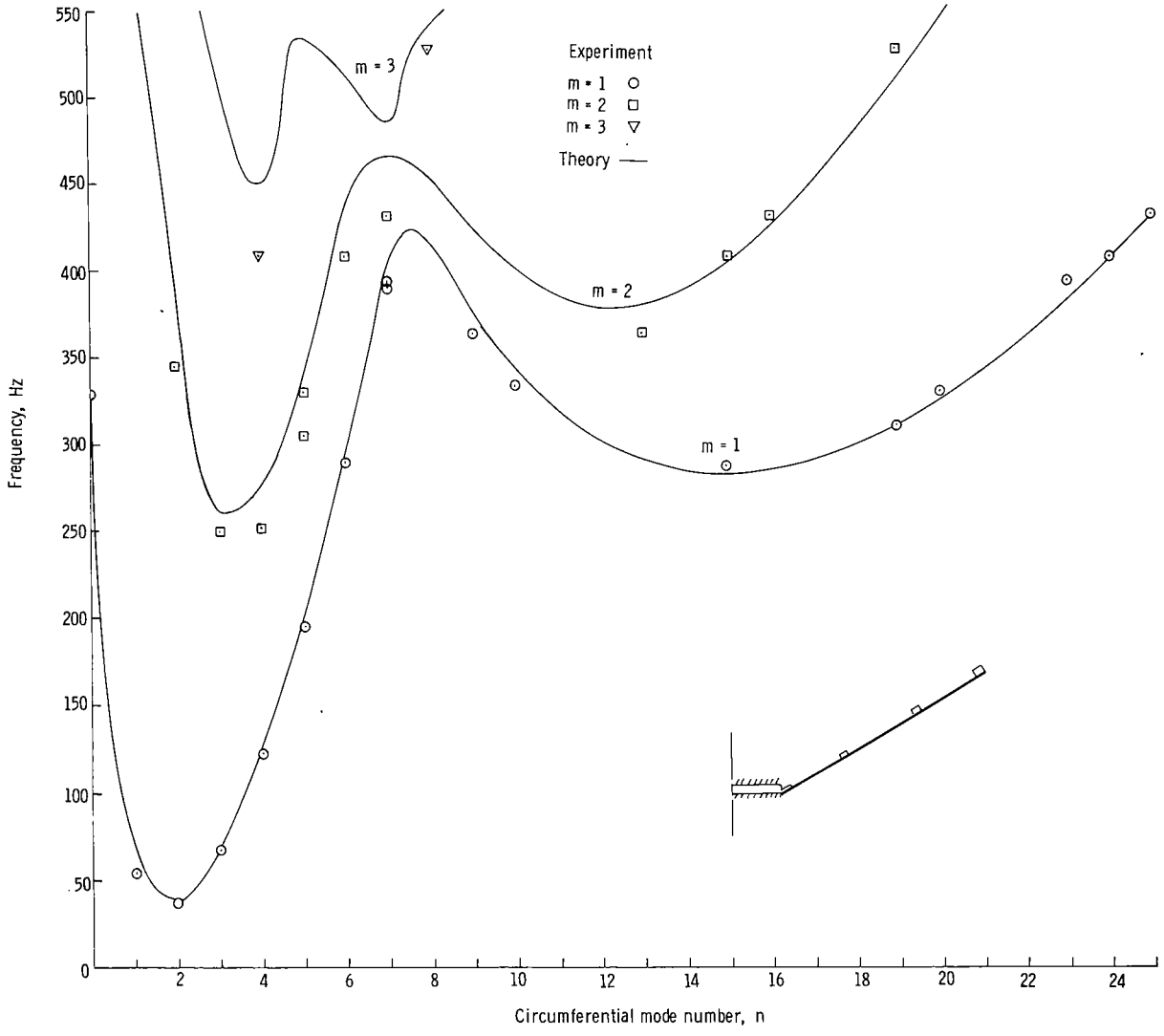

(a) Frequency.

Figure 14.- Comparison of analysis and experiment for model configuration 6.

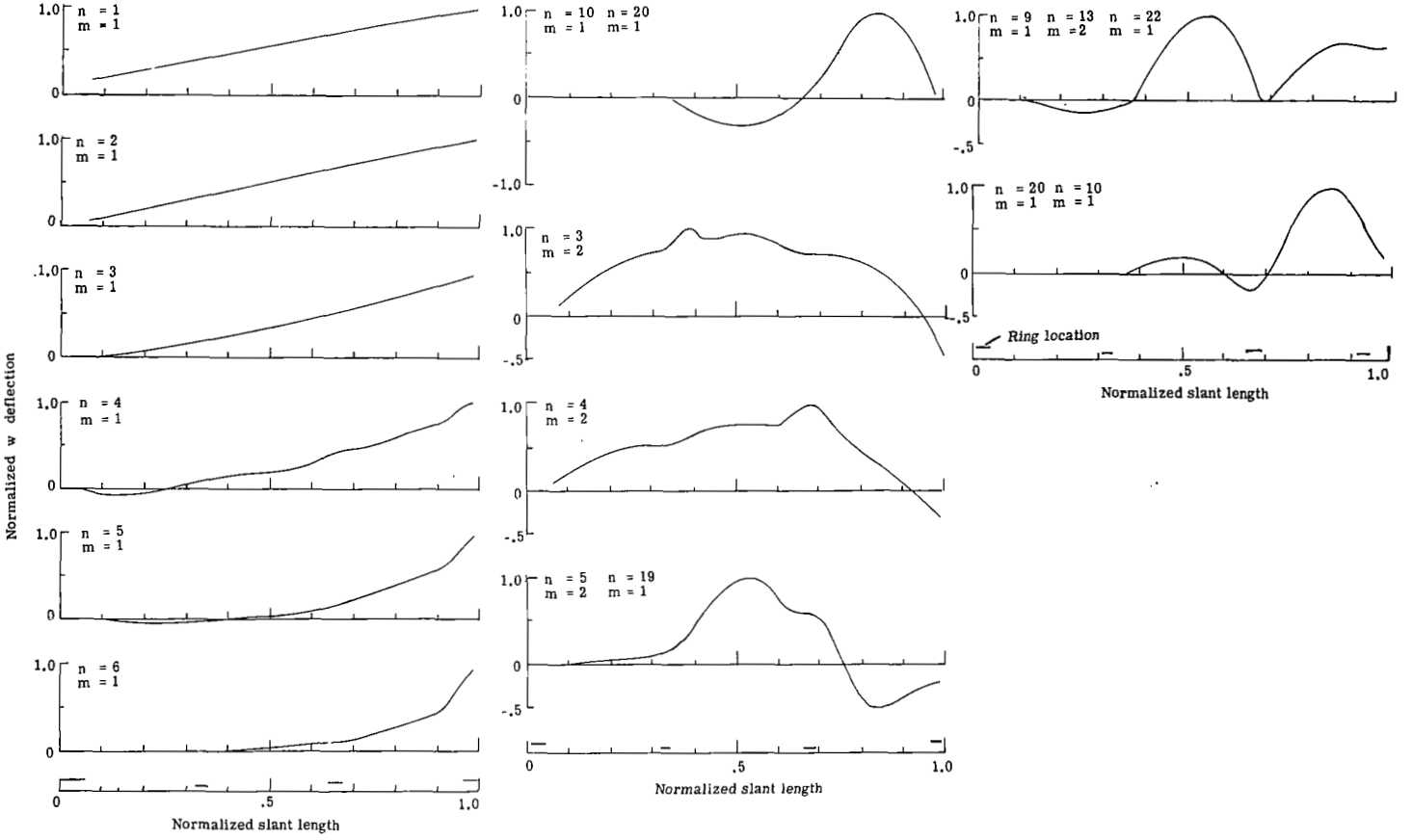

(b) Normalized experimental mode shapes.

Figure 14.- Concluded.

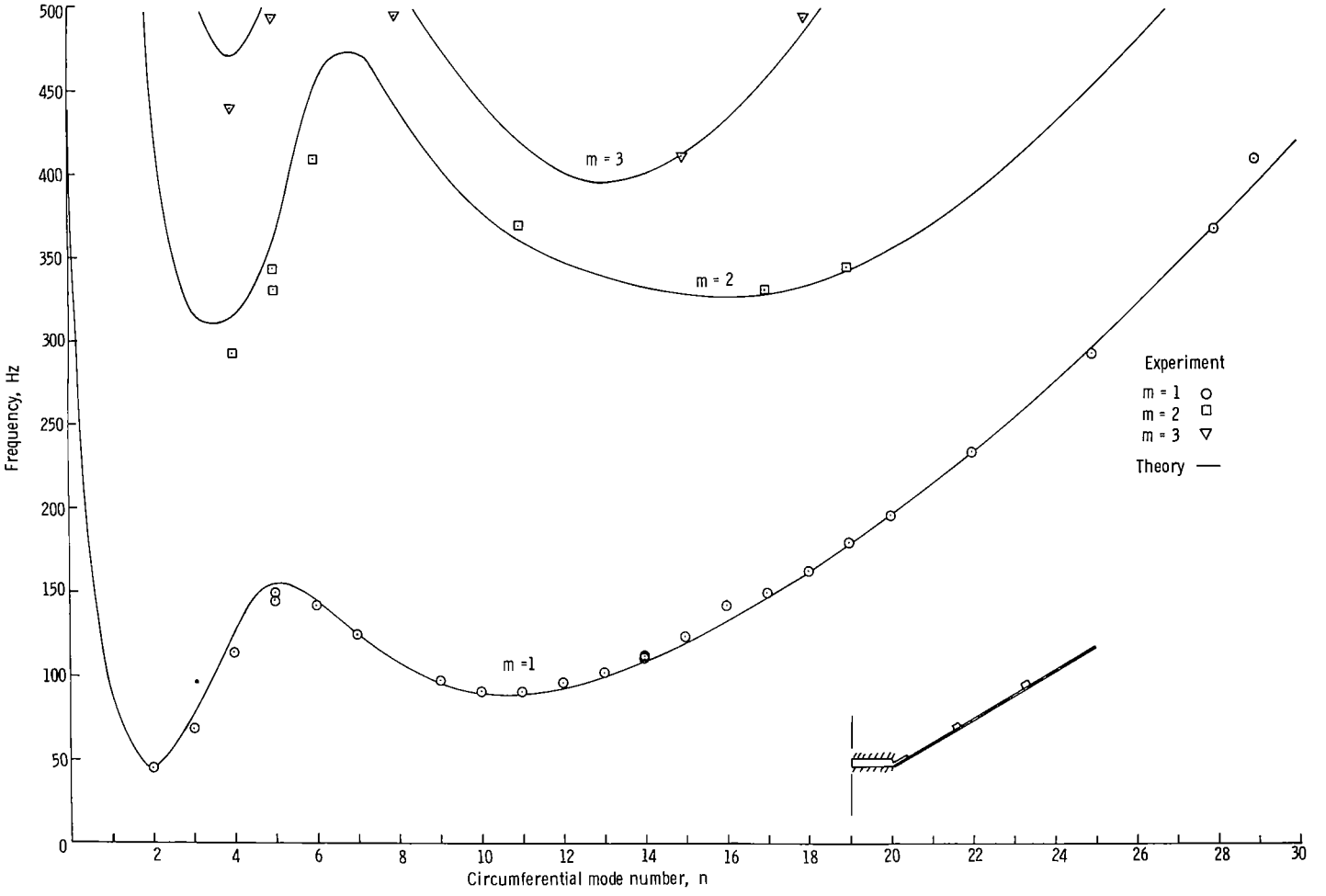

(a) Frequency.

Figure 15.- Comparison of analysis and experiment for model configuration 7.

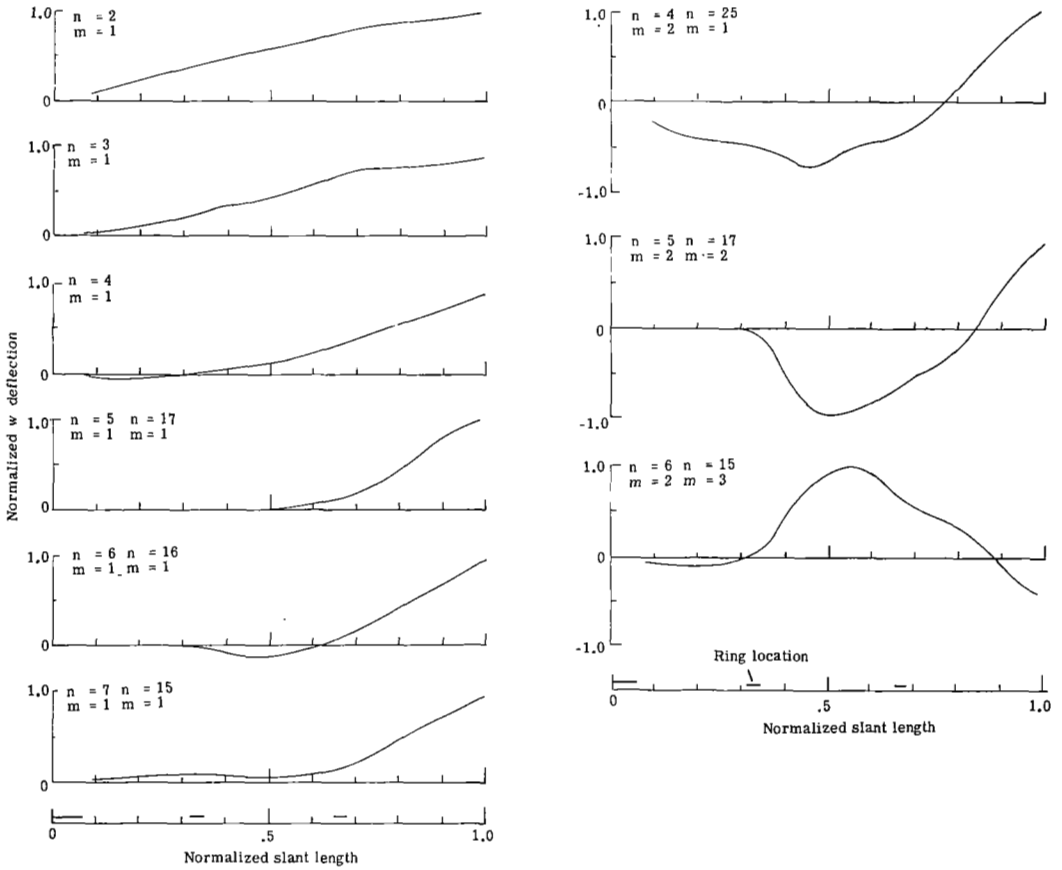

(b) Normalized experimental mode shapes.

Figure 15.- Concluded.

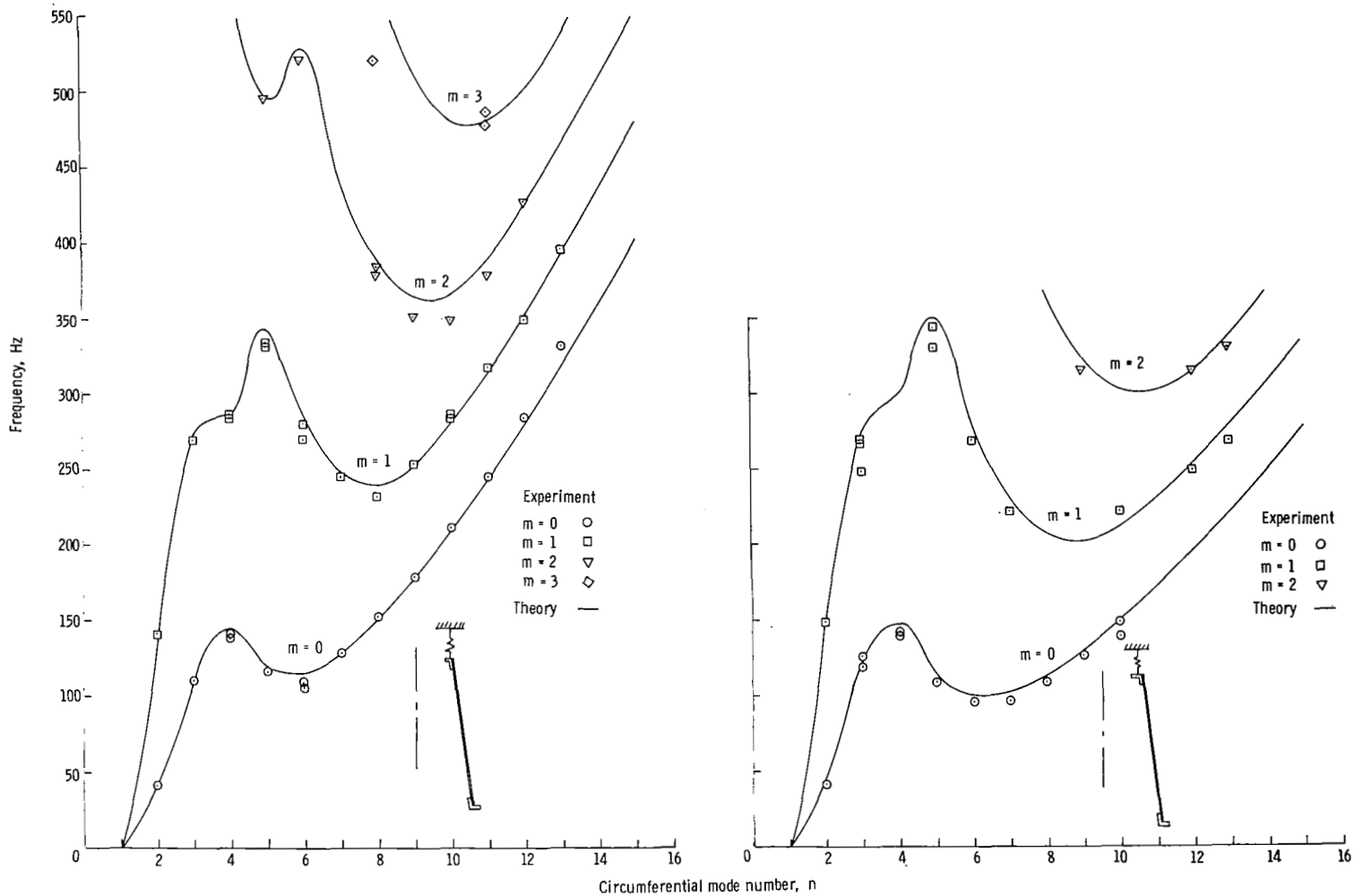

(a) Model configuration 8 – frequency.

(b) Model configuration 8A – frequency.

Figure 16.- Comparison of analysis and experiment.

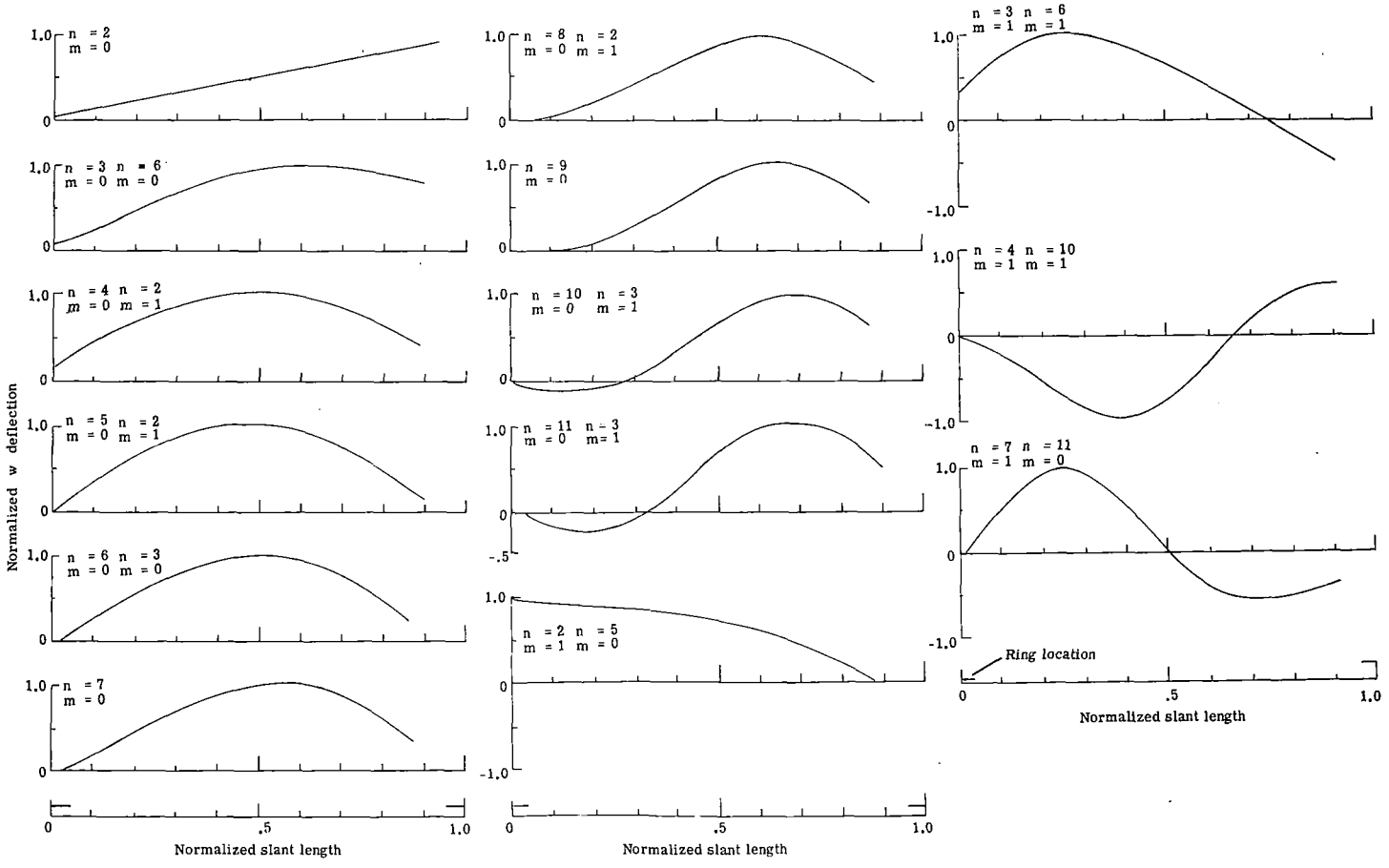

(c) Normalized experimental mode shapes for model configuration 8.

Figure 16.- Concluded.

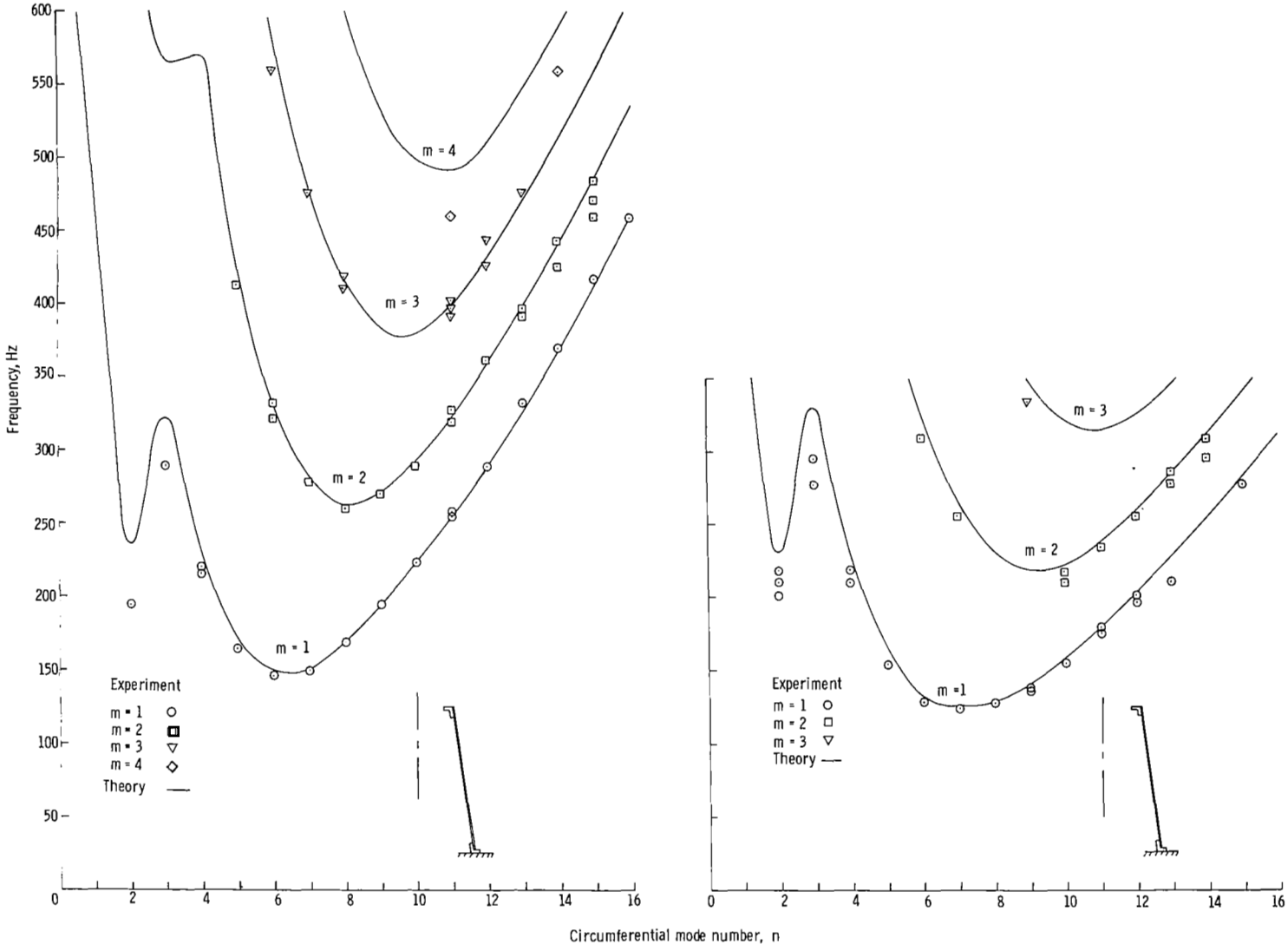

(a) Model configuration 9 – frequency.

(b) Model configuration 9A – frequency.

Figure 17.- Comparison of analysis and experiment.

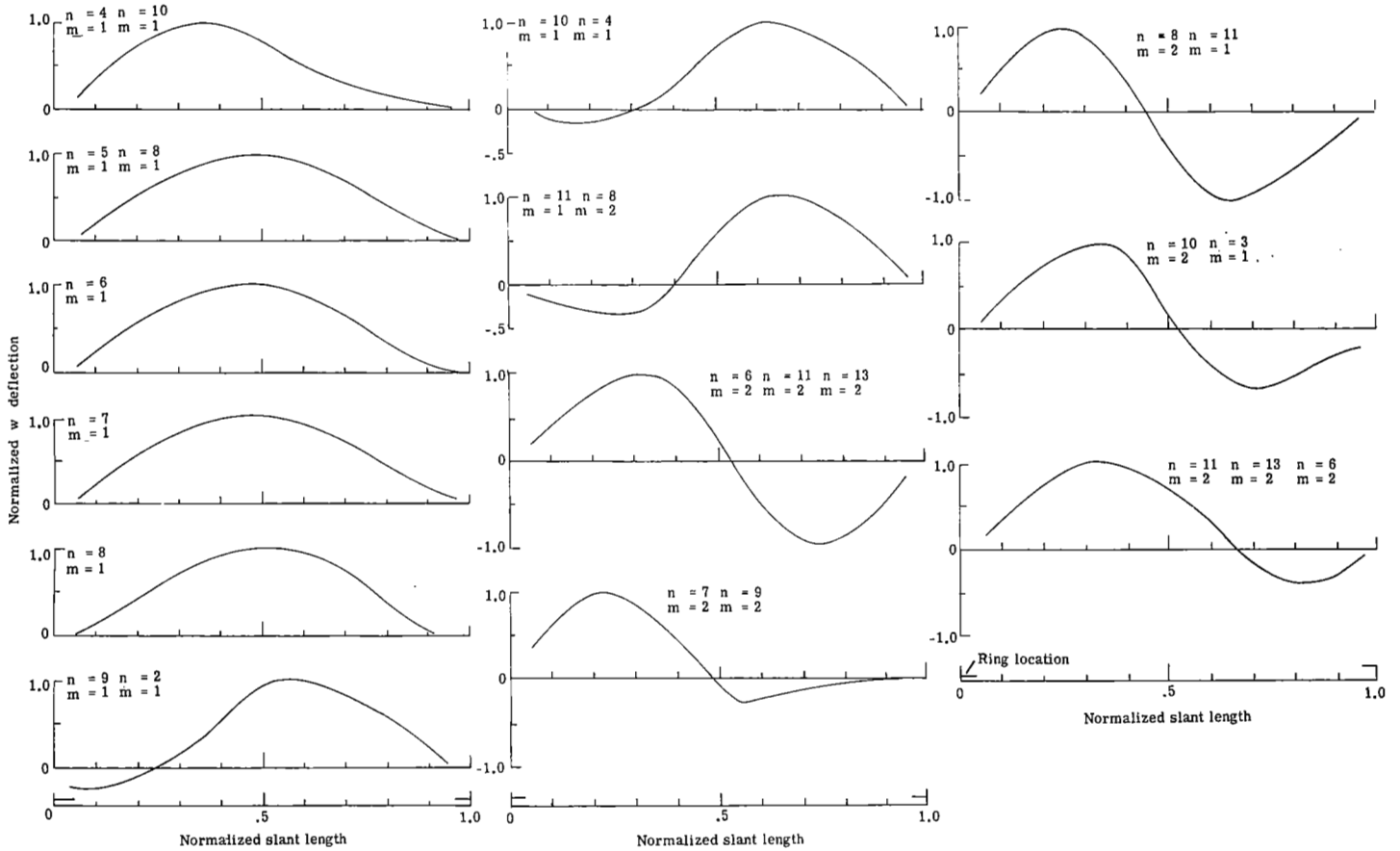

(c) Normalized experimental mode shapes for model configuration 9.

Figure 17.- Concluded.

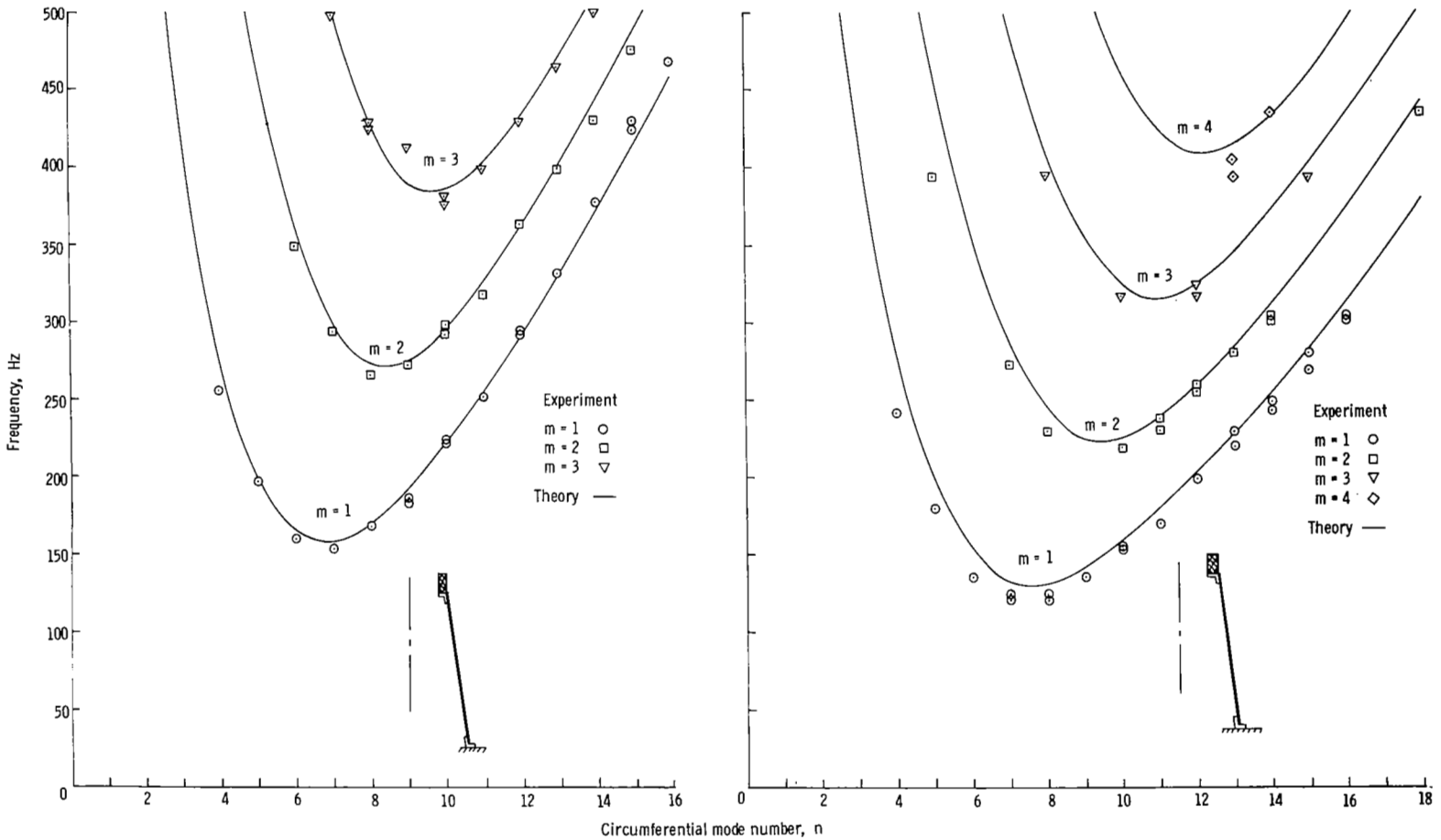

(a) Model configuration 10 – frequency.

(b) Model configuration 10A – frequency.

Figure 18.- Comparison of analysis and experiment.

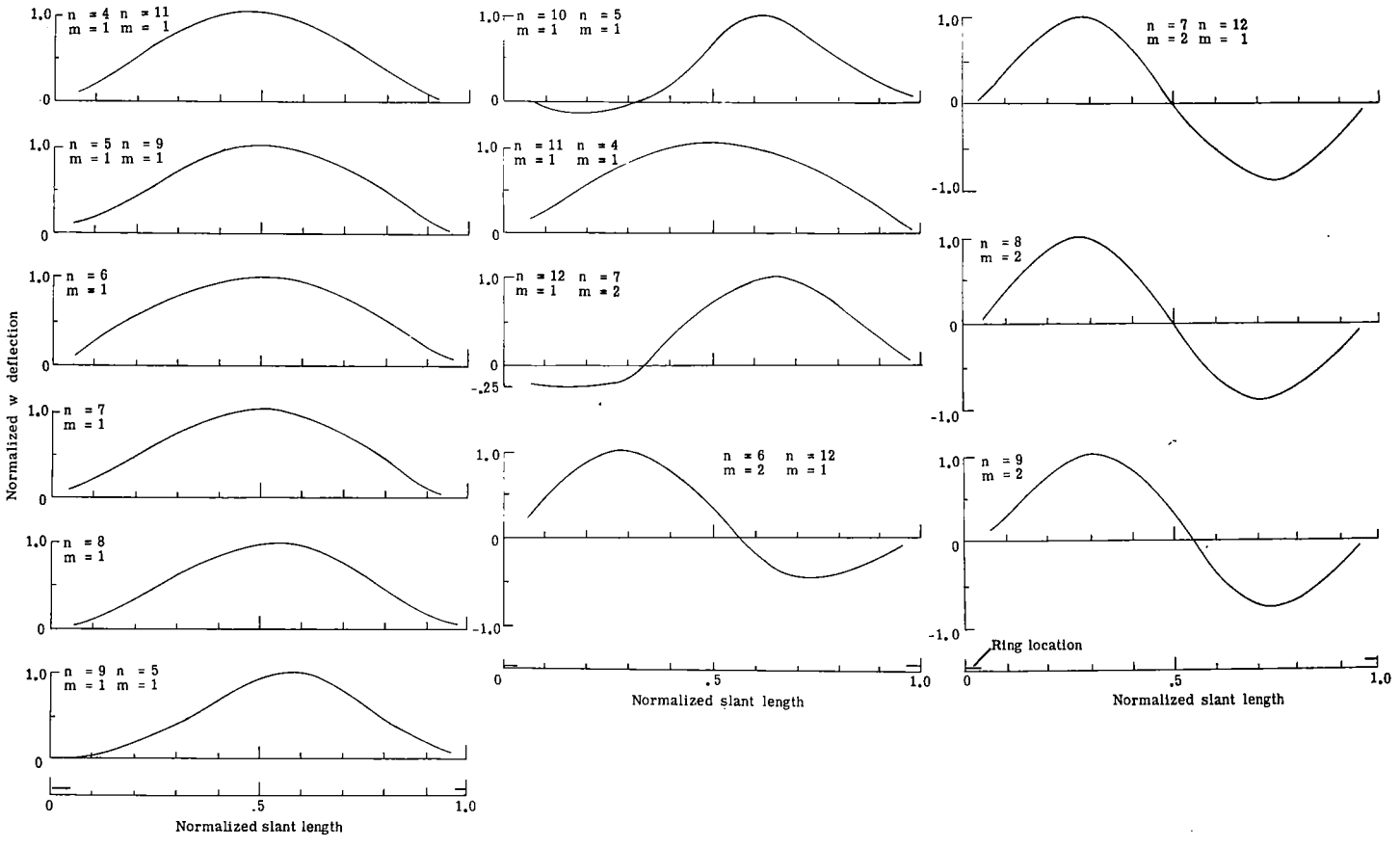

(c) Normalized experimental mode shapes for model configuration 10.

Figure 18.- Concluded.

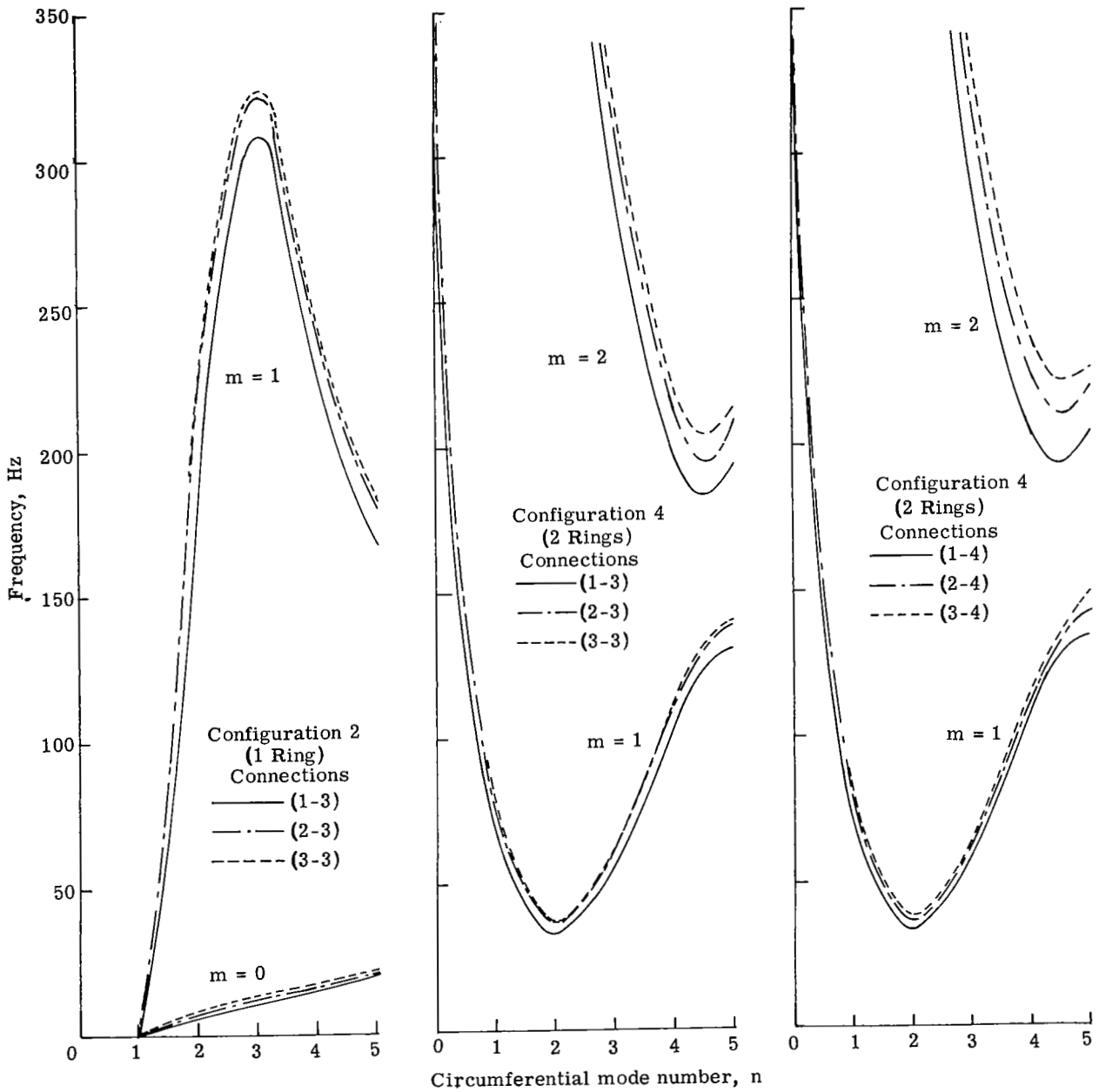

Figure 19.- Comparisons of calculated frequencies for various numbers of attachment points per ring stiffener.

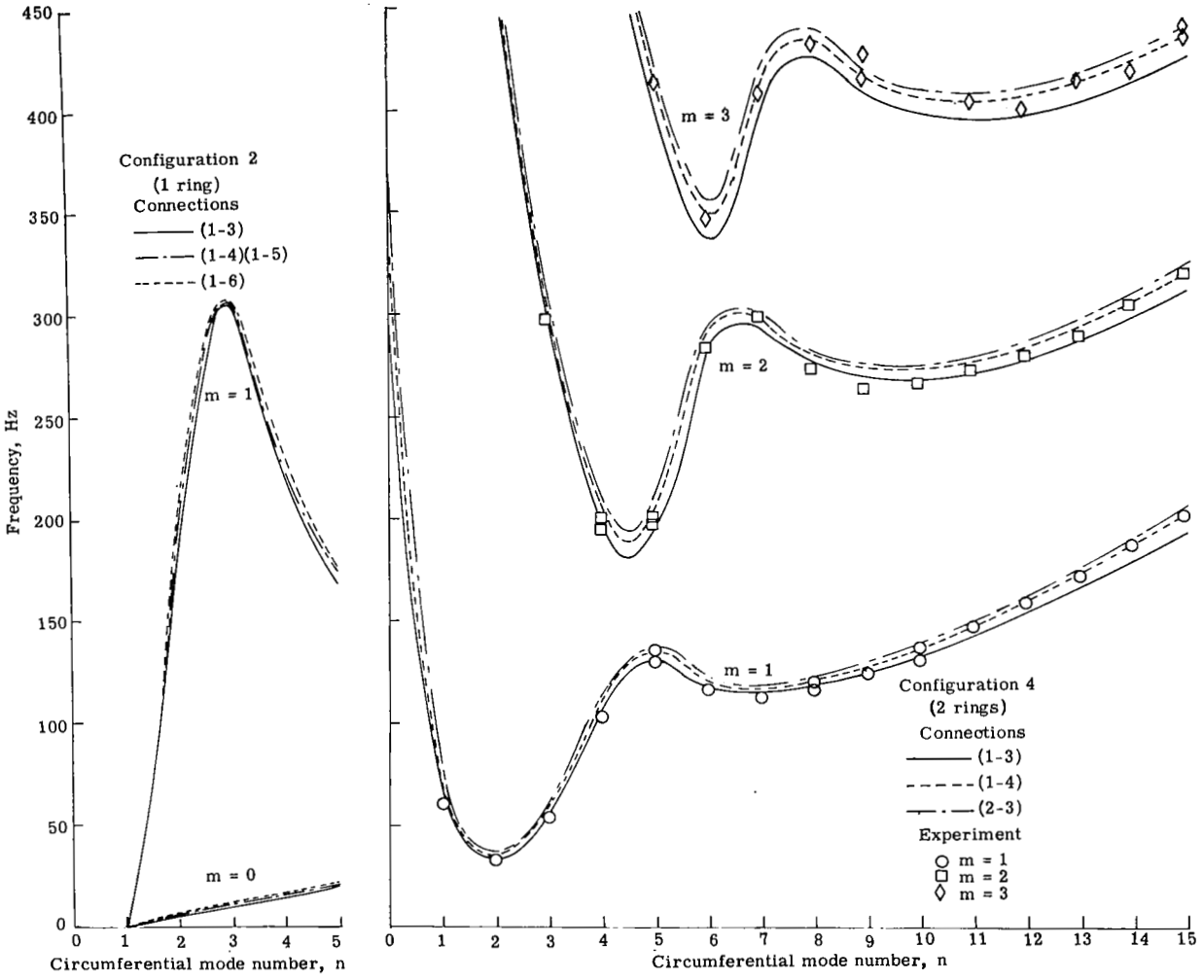

(a) Configuration 2.

(b) Configuration 4.

Figure 20.- Comparisons of calculated frequencies for various numbers of constraint equations per attachment circumference.

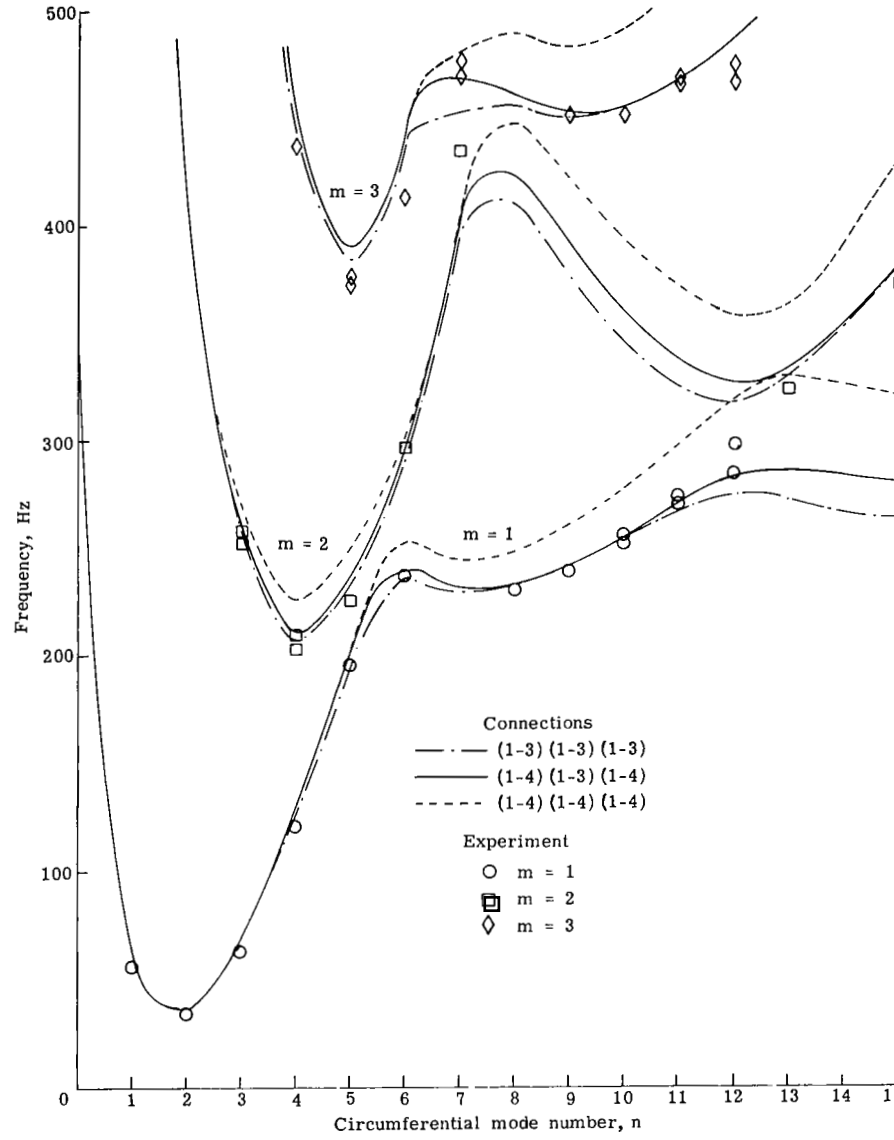

(c) Configuration 5.

Figure 20.- Concluded.

NASA-Langley, 1971 —— 32 L-7228